Technische Universität München
TUM School of Natural Sciences

Rapid Element Quantification in Metallic Particles via Laser-Induced-Breakdown-Spectrometry

Maria Katharina Sendlinger

Vollständiger Abdruck der von der TUM School of Natural Sciences der Technischen Universität München zur Erlangung einer

Doktorin der Naturwissenschaften (Dr. rer. nat.)

genehmigten Dissertation.

Vorsitz: Prof. Dr. Michael Schuster

Prüfende der Dissertation:

1. Priv.-Doz. Dr. Natalia P. Ivleva
2. Prof. Dr. Klaus Köhler

Die Dissertation wurde am 11.07.2025 bei der Technischen Universität München eingereicht und durch die TUM School of Natural Sciences am 25.09.2025 angenommen.

Ich habe gelernt, dass der Weg des Fortschritts

weder kurz noch unbeschwerlich ist.

- Marie Curie

Danksagung

Zunächst möchte ich mich bei PD Dr. Natalia Ivleva, Prof. Dr. Michael Schuster und Dr. Stephanie Kaufmann für die hervorragende Betreuung während meiner Doktorarbeit bedanken. Ihre Unterstützung und die vielen interessanten Gespräche und Diskussionen haben es mir ermöglicht, sowohl fachlich als auch persönlich zu wachsen und viel dazu zulernen.

Ebenso bin ich Dr. Dominik Huber zu großem Dank verpflichtet, der mich bereits in meiner Masterarbeit betreut und mich so für eine Promotion in diesem Bereich motiviert hat. In diesem Zusammenhang möchte ich auch Florian Mume, dem Leiter meiner Arbeitsgruppe, danken, der mir diese Promotion ermöglicht und mir als Mentor zur Seite gestanden hat.

Fachlich bin ich Thomas Glabik für die Durchführung der µRFA-Messungen sowie Christiane Pöppel und Stefanie Hengstberger für ihre Unterstützung bei den Mikrostrukturanalysen sehr dankbar. Ebenso danke ich Virginia Merk, Lutz Pfeiffer und Sven Merk von der Laser Technik Berlin (LTB) für die Weiterentwicklung des CORALIS und die stets sehr freundliche und unkomplizierte Zusammenarbeit und Beratung.

Auch den Studierenden Alexander Thomas, Jannis Gehrlein, Kevin Li, Besiana Emini und Eloise Hosseini bin ich für ihre engagierte Forschungs- und Abschlussarbeiten zu Dank verpflichtet, da ihre Beiträge zum Erfolg dieser Dissertation beigetragen haben. Ich hatte immer viel Spaß mit euch zusammenzuarbeiten.

Darüber hinaus möchte ich mich bei der gesamten Raman- und SEM-Gruppe der TU München bedanken. Obwohl ich nicht oft vor Ort war, habt ihr mich stets mit offenen Armen empfangen und mir bei Problemen mit Rat und Tat zur Seite gestanden.

Ganz besonders danke ich an dieser Stelle Dr. Dominik Huber, Alexander Thomas und Jannis Gehrlein für die vielen gemeinsamen Kaffeepausen, offene Ohren, Tischtennismatches, Weihnachtsfeiern, Sommerfeste und Nachmittage im Olympiapark. Ohne euch wäre die Zeit der Promotion nicht halb so schön gewesen!

Abschließend möchte ich mich bei meiner Familie und meinen Freunden bedanken, die mich durch mein gesamtes Studium begleitet haben. Ohne eure Unterstützung wäre ich nicht bis hierhin gekommen!

Content

List of Publications

This work is a cumulative dissertation, based on the lead author publications listed in the following. Additionally, the co-author publications as well as oral and poster presentations of the author are shown.

Lead author publications

Lanzinger M.; Huber D.; Merk V.; Kaufmann St.; Schuster M.; Ivleva N. P., Development of Laser-Induced Breakdown Spectroscopy-Methods for Rapid Element Quantification in Alloy Particles in Technical Cleanliness Analysis, Spectrochim. Acta Part B At. Spectrosc. 205 (2023) 106691.

Lanzinger M.; Kaufmann, St.; Schuster M.; Ivleva N. P., LIBS as a Fast and Reliable Alternative to µXRF and SEM-EDX for Quantitative Analysis of Aluminium Alloy Particles in Technical Cleanliness Analysis. Microchemical Journal. 207 (2024) 111782.

Co-author publications

von der Esch, E.; **Lanzinger, M.**; Kohles, A. J.; Schwaferts, C.; Weisser, J.; Hofmann, T.; Glas, K.; Elsner, M.; Ivleva, N. P., Simple Generation of Suspensible Secondary Microplastic Reference Particles via Ultrasound Treatment. Frontiers in Chemistry, section Analytical Chemistry 2020.

Sedlmeier C.; **Lanzinger M.**; Gasteiger H.; Drifts (Diffuse Reflectance Infrared Fourier Transform Spectroscopy) - a Way to Assess the Reactivity of Solid Electrolytes with Ambient Air. Meet. Abstr. 2020.

Oral presentations

Huber, D.; **Lanzinger, M.**, Anwendung der LIBS-Raman-Spektrometrie zur Charakterisierung und Identifizierung von partikulären Verunreinigungen im Bereich der technischen Sauberkeitsanalyse. *12. Fachtagung Technische Sauberkeit*, 24.-25.05.2022, Bad Göggingen, Germany.

Poster presentations

Lanzinger, M.; Huber, D.; Kaufmann St.; Schuster M.; Ivleva, N. P., Application of quantitative Laser-Induced Breakdown Spectroscopy in Technical Cleanliness. Analytica Conferences, 21.-23.06.2022, Munich, Germany.

Lanzinger, M.; Schuster M.; Ivleva, N. P., Laser-Induced Breakdown Spectroscopy in Technical Cleanliness. BMW Dialogtag, 14.09.2022, Munich, Germany.

Lanzinger, M.; Kaufmann St.; Schuster M.; Ivleva, N. P., Comparative Study of EDX, µXRF and LIBS for Element Quantification in Metallic Particles. ANAKON, 11.-14.04.2023, Vienna, Austria.

Summary

In the context of high-quality production, quality assurance and process control, the characterization of metal alloys and their respective particles is a commonly applied tool. One example for such an application is *technical cleanliness analysis* (TCA) in the automotive industry, where more and more sensitive and highly technologized products place increasingly high demands on the product quality. Already small impurities and (particle) contaminations in a size range between roughly 50 and 1000 µm, can lead to serious failures and damage, for example by blocking of mechanical components or short-circuiting of electrical systems. Therefore, limits for particle contamination are tightened in today's and future's automotive production to guarantee high-quality and safe goods. Even though TCA is known and executed in the automotive industry for over 20 years, with the shift to electromobility and to more sensitive components, the demand for more accurate and precise analytical tools in TCA increases accordingly.

Currently, the commonly used TCA techniques for material characterization are optical microscopy and automated *scanning electron microscopy coupled with energy dispersive X-ray spectroscopy* (SEM-EDX). However, these methods only provide information about rough material classes, like metallic-reflective and not metallic-reflective (optical microscopy), and alloy classes, like iron or aluminium based (SEM-EDX). With only this rough material classification the identification of a contamination source is not possible. Only with an in-depth characterisation of the particle, a fast and efficient origin recognition and solution process is enabled. Considering the fast-paced industrial production, also the time necessary for analysis and evaluation is a key factor in the context of TCA.

To increase the analytical performance and reduce analysis time, therefore, increasing efficiency, other methods than SEM-EDX and optical microscopy are under review. In this dissertation, *laser-induced breakdown spectrometry* (LIBS) studied in this context. LIBS offers a fast measurement, little to no sample preparation as well as high sensitivity for qualitative and quantitative analysis. Additionally, only small sample volumes are necessary for LIBS, enabling TC particle characterization.

In this thesis, the fitness of LIBS for the use in industrially applied particle analysis, like TCA, is studied und improved models for quantitative analysis are built. The quantification models are specifically developed for and applied to the characterization of aluminium alloy particles using the multivariate data analysis algorithm "*Partial Least Squares*" (PLS) -regression. Employing and training with 49 *certified reference materials* (CRM) quantification models for

ten analytes in aluminium alloy matrices are established. By additionally pre-selecting evaluation wavelengths and implementing sub-calibrations, large concentration ranges are calibrated with low *limits of quantification* (LOQ). For validation cross-validation as well as samples not included into developing the calibration are utilized. This way, the stability of the models is presented for varying sample matrices.

The developed models are then applied to the analysis of in-house generated reference particles for the use in TCA. As these reference particles are shaved from bulk samples before being pestled and sieved, they are variable in size and composition, easily and economically produceable as well as similar to TC-particles found in the production environment. Using the previously developed calibration models it is shown that (i) the composition of the reference particles is not dependent on their size and (ii) the developed models are fit to be used for the analysis of TCA relevant particles.

Finally, the results of the developed LIBS PLS-regression quantification models are compared to widely established X-ray-based metallic particle characterization methods (SEM-EDX, *µ-X-ray-fluorescence-spectrometry*: µXRF). Four CRMs in particle form are analysed subsequently with all three methods to directly compare the quantitative results for different aluminium alloy matrices and compositions. Additionally considering the respective analysis volume for each method, the results showcased, a high comparability of LIBS to the established methods, independent of sample composition.

The results of this dissertation showcase the possibilities and advantages of applying LIBS in industrial particle analysis, like TCA. The developed multivariate models are fit to characterize metallic particles in detail, yielding comparable results to widely established analytical techniques with significantly reduced analysis time and sample preparation effort. By developing and optimizing further quantification models, for example for iron or copper matrices, LIBS can be further established as a rapid and reliable analysis method for particle characterization in industrial applications; both as an alternative as well as an addition to established metallic material characterization techniques.

Kurzzusammenfassung

Im Kontext einer hochwertigen Produktion, der Qualitätssicherung und der Prozesskontrolle, sind die Charakterisierung von Metalllegierungen und deren Partikeln ein häufig angewendetes Werkzeug. Ein Beispiel für eine solche Anwendung ist die technische Sauberkeitsanalyse (*engl. technical cleanliness analysis*, TCA) in der Automobilindustrie, in der immer sensiblere und hoch-technologisierte Produkte zu zunehmend höheren Anforderungen an die Produktqualität führen. Schon kleine Verunreinigungen und (Partikel-) Kontaminationen in einer Größenordnung von etwa 50 bis 1000 µm können zu ernsthaften Ausfällen und Schäden führen, zum Beispiel durch das Blockieren von mechanischen Komponenten oder das Erzeugen von Kurzschlüssen in elektrischen Systemen. Daher werden Partikelgrenzwerte in der heutigen und zukünftigen Automobilherstellung immer weiter verschärft, um hohe Qualität und sichere Produkte zu gewährleisten. Obwohl TCA seit über 20 Jahren in der Automobilindustrie bekannt ist und verwendet wird, steigt mit dem Übergang zur Elektromobilität und zu empfindlicheren Komponenten auch die Nachfrage nach genaueren und präziseren analytischen Methoden in der TCA.

Momentan sind die üblicherweise in der TCA verwendeten Methoden zur Materialcharakterisierung die optische Mikroskopie und die automatisierte Rasterelektronenmikroskopie gekoppelt mit energiedispersiver Röntgenspektroskopie (*engl. scanning electron microscopy coupled with energy dispersive X-ray spectrometry*, SEM-EDX). Diese Methoden liefern jedoch nur Informationen über grobe Materialklassen, wie metallisch-reflektierend und nicht metallisch-reflektierend (optische Mikroskopie), und Legierungsklassen, wie eisen- oder aluminiumbasiert (SEM-EDX). Mit nur dieser groben Materialklassifizierung ist die Identifizierung einer Kontaminationsquelle nicht möglich. Nur mit einer eingehenden Charakterisierung des Partikels wird ein schneller und effizienter Quellenidentifikations- und Lösungsprozess ermöglicht. In Anbetracht der schnelllebigen industriellen Produktion ist auch die für Analyse und Bewertung notwendige Zeit ein Schlüsselfaktor für die Industrie im Kontext der TCA.

Um die analytische Leistung zu steigern, die Analysezeit zu reduzieren und damit die Effizienz zu erhöhen, werden zusätzliche Methoden zur SEM-EDX und optischen Mikroskopie auf ihre Anwendbarkeit überprüft. In dieser Dissertation wird die laserinduzierte Plasma-Spektrometrie (*engl. laser-induced breakdown spectrometry*, LIBS) in diesem Kontext untersucht. LIBS bietet eine kurze Messzeit, wenig bis keine Probenvorbereitung sowie eine hohe Empfindlichkeit für

qualitative und quantitative Analysen. Zusätzlich werden für LIBS nur kleine Probenmengen benötigt, was die TC-Partikelcharakterisierung ermöglicht.

In dieser Arbeit wird die Eignung von LIBS für den Einsatz in industriell angewendeten Partikelanalysen, wie TCA, untersucht und verbesserte Modelle für quantitative Analysen erstellt. Die Quantifizierungsmodelle werden speziell für die Charakterisierung von Aluminiumlegierungspartikeln unter Verwendung des multivariaten Datenanalysealgorithmus "*Partial Least Squares*" (PLS) Regression entwickelt und angewendet. Durch die Verwendung und das Training mit 49 zertifizierten Referenzmaterialien *(engl. certified reference material,* CRM) werden Quantifizierungsmodelle für zehn Analyten in Aluminiumlegierungsmatrizen entwickelt. Durch die zusätzliche Vorauswahl von Wellenlängen zur Auswertung und die Implementierung von Sub-Kalibrierungen werden große Konzentrationsbereiche mit niedrigen Quantifizierungsgrenzen (*engl. limit of quantification*, LOQ) kalibriert. Zur Validierung werden Kreuzvalidierung sowie Proben, die nicht in die Entwicklung der Kalibrierung einbezogen wurden, verwendet. Auf diese Weise wird die Stabilität der Modelle für unterschiedliche Probenmatrizen gezeigt.

Die entwickelten PLS-Regressionsmodelle werden dann auf die Analyse von selbst hergestellten Referenzpartikeln für den Einsatz in der TCA angewendet. Da diese Referenzpartikel aus Bulk-Materialien geschnitten werden, bevor sie gemörsert und gesiebt werden, sind sie in Größe und Materialzusammensetzung variabel, wobei sie leicht und wirtschaftlich herstellbar sind und gleichzeitig hohe Ähnlichkeit zu in der Produktion vorkommenden TC-Partikeln aufweisen. Mit den zuvor entwickelten Kalibrierungsmodellen wird gezeigt, dass (i) die Zusammensetzung der Referenzpartikel nicht von ihrer Größe abhängig ist und (ii) die entwickelten Modelle geeignet sind, um für die Analyse von TCA-relevanten Partikeln verwendet zu werden.

Schließlich werden die Ergebnisse der entwickelten LIBS-PLS-Regressionsmodelle mit weit verbreiteten röntgenbasierten Methoden zur Charakterisierung metallischer Partikel (SEM-EDX, *µ-Röntgenfluoreszenzspektrometrie*: µXRF) verglichen. Vier CRMs in Partikelform werden hierfür nacheinander mit den drei Methoden analysiert, um die quantitativen Ergebnisse für verschiedene Aluminiumlegierungsmatrices und -zusammensetzungen direkt zu vergleichen. Unter Berücksichtigung des jeweiligen Analysevolumens jeder Methode zeigen die Ergebnisse eine hohe Vergleichbarkeit zwischen LIBS und den etablierten Methoden, unabhängig von der Probenzusammensetzung.

Diese Dissertation zeigt die Möglichkeiten und Vorteile der Anwendung von LIBS in der industriellen Partikelanalyse, wie zu Beispiel TCA, auf. Die entwickelten multivariaten

Quantifizierungsmodelle sind geeignet, um metallische Partikel detailliert zu charakterisieren und liefern vergleichbare Ergebnisse zu weit verbreiteten Techniken mit deutlich geringerer Analysezeit und Probenvorbereitungsaufwand. Durch die Entwicklung und Optimierung weiterer Quantifizierungsmodelle, zum Beispiel für Eisen- oder Kupfermatrizen, kann LIBS weitreichend als schnelle und zuverlässige Analysemethode für die Partikelcharakterisierung in industriellen Anwendungen etabliert werden; sowohl als Alternative als auch als Ergänzung zu etablierten Methoden zur Charakterisierung von metallischen Partikeln.

Abbreviations

CRM	Certified Reference Material
GF-AAS	Graphite Furnace Atomic Absorption Spectrometry
ICP-OES	Inductively-coupled Plasma Optical Emission Spectrometry
ICP-MS	Inductively-coupled Plasma Mass Spectrometry
IR	Infrared
LA-ICP-OES	Laser Ablation Inductively-coupled Plasma Optical Emission Spectrometry
LASSO	Least Absolute Shrinkage and Selection Operator
LIBS	Laser-induced Breakdown Spectrometry
LOD	Limit of Detection
LOQ	Limit of Quantification
LTE	Local Thermodynamic Equilibrium
R^2	Coefficient of Determination
RMSEC	Root Mean Square Error of Calibration
RMSECV	Root Mean Square Error of Cross Validation
MC	Mixed Crystals
MDA	Multivariate Data Analysis
Nd:YAG	Neodymium-Doped Yttrium Aluminium Garnet
NIST	National Institute of Standards and Technologies
PC	Principle Component
PCA	Principle Component Analysis
PLS	Partial Least Squares
SEM-EDX	Scanning Electron Microscopy coupled with Energy Dispersive X-ray Spectrometry
SNR	Signal-to-Noise-Ratio
TC	Technical Cleanliness
TCA	Technical Cleanliness Analysis
VDA	Ger.: Verband Deutscher Automobilhersteller
µXRF	µ-X-Ray Fluorescence Spectrometry

1. General Introduction

1.1. Necessity of Detailed Particle Characterization in the Automotive Industry

The more complex a system or product is, the more sensitive it is to contaminations. The powertrains in modern motor vehicles improve their performance and, as a result, their technological complexity. They have been evolving to be more fuel-efficient, partly or fully electrically powered while at the same time offering speed, safety, and longevity. To fulfil these requirements, the cars are built in a way that, e.g., high-performance batteries are packed compactly in the vehicle body, the engine components interact smoothly and communication between automotive software, various sensors and the mechanical machineries works without difficulties. [1-3] If the carefully balanced system is hampered by e.g. contaminations in the battery storage unit, the automotive's performance regarding distance, speed and acceleration, as well as its safety can be impaired. If such failures occur, not only the safety of the passengers might be at risk, but also costly recall campaigns can be necessary. Therefore, producers facilitate high efforts to minimize component contamination in critical areas. [4,5] At the same time, exaggerated cleanliness measures and procedures can skyrocket costs, forcing the manufacturers to balance between cleanliness and production efficiency. [3]

These issues of clean parts and related cleaning and prevention processes are summarized in the term *technical cleanliness (TC)* in the automotive industry. The *German Association of the Automotive Industry* (*VDA: ger.: Verband Deutscher Automobilhersteller*) recognized TC as a vital factor early on, developing the standardized documents VDA 19.1 [6] and VDA 19.2 [7] in 2004. They define relevant prevention and analysis measures for particulate contamination. Especially metallic particle contaminations are thoroughly discussed, as they are one of the most critical contaminations in TC in the automotive industry due to their abrasive, hard and conductive nature. To address current analytical challenges, especially regarding the technology change to electromobility, the documents are revised since 2023, however have not yet been published at the time of this dissertation. [8]

A major contributor to a product's TC contamination is the initial cleanliness state of the single components, as such particles are introduced with the component in potentially critical areas of the product. Often the particles are generated in the manufacturing processes steps, like cutting or grinding, and remain on the component due to insufficient cleaning. Another common source of TC relevant particles is the production environment, where e.g. construction or

maintenance measures lead to particle generation and, therefore, a risk of product contamination. Additionally, the production processes themselves can be a source of particulate contaminants. For example, in laser welding, where a laser is used to heat, melt, and fuse two materials, welding beads can be generated due to, among others, surface contaminations, like particles or organic films on the surface. [9,10]

In the case of welding beads, the particle source and the generation process can be identified easily due to the characteristic globular shape of the particles. However, in the other named cases of origin, the identification of the particles' source is more challenging. All metal components and tools used for producing and handling them can be possible sources of contamination, opening a large variety of metal alloys and alloy compositions, that need to be considered in origin determination. [4,11] To identify the source of such particles and efficiently start a solution process, a detailed characterization of such particles is necessary.

In VDA 19.1, *optical microscopy* and automated *scanning electron microscopy coupled with energy dispersive X-ray (SEM-EDX)* are suggested as primary analytical methods for *technical cleanliness analysis (TCA)*. They are used for the rough classification of contaminants: optical microscopy often equipped with polarized and non-polarized light is applied to distinguish between metallic and non-metallic reflective materials, while automated SEM-EDX commonly differentiates particles into material classes of, e.g., low- and high-alloyed iron, low-alloyed aluminium, aluminium-silicon-alloy, or bronze. [6]

This ambiguity in the material characterization poses a problem for the root cause analysis. For example, an unspecified aluminium-silicon alloy can be attributed to both a workpiece carrier and a component. However, with a more in-depth characterization of the material composition the differentiation of such similar alloys is possible, and the source material or process step can be pin-pointed. Therefore, other analysis methods than optical microscopy and automated SEM-EDX must be explored for application in TCA.

A possible candidate explored in this thesis is *laser-induced breakdown spectrometry (LIBS)*. This technique has high multi-element detection accuracy with minimal sample preparation effort and is short in measurement time, offering to keep up with fast-paced industrial production. [12-14] However, LIBS is still a fairly novel method, with challenges especially regarding quantitative analysis, making it necessary to develop and facilitate improved approaches e.g. in multivariate data analysis. This work will carefully assess LIBS' capabilities and limitations to add quality and value to the application of metallic particle characterization in the context of TCA by applying and optimizing multivariate data analysis models to LIBS data.

1.2. Material Characterization using Laser-Induced Breakdown Spectrometry

Using LIBS, multi-element analysis of gaseous, liquid, and solid samples can be performed. For this, a high-energy laser vaporizes a small fraction of the specimen, generating a plasma. During the decay of the plasma element characteristic radiation is emitted, which can be used to gain qualitative and quantitative information. An in-depth description of the complex processes during LIBS is provided in chapter 2.3.

The main advantages of LIBS analysis are the small necessary sample volume, the fast measurement (< 1 s), little to no extensive sample preparation and the in-situ removal of surface contaminants, such as organic films. [12-15] Additionally, the measurement atmosphere can be adjusted to fit the analytical requirements, ranging from vacuum in space exploration [16-18] over inert gas, such as argon [19,20] to measurements under ambient air. [21-23] LIBS has been used for a variety of samples and applications, e.g., polymers [24-26], glass [22,27], biomaterials [28-30], food derivatives [31-35], as well as metals and their alloys [12,36-38]. Metal analysis using LIBS includes, among others, classification for sorted recycling [38-40], characterization of artifacts in archelogy [41,42] and process control in, e.g., metal production and recycling. [43-46] In the context of TCA, LIBS has not been scientifically discussed in detail yet. However, it offers great advantages in this field of study, as the method promises the opportunity to rapidly characterize particle samples with little to no mandatory sample preparation, as has been shown by D. Huber. [47]

In the referenced dissertation, LIBS is used to classify engine components, enabling the development of engine component databases to identify particle sources. [47] Following up on this, the presented thesis applies LIBS to particle characterization by specifically developing quantitative models for metal alloy matrices and the analysis of the respective particle material. As the identification by qualitative means classifies according to differences in spectral features and does not primary include *certified reference materials (CRMs),* it is limited by the qualitative differentiability of the samples. Alloys that are highly similar in their composition and e.g., only differ in the concentration of single alloy elements, often cannot be discriminated by classification models. Applying quantification, improves the differentiability of such materials, in turn, also improving the chance of identifying the contamination source and, therefore, pin-pointing the generation process.

However, quantitative LIBS is still considered challenging in the scientific community. This is especially the case for the sample class of metal alloy particles relevant in TCA, as will be described in the following chapter.

1.3. Challenges in Quantitative LIBS-Analysis of Metal Alloy Particles

In quantitative LIBS analysis of metal alloy particles relevant for TCA both the sample size, the local sample composition (matrix), and the properties of the method itself pose challenges. Therefore, the present effects must be carefully considered to generate meaningful and accurate results.

The first challenge in quantitative analysis of metal alloy particles is inhomogeneity, which is present in all metal alloys. As an example, a microstructure image of an aluminium-silicon alloy is shown in figure 1. Here, different crystal phases in shades of white and grey can be observed. They refer to α-aluminium and Al-Si phases, which differ most dominantly in their silicon content. While 11.7 $\%_{wt}$ of silicon is present in Al-Si phases, almost no silicon is solved in the white aluminium phases. [48, 49] This results in locally different matrix compositions at different analysis spots.

Additionally to the overall sample inhomogeneity in metal alloys, the microstructure is highly dependent on various crystallization parameters, like the temperature gradient and the geometry of the resulting component. In figures 1 (a) and (b) this variability in microstructure evolution in different samples is showcased, with (a) displaying white α-aluminium phases with a size of roughly 250 µm, while phases in (b) are significantly smaller with roughly 100 µm. The process of microstructure evolution is a complex topic and, therefore, will be described in detail separately in chapter 2.2. These differently sized and distributed phases of course impact the representativeness of a measurement for the whole bulk composition.

The challenge of representativeness is reinforced by a central property and actually advantage of LIBS: the small analysis volume. Considering the phases' sizes of up to 250 µm in figure 1 and a LIBS laser diameter of only 20 µm used in this study, the impact on the quantitative result of a single measurement is obvious. This can hamper the representativeness of a single LIBS measurement for the whole bulk material and, therefore, the identification of a TC particle source. [12,50]

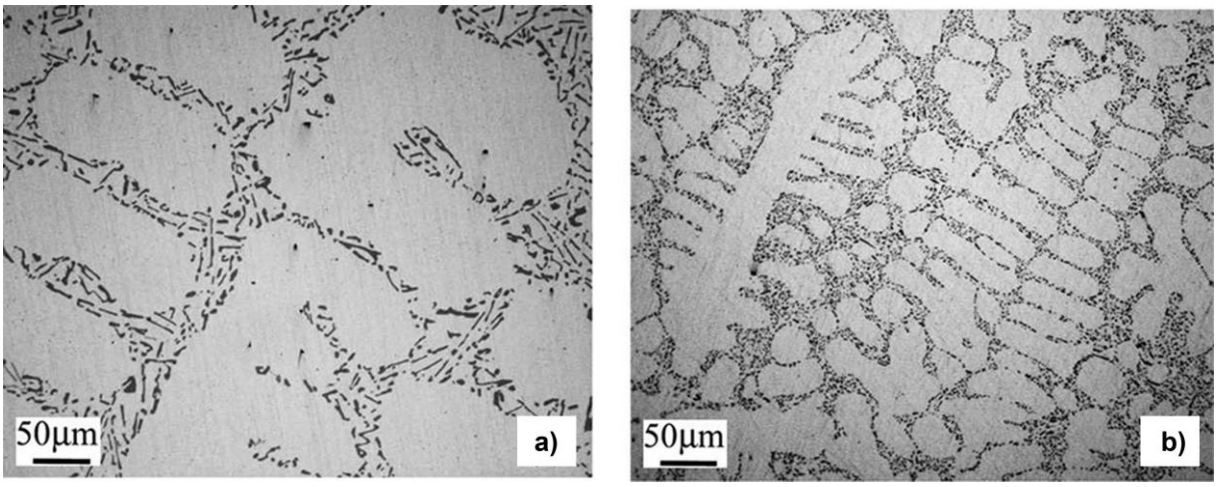

Figure 1: Microscopic images of aluminium-silicon structures (cast alloy), with differently sized dendritic phases (a), (b). In the light phases α-aluminium crystals and in the dark spotted phases eutectic Al-Si systems can be seen. The grey spots and needles correspond to silicon crystals. Taken from [49].

Additionally, (locally) varying composition also impact the LIBS excitation process. The changing sample compositions lead to locally different physical properties, like heat capacity or melting temperature influencing the laser-sample interaction and, e.g. the transfer of analytes to the plasma state. [51] Such so-called *matrix effects* obscure the correlation of analyte concentration in the sample and resulting optical emission signals, making quantification and calibration by LIBS more challenging. [12] Dissolving the sample and diluting the matrix to reduce these effects, as is done in inductively-coupled plasma optical emission spectrometry (ICP-OES) or mass spectrometry (ICP-MS) analysis [52], is, however, not possible and, in case of TCA, not desired, since a rapid and easy measurement is aimed for.

Another challenge for developing calibration models are disturbances in the OES spectra. The main spectral challenge in LIBS analysis is *self-absorption*. During self-absorption, photons emitted during relaxation are re-absorbed in the plasma, resulting in signal broadening and possibly intensity decrease. [53,12] As some wavelengths of the same analyte are more prone to be affected by self-absorption than others, undisturbed signals need to be identified and selected for accurate analysis. For more information on physical processes in LIBS, including self-absorption the reader is referred to chapter 2.3.

Up to this point, only bulk (> 30 mm) [54,55], scrap (~1 mm to over 30 mm) [21,39] and nano- [56,57] sized metallic samples have been studied in the context of quantitative LIBS. However, the sizes relevant for TCA (~45 µm to over 1 mm) bring their own associated challenges, which are not completely transferrable to the sample sizes analysed so far.

While scrap or bulk samples have a volume large enough to spread multiple LIBS measurement locations over the sample surface, thereby reducing the effect of local inhomogeneities, TCA particles are smaller in their volume. Therefore, only one or a few measurements can be performed on each sample. As every isolated TCA particle can possibly be from a separate source material, all particles must be considered individually.

At the same time, the sample volumes are large enough to display inhomogeneities of their own, possibly not being representative for the origin material composition. Especially, since the particles are mostly generated from a specific location of the bulk, like edges and/or the surface. Such areas generally are strongly impacted by inhomogeneities (like segregation), possibly leading to decreased representativeness of the generated particles for the original bulk. Further, metallic particles in TCA mostly have been subjected to high forces, pressures, and temperatures in the engine before they are isolated and analysed. Such energy intake can damage the microstructure of the particles, impacting their element composition. Therefore, their representativeness for the bulk material can be impaired.

Due to these challenges, the quantitative analysis of TCA relevant metal alloy particles using LIBS is considered challenging. However, with the right tools, these challenges can be tackled, and quantitative LIBS can be optimized and applied to TCA.

1.4. Approaches to Enable Quantitative LIBS Analysis

Quantitative LIBS offers the chance in TCA for rapid and accurate particle characterization to identify contamination sources and efficiently target TC problems. However, due to the challenges described in chapter 1.3, quantitative LIBS is still in need of research and development, especially its application in metallic particle characterization.

TC relevant samples have an inhomogeneous matrix, impacting the representativeness of a single measurement for the whole material. Spreading multiple measurement points over the sample and including a more significant volume can help to decrease these inhomogeneity effects. Therefore, as much measurement locations and sample volume as possible should be included into the analysis.

To overcome the matrix effects due to varying sample compositions, a known calibration approach is to *matrix match* the reference materials to the unknown sample's composition. This way the matrix effects are already displayed in the calibration and the sample composition can be calculated more accurately. This approach can also be used in LIBS analysis. However,

when characterizing inhomogeneous material classes with a broad range of analytes and compositions, like metal alloys, it is not possible to depict every possible sample's matrix individually.

Therefore, advanced evaluation and data treatment algorithms need to be employed. In literature, often multivariate data evaluation techniques, like *principal component analysis* (PCA) [47,58-60] and *partial least squares* (PLS) *regression* [54,59-62] are used in LIBS. Such multivariate analysis methods allow the implementation of multiple variables in the evaluation and can reduce matrix effects by identifying correlations between the variables. [63] This way, the effect of varying and unknown on the quantification result can be minimized, even for complex matrixes not included in the calibration model. A detailed description of multivariate methods is provided in chapter 2.4.

Combining, adjusting and developing the named approaches to tackle the challenges of quantitative LIBS, the technique might be a valuable addition to industrial applications, like TCA. One step, to enable the use of LIBS in this context is offered in this dissertation.

1.5. Objectives

In this thesis, the applicability of LIBS for quantitative characterization of metal alloys in particle form, especially for the use in technical cleanliness analysis (TCA) in the automotive industry, is studied. For this purpose, multivariate quantification models (PLS-regression) for LIBS analysis specifically optimized for the characterization of metallic particle samples commonly found in automotive production environments are developed and validated. The studied material class is aluminium alloys, as they show a broad range of alloying composition and are commonly used in the automotive industry. [48] The sample sizes in this dissertation are roughly between 45 µm to over 1 mm, which is the mainly relevant sample size in TCA.

Considering the challenges and solution approaches described in the previous chapters, the first objective is to develop and validate PLS-regression quantification models for aluminium alloys for the characterization of samples relevant in TCA (see chapter 3.1). The measurement and evaluation parameters of the developed quantification models are optimized for the analysis of TC metal alloy particles. After validation using bulk CRMs, the calibrations are applied to characterize in-house generated, reference aluminium-alloy particles in different size classes (45 – 100 µm, 100 – 250 µm, 250 – 500 µm, 500 – 1000 µm, > 1000 µm) and the results compared to their respective bulk material. The particles used for validation cover a broad range of analyte concentration specifically adjusted to common aluminium alloys in industrial use. The procedure of reference particle generation is easily transferred to other materials and enables the in-house generation of TCA relevant references categorised in both element composition and size class.

The second objective (see chapter 3.2) is, to conduct a comparative study of the developed models and established analysis models to validate the use of the developed models against already established metallic particle characterization methods. This way, the use of the novel models for industrially applied analysis is enabled. The most common analysis methods for metal particle characterization are SEM-EDX and µXRF. In routine TCA, the quantitative evaluation is performed automatically by pre-developed algorithms, minimizing the necessary work effort to mere recalibration. To use the developed LIBS evaluation models in regular industrial analysis, their comparability to these already established methods is essential. Therefore, the described comparative study evaluates the methods performance regarding the determined alloy composition of four CRMs in particulate form. To enable comparison between the analysis techniques, first a theoretically minimal volume is determined based on microstructure analysis. Comparing the theoretical value to the approximated analysis volume

of each technique enables comparison between the methods, presenting LIBS as a reliable and fast alternative to established X-ray-based methods.

By studying the metal alloy particles using LIBS in the context of analytical chemistry, an alternative approach to alloy characterization is developed. Even though it is based on questions regarding TCA, the here described findings and analytical evaluation models can be transferred to other applications.

2. Theoretical Background and Methodology

In the following chapter, the theoretical background and the methodology of this project is described. First, the context of *technical cleanliness* (TC) is presented, including its necessity in industrial production, the sampling, and the following analysis. Next, metal alloys and their composition are discussed to showcase the complexity of their characterization, especially regarding inhomogeneity and microstructure evolution. The chapter's third part describes *laser-induced breakdown spectrometry* (LIBS), the central analysis method in this thesis, regarding excitation, plasma generation as well as experimental considerations. Lastly, LIBS evaluation and quantification methods are showcased, with partial least squares regression described in most detail. Here, also the importance and effects of data treatment on the multivariate analysis method are shown.

2.1. Technical Cleanliness

In the construction of complex products, the production processes need to be defined and acted out thoroughly to ensure high quality and safety. This includes the absence of impurities like dust, dirt, oil, or other foreign substances on critical surfaces. Contaminations can damage the components, causing costly failures and image loss, especially for luxury products like (premium) cars. The automotive industry has therefore defined TC standard documents VDA 19.1 (Quality Management in the Automotive Industry – Inspection of Technical Cleanliness) [6] and VDA 19.2 (Quality Management in the Automotive Industry – Cleanliness in Assembly). [7]

The documents provide regulations for avoiding contamination in general and *TC analysis (TCA).* The latter includes both the process of component sampling to test their cleanliness and the proceeding analysis to characterize the contaminations in detail. [6,7] The international equivalent to the VDA 19 documents is ISO 16232 [64], but the VDA 19 documents will be used as main references here.

While, in general, liquid contaminations disturb processes like chemical resistance and adhesiveness, solid particles can cause damage to the components due to their volume, abrasiveness, hardness, and electrical conductivity. [65-67] Solid contaminations in TCA are generally distinguished in non-metallic (e.g. polymers, minerals) and metallic particles.

Polymers are vastly used in today's industry e.g., as adhesives or for packaging in logistics. They generally are non-conductive, non-abrasive, and soft, but can block inlets, filters, or valves. Polymer particle contaminations are mainly generated by ripping or wear of logistical packaging. Especially the repeated use of transport boxes or similar wrapping to improve sustainability can augment this contamination mechanism. Therefore, the multi-use packaging needs to be cleaned thoroughly between cycles. [6]

Minerals are used in various processes as blasting agents to pre-treat surfaces or to abrasively remove rust or old varnish. As their application states, they are highly abrasive and hard, damaging components by increased wear or rapid corrosion occurrence. [4,11]

Metals are the most common materials in the automotive industry both in the products and tools used. They combine all previously mentioned critical properties – hardness and abrasiveness – with being electrically conductive. Especially for electrical components, like sensors and battery components, metallic particles, therefore, pose the risk of short circuits and performance loss. [3] Therefore, avoiding metallic particle contamination is a critical factor in the automotive industry. [4,11]

Avoiding all particle contaminations in the production and on the components is costly, as the installation of multiple cleaning steps and an immaculate production environment would be necessary. To reduce production costs, the limits of still possible TC levels are carefully assessed and adjusted according to the principle "as clean as necessary, as dirty as possible". [3,65] On one side, this saves costs as not all elements need to be handled with special care to be cleaned and kept clean but used in a lower state of cleanliness. On the other hand, this implies that the necessary cleanliness status of each component needs to be defined individually and kept consistent throughout the production line. This consistency is crucial, as all the effort (and costs) invested in keeping one component clean can be for nothing if it is contaminated due to contact with a dirtier piece, either directly or a transport medium like flowing air, cooling fluid, or oil. [4]

To define the necessary cleanliness, the critical processes in the product and its production need to be known in detail. Using methodologies like theoretical simulation and calculations the limits can be assessed using only drawings and models of the system. Additionally real-life experiments can be performed, by introducing particles with defined characteristics (number, material, morphology, etc) in critical areas. This option is the most expensive, as the product will not be usable afterwards, however is a methodically easy way to qualitatively assess the stability of the system. [6]

During production regular TC sampling and analysis of components as well as the production environment provides essential information for process analysis and enables tracking effects of material or production changes in the production of individual parts and the final product. [4,6]

Multiple contamination characteristics must be considered to ensure and assess present TC standards in the production, including **particle number** and **size**, **type of particle** (non-metallic, metallic), and **chemical composition**. The characterization of the contaminants enables both quality assurance and source identification as (i) the criticality of contaminations can be assessed and (ii) a targeted problem management process is facilitated. Therefore, the detailed analysis of contamination materials is an essential goal in TCA, in addition to regular cleanliness assessments. Both will be discussed in the following chapter.

2.1.1. Technical Cleanliness Inspection and Analysis

Detection, collection, and characterization of (particle) contamination on critical components are crucial in identifying the source and tackling quality issues efficiently. The following chapter describes the analytical practice – from sampling procedures, including transporting the sampled components to the laboratory, to isolating contaminations and their characterization.

In TCA, sample collection can be divided into two procedures with different analytical questions: [6]

- Sampling of the environment to study a process or the cleanliness of the environment. As particle contaminations can be transferred from the environment to the components, this procedure can indirectly provide information on the cleanliness status of the process as well as the used parts.
- Sampling of a component to directly study its cleanliness and detect contaminations from production, handling, or logistics.

Figure 2: An example for a particle stamp used for sampling of surfaces for TCA from CleanControlling. [68]

The cleanliness of the production environment is mainly studied using particle traps or stamps, which are placed close to the location to be examined or used to directly sample areas or component exteriors. The sticky surface fixates the particle contaminations, enabling fast and easy snapshots of the sample surface or the environmental cleanliness. For transport, the stamps or traps are closed with a lid to avoid cross-contamination. A particle stamp is shown in figure 2.

As the stamps cannot be used for complex geometries, small openings, or large areas, sampling whole components is mainly done using an extraction medium.

The component itself mainly determines the extraction medium used to sample components. The used medium must not damage the sampled piece and must be able to extract the particles efficiently. The most common extraction media are organic solvents and pressured air in the sense of suction or blowing extraction. The organic solvent can extract particles from components, even when they are sticking to, e.g., an oil film, and is non-corrosive for metallic materials. Additionally, it can be easily removed from the sample afterward by drying, improving handling speed. Vacuuming the component is mainly used for parts sensitive to solvents, e.g., electric sensors or platins. Figure 3 shows (a) particle suction extraction system and (b) solvent extraction cabinet.

Figure 3: Particle extraction systems. a) Particle suction extraction system C|PS² by CleanControlling Technical, Dresden, Germany [69]. b) Cleanliness cabinet by PALL, New York USA. [Image by M. K. Lanzinger]

Extraction parameters like time, volume flow, and area to be sampled are defined for each component individually. This way, comparability between different component samples and laboratories is ensured. [6] Independent of the extraction method, the particle contaminations are generally collected on a filter. The filter's mesh size can be adjusted according to the components' cleanliness specification. Typically mesh sizes between 5 – 200 µm are used. In case of high contamination, filter cascades are applied to reduce the number of particles on the individual filters. In figure 4, a microscopic image of a filter used in TCA with multiple particles as well as a detail image of a metallic contaminate is shown.

Residues of extraction fluid can hamper the following analysis. Therefore, the filters are dried in a drying cabinet, if applicable. After the samples are prepared on the filters, the analysis can be conducted, characterizing the contaminants' number, size, and material, depending on the analytical question.

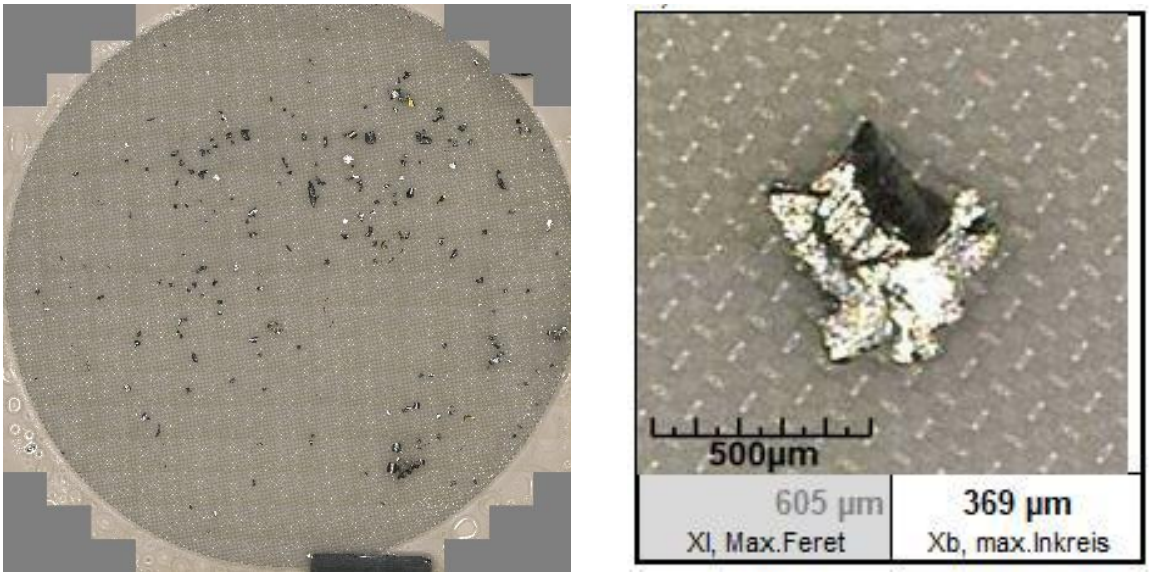

Figure 4: TCA analysis. Left: overview image from a self-prepared TCA filter. Right: metallic particle from experimental testing. [Images by M. K. Lanzinger]

2.1.2. Particle Characterization in Technical Cleanliness Analysis

In VDA 19.1 [6], two procedures of TCA are described. The *standard analysis* is used for, as the name states, standard procedures, while the *advanced analysis* investigates the particle characteristics in more detail. Easy and fast methods namely gravimetry and optical microscopy are applied during the standard analysis. These procedures are performed independently of the visible particle load on the sample or filter. Analogue to the sampling procedures, parameters applied in standard analysis are defined for each method and sometimes component, to ensure comparability between individual components and different laboratories.

In gravimetry, the mass of the filter is compared before and after sampling, providing a quick and easy way to assess the combined mass of all contaminations. However, this analysis method does not provide information on particles' size, number, or material type. These parameters can be determined by optical microscopy. Using optical microscopy, the particles are assigned to one of three categories: metallic reflective, non-metallic reflective, and fibres. The classification is done according to the particles' reflectivity towards polarized light as well as its shape. While metallic materials reflect polarized light like a mirror without changing the polarization, non-metallic samples, including fibres, randomly change the polarization to basically non-polarized. A second polarizer, perpendicular to the incident light's polarization,

filters the still polarized light reflected from the metallic particles. As only the depolarized radiation passes this second polarizer, metallic and non-metallic reflecting particles can be differentiated. Figure 5 shows a scheme of this process. If the particle is long and thin – exact specifications of the length to width ratio may vary between companies – the particle is assigned to the fibre class.

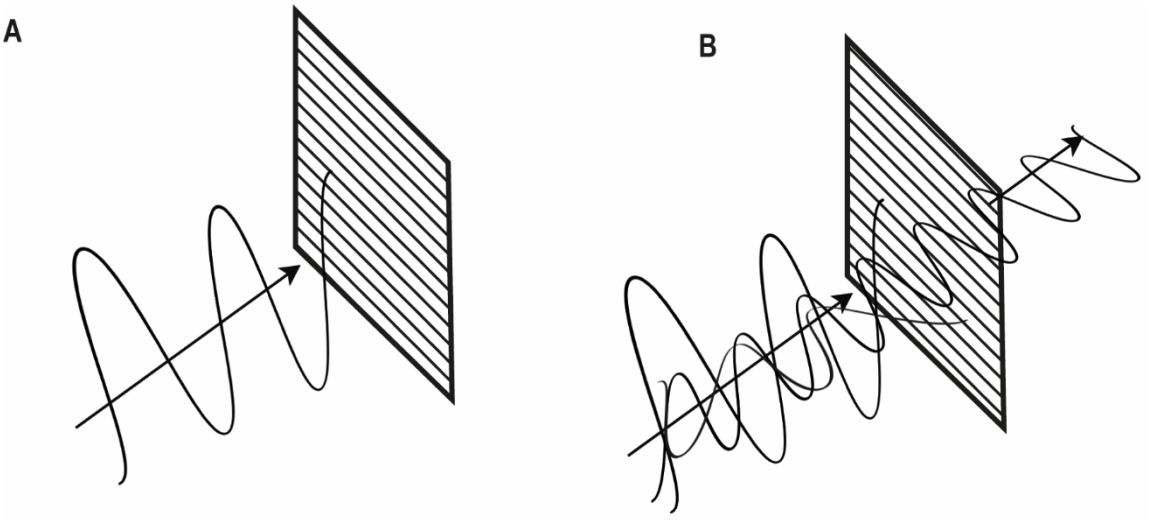

Figure 5: Scheme of differentiation between metallic reflective and non-metallic reflecting materials using polarized light. (A): Light polarized perpendicular to the polarizer cannot pass the barrier. (B) Non-polarized light passes through any polarizer. Adapted from [70]

The standard analysis in TCA uses fast, easy, and partly automated analysis methods to determine the cleanliness status of the sample by determining the weight of the particle load and the number, size class, and material category of the contamination. Generally, this information is enough to determine whether a process fulfils the cleanliness requirements or not. If additional information is necessary e.g., because the cleanliness criteria are not fulfilled and measures need to be taken, the advanced analysis is applied e.g., to identify the contamination source(s).

Advanced TCA includes methods determining particle characteristics like 3D-morphology, material class or composition. VDA 19.1 [6] proposes the use of *scanning electron microscopy coupled with energy dispersive X-ray* (SEM-EDX), Raman and infrared (IR) spectroscopy, or LIBS. Of the named methods, Raman and IR are mostly used to study non-metallic particles like polymers or minerals. They are non-destructive analysis methods identifying the material by the characteristic interaction of electromagnetic radiation with the rotational and vibrational modes in the sample molecules. Consequently, materials are characterized on their molecular level. [71]

LIBS and SEM-EDX, on the other hand, characterize materials on an elemental level. They are mainly used to analyse metallic materials in TCA to determine their corresponding alloy composition. SEM-EDX is a non-destructive method using a high-energy electron beam to remove electrons close to the nucleus. By re-filling the electron holes close to the nucleus, element characteristic X-ray radiation is emitted, enabling qualitative and quantitative evaluations of analyte elements. Additionally, the SEM-part of the SEM-EDX method, can be used to study the morphology and topology of the particle's surface. [72]

In TCA, the characterization of particles using SEM-EDX is an automated process. The particles are identified and localized using the material contrast of the organic filter and metallic particles in SEM and subsequently analysed via EDX. The measurement time in this automated process is limited to a few seconds per particle; otherwise, the measurement time of more than 50 particles on a TCA filter would be too long to be cost-effective. However, in such a short time, of course a detailed quantitative analysis is not possible. To decrease the total time necessary for the automated SEM-EDX analysis of a whole TCA filter by implementing location transfer between microscope and SEM-EDX, developed and described in detail by D. Huber. [47] The short measurement time, combined with the automated set-up, maximizes the analysis speed while reducing the sensitivity and accuracy of the results. Therefore, in the standard TC laboratory set-up, SEM-EDX provides only material classes, e.g., aluminium-alloy, aluminium-silicon-alloy, high- and low-alloyed steel, or bronze as a result instead of quantitative sample compositions and analyte concentrations.

To differentiate in more detail between metallic materials, LIBS can be applied. In LIBS, a small sample volume is evaporated using a high-energy laser, forming a plasma. By recombination of electrons and positively charged atom bodies in the plasma element characteristic radiation is emitted, which can be used for qualitative and quantitative analysis of the sample. The detailed physical processes of LIBS are discussed in chapter 2.3. In TCA, the information from LIBS is used for particle source identification. By characterizing the composition of the metallic contaminates in detail, their origin alloy can be determined. With the source alloy known, components of the respective composition in the process can be identified, enabling a targeted solution process.

On the one hand, TCA's goal is to supervise cleanliness standards of e.g., the production environment and the used components. On the other hand, found contaminations are to be analysed to (i) determine their criticality to the product and (ii) identify their source. Identification of this origin material requires detailed knowledge about the particle composition and source. Metal alloys pose a specifically challenging sample class in this context due to their high

variability in composition and inhomogeneous nature. Therefore, matrix composition and metal alloy microstructure will be the topic of the following chapter.

2.2. Metal and Metal Alloy Science

Throughout history, metal alloys have significantly shaped the world as we know it today. Even though there is more to the concept of societal progression than the craft of producing and working with metals and alloys, the distinction between e.g., stone- (pre-metal), bronze- and iron-age is still used to differentiate between historical periods using predominantly the named material for weapons and tools. [73] In today's industrialized production, metals and alloys are highly optimized to fit their use, whether it be high corrosion resistance, hardness, or deformability. [74,75] Due to their extraordinary versatility, engineerability, and adaptability they are indispensable in numerous industries and applications.

One branch of industry that relies heavily on metal alloys is the automotive industry, as it is faced with constant pressure for technological advancements, including engineering, safety, and design developments. [4] With their exceptional and tuneable properties, metal alloys are crucial in meeting these demanding requirements. From lightweight and high-strength alloys for structural components to corrosion-resistant and durable alloys for stressed parts, alloys enhance vehicle performance, efficiency, and safety. As these materials are omnipresent in production, they can originate TCA-relevant contaminations during, among others, mechanical processes like cutting, welding, or drilling. [6] To understand the challenges in identifying these particles accurately and efficiently, in turn, identifying the origin materials and their composition is essential.

Therefore, the following chapters explain metallic structures and the effect of alloying in basic concepts. Further, the crystallization process in metal alloys and the resulting microstructure are discussed, including considerations on inhomogeneity. To illustrate the variety of metal alloys, two different ones are showcased in the following chapters: aluminium and iron based alloys.

2.2.1. General Properties of Metal Alloys

Metallic materials are composed of positive metal ions in a *crystal lattice* surrounded by *electron gas*. These delocalized electrons, which are highly mobile in between the metal

cations, lead to the characteristic metallic properties, like high thermal and electrical conductivity. Additionally, the electron gas is vital for their high plastic deformability. In contrast to ionic bonds, like salts, a deformation of the metal crystal lattice does not lead to a line-up of two particles of the same charge, resulting in a repulsion and thus break. Instead, the delocalized electrons buffer the strain, enabling material deformation without breaking. [76-78]

The crystal lattice results from the atoms organizing in optimal distance, according to their attractive and repulsive interactions. Typical metallic unit cells are *face-centred cubic* (*fcc,* e.g., aluminium [79]), *body-centred cubic* (*bcc,* e.g., iron [78]) and *close-packed hexagonal* (*cph,* e.g., magnesium [78]) (see figure 6).

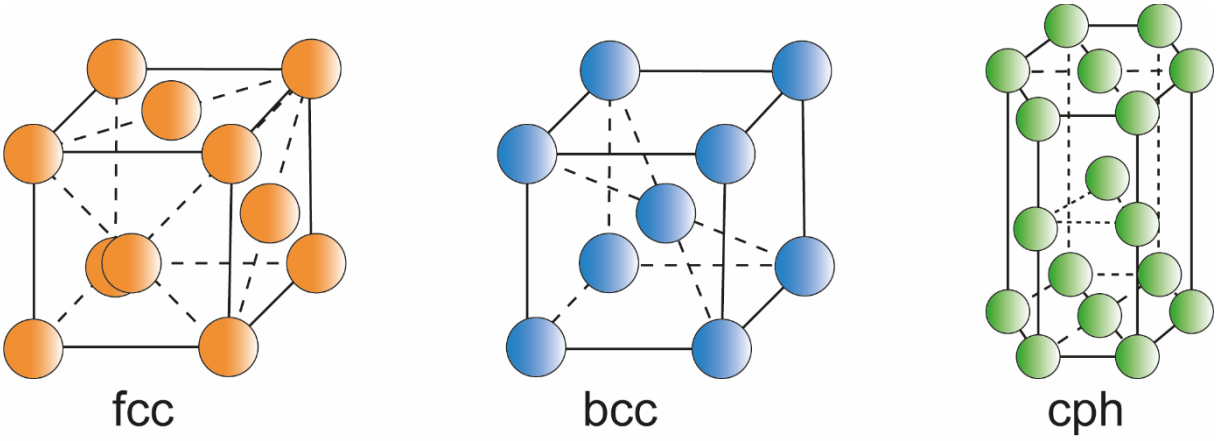

Figure 6: Most common crystal lattice structures in metallic materials: face centred cubic (fcc, e.g., in aluminium), body centred cubic (bcc, e.g., in iron), and close packed hexagonal (cph, e.g., in magnesium). Scheme adjusted from [78].

The lattice of the pure metal differs from its alloys, as alien elements are integrated into the structure by occupying an *interstitial site* between the lattice atoms or by *substituting* a lattice atom. Already at concentrations of 0.001 $\%_{wt}$ of alien atoms, the system is referred to as *mixed crystal (MC)*. This defect in the ideal lattice leads to increased tension in the structure, which favour material characteristics like hardness. Depending on the concentration of matrix and alloy element, metal alloy properties can be precisely engineered to specifically fit the desired properties. [77]

The respective change in material properties can be understood by correlation of phase diagram and microstructure analysis. This will be the topic of the next chapter.

2.2.2. Evolution of Microstructure

Alloys are produced from the melt of the main (matrix) element and one or multiple alloying elements in a defined mixing ratio. The elements' melts can be completely, partially, or not soluble in each other. An example of *complete solubility* is the Cu-Sn system, which forms a single (melt) phase at any ratio. *Partially soluble* systems, like Cu-Pb, show this behaviour only for distinct compositions. If these conditions are not met, the melts behave like *insoluble systems* (e.g. Fe-Pb), and complete separation in two phases occurs. Such insoluble phases can be mixed macroscopically only by stirring or shaking the emulsion. [74]

As the melts cool, they become solids, forming *phases of crystals* or *solid solutions* of the constituent elements. These phases are homogeneous in composition but can be distinguished from each other using crystallographic means.

Technically used metals and alloys generally crystallize *poly-crystalline*, meaning they are composed of multiple *crystals* or *crystal phases* forming independently in the melt. Multiple crystals or crystal phases make up a so-called *grain*, whose combined structure is called *microstructure.* The microstructure can be imaged through metallographic grinding, polishing, and, if necessary, etching. Subsequently, optical or secondary-electron microscopy can be used to visualize and characterize the microstructure, including information on the crystallization process and the alloy composition. [73,79-82]

The speed of crystal growth is *anisotropic*, meaning it depends on the crystals' orientation and varies for different paths. As some directions grow faster than others, needle and plate-like structures are formed in the microstructure. They are also called *dendrites* due to their tree-like morphology. [73,78]

In a melt, not one but multiple nucleation processes take place, making multiple *grains* (combinations of crystal phases) grow simultaneously. Generally, materials with smaller grains have more favourable strength and surface properties during later forming processes. For example, materials with a coarse microstructure tend to scar during shaping, while finely structured ones display smoother surfaces. [73,78] To decrease the grain size in the final product the *primary microstructure* is, therefore, often subjected to recrystallization and welding, leading to a finely structured *secondary microstructure*.

The solidification behaviour and microstructure evolution of melts to form a metal alloy can be understood in phase diagrams. The phase diagram of a two-component system depicts its specific solubilities and crystal phases for the respective compositions and temperatures. As

an example, the Fe-C phase diagram (figure 7) is described. The gathered knowledge will then be transferred to the Al-Si system (figure 8).

Generally, iron-alloys are distinguished in steel and cast iron, with carbon concentrations below and above 2.06 $\%_{wt}$, respectively. Iron-based alloys above 6.67 $\%_{wt}$ of carbon are technically not applied due to their composition being mostly *cementite* (Fe_3C), which is a Fe-C-phase with hard and brittle attributes. The presence of cementite, therefore, results in non-favourable properties regarding its machinability, making it hardly applicable in the production of components or mechanical tools. [74]

In the phase diagram (figure 7), *L* denotes the liquid melt, and the line separating this melt from the (partly) solid phases is called the *liquidus line*. Any temperature above this line indicates that all components are liquid. Below the liquidus line, solid solutions/MCs, surrounded by residue melt, start forming until the *solidus line* is attained. Here, the liquid has entirely solidified. The system includes two *eutectic points*: 0.83 $\%_{wt}$ of carbon for steel (E_1) and 4.3 $\%_{wt}$ of carbon for cast iron (E_2). Whenever the system passes through either of these two points during the cooling process, the remaining melt cools into very finely-grained crystals, called *eutectic phases*. Eutectic phases are the thermodynamic equilibrium of mixtures of substances. They are homogeneous and solidify and melt at a single temperature, which is lower than the melting point of both single constituents. Melts with concentrations below the eutectic are called *hypoeutectic*, above, *hypereutectic*. [74,78]

In the area between the liquidus and solidus curves, where MC and the liquid melt coexist, it is possible to determine the carbon concentration in each. For this purpose, the initial concentration is taken, and a line is drawn perpendicular at the current temperature. The intersection with the solidus curve provides the current carbon concentration in the MCs. Its intersection point with the liquidus line offers the concentration of carbon in the remaining melt.

Depending on the temperature and carbon concentration, different MCs form. These are:

- *α*-MCs / *α*-ferrite
- *γ*-MCs / austenite
- *δ*-MCs / *δ*-ferrite
- Fe_3C / cementite

Additionally, perlite and ledeburite can occur. However, these are in fact not MCs but eutectic phases of cementite with *α*-ferrite in steel (perlite) and cementite with austenite in cast iron (ledeburite), respectively. [78]

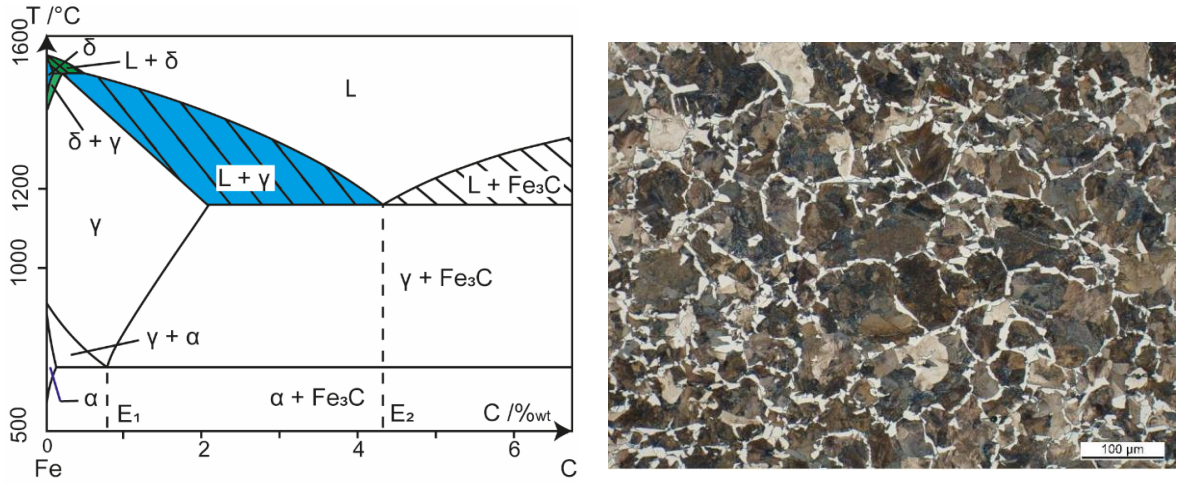

Figure 7: Left: Phase diagrams of Fe-C adapted from [78]. Right: Microstructure of Fe-alloy C38 (0.3-0.4 $\%_{wt}$ of carbon [83]), etched (3 % alc. HNO_3). [Image by M .K. Lanzinger]

An exemplary cool down shall be explained to help understand the solidification and conversion processes. Assuming an initial eutectic steel composition of the melt (E_1, c_C = 0.83 $\%_{wt}$), first austenite crystallizes in the melt after the temperature falls below the liquidus line. Once the solidus line is reached, the entire melt has solidified as austenite. Until reaching the eutectic temperature of 723 °C, no structural conversion occurs. However, below this temperature, the austenite recrystallizes to *α*-ferrite and cementite, forming eutectic perlite. This phase is the most stable thermodynamically and does not transition further with decreasing temperature.

For hypoeutectic carbon concentrations, transitions of *δ*-ferrite to austenite, followed by austenite to *α*-ferrite, occur. The latter two MC can now also form perlite phases. However, perlite will still be accompanied by α-ferrite in the microstructure, as the carbon content does not suffice for a complete eutectic phase. In figure 7, right, this is clearly visible as the brown-shaded perlite phases are surrounded by white ferrite phases. The different shading of the brown perlite phases does not correspond to a composition difference but to a different orientation of the crystals to the incident light.

The Al-Si phase diagram (figure 8, left) is less complex than the Fe-C system. Here basically only two crystal phases are formed:

- *α*-MCs of silicon solved in aluminium.
- *β*-MCs of aluminium solved in silicon.

If the melt solidifies at a concentration of 11.7 $\%_{wt}$ of silicon, the eutectic point is crossed, and the fine-grained eutectic of *α*- and *β*-phases is formed in a very regular distribution. If the composition of the melt is hypoeutectic (c_{Si} < 11.7 $\%_{wt}$) and the temperature drops below the liquidus curve, *α*-crystals start forming in the melt. As the solubility of silicon in these α-phases is very little, the melt becomes enriched with the alloy element. Moving along the liquidus curve, the silicon concentration increases, possibly until the eutectic point is reached. In this eutectic composition, the melt solidifies completely, crossing the solidus curve. [74,84]

In the displayed microstructure (figure 8, right), finely-grained eutectic phases (arrow 1) are visible in the grey-lined areas surrounded by white *α*-aluminium matrix (arrow 2). The dark grey areas are primarily silicon crystals (arrow 3), while the small black dots (arrow 4) are inclusions of copper- and FeMn/FeMg MCs.

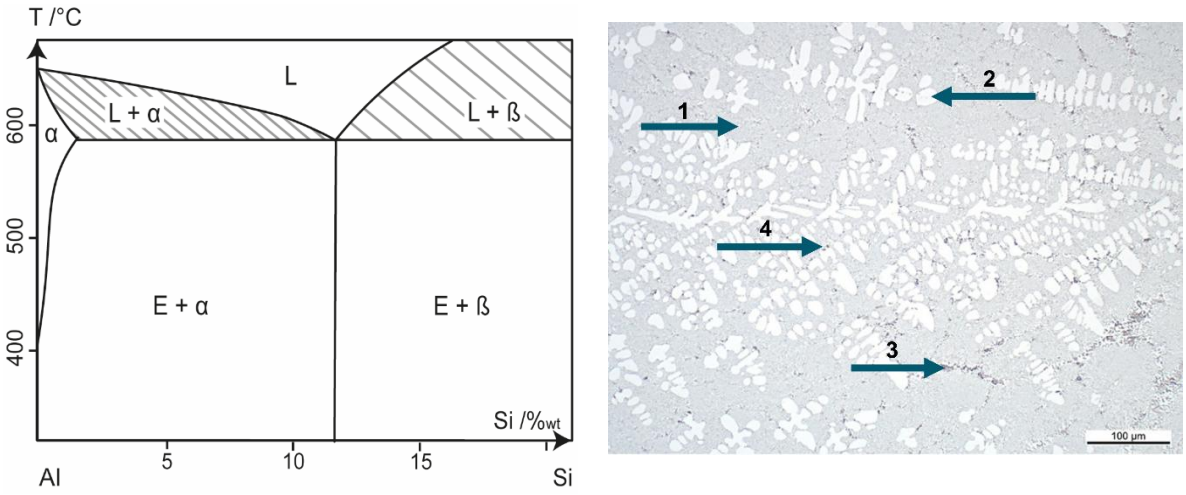

Figure 8: Left: Phase diagram of Al-Si adapted from [78]. Right: Microstructure image of Al-Si-alloy AlSi17Cu4Mg. 1: Al-Si-eutectic phase, 2: α-aluminium phase, 3: primary silicon crystals, 4: Cu- and FeMn/FeMg-inclusions. [Image by M. K. Lanzinger]

As shown in the microstructures in figures 7 and 8, inhomogeneities are present in all metal alloys. [81,85] Such inhomogeneous distributions of alloy elements are called *segregations*. *Micro-segregations* describe concentration differences in crystal phases or grain boundaries. Their formation can be mainly attributed to differences in solubility in the solid phase. If alloy components are not or hardly soluble in the solid phase, they stay in the melt as long as possible, crystallizing on the borders of crystal phases. Micro-diffusion can be induced by heat treatment, reducing such micro-segregations. However, on a macro scale the segregations cannot be decreased as easily, as the distance between the areas of different concentrations is too large to be overcome by diffusion. *Macro-segregations* are, for example, gravity and

ingot segregations. While ingot segregation is the macro analogue to micro-segregation, gravity segregation is due to density differences of alloy components. [74,78]

In addition to physical limitations regarding homogeneity, industrially applied alloys are sometimes treated multiple times to adjust the microstructure according to the respective application. For example, Fe-C alloys are often hardened by heating the component in a carbon-rich environment. The carbon diffuses into the surface, fortifying the affected area. This treatment actively changes the element composition in the surface volume of the component, increasing the already present inhomogeneity on a macro scale.

Especially for small sample volumes e.g., particles, such segregations and inhomogeneities can be challenging. Additionally, as particles generally are generated from edges and surfaces, which are more susceptible to inhomogeneities, their representativeness for the composition of the whole bulk material can be impaired. As in this thesis, the mainly used method, LIBS, only examines a small volume, these considerations will be necessary for further discussion and should be kept in mind.

2.3. Laser-Induced Breakdown Spectrometry

Exposing atoms or molecules to sufficiently high energy predominantly excites their valence electrons to a higher energy level or altogether removes them. As a result, a medium of free charge carriers with a high degree of ionization, a *plasma*, is formed. Naturally generated plasmas are observable in lightning or solar winds. In chemical analysis, plasmas are formed selectively to determine the elemental composition of solid, liquid, or gaseous samples. [12,13] For this purpose, the magnetic, electronic and spectroscopic properties of the ions can be exploited, e.g., in *inductively coupled plasma mass spectrometry* (ICP-MS) or ICP – *optical emission spectrometry* (ICP-OES).

While in these analytical techniques, an inductively coupled electric field is used to generate the plasma, a high-energy laser can also be applied, as is the case in *laser ablation ICP-MS* (LA-ICP-MS) and LIBS analysis. In both cases the laser radiation is applied to excite and ablate the sample, however the coupled analysis methods differ. While LA-ICP-MS is using mass spectrometry for detection, for a LIBS measurement, the plasma excitation by laser radiation is coupled with an optical spectrograph to gain qualitative and quantitative information with cheaper and less sophisticated set-ups.

Ablation using laser radiation has several advantages over other analysis methods, making it a popular choice for a wide range of applications. One of the critical benefits is the minimal sample preparation compared to other analytical techniques, especially in the analysis of solid samples. Instead of time-consuming preparation, like digestion and dilution in ICP-OES, the sample can be analysed directly using LIBS. Compared to other direct methods, e.g. SEM-EDX, and µXRF, which also need less sample preparation, the short measurement time of LIBS is beneficial. While SEM-EDX measurements take at least a few seconds (automated, non-quantitative) up to several minutes (manual, quantitative), a LIBS measurement – independent of qualitative or quantitative analysis – can be performed at times below one second. [12,13]

Another advantage of LIBS is the rapid on-site removal of surface contaminations. While (µ-) XRF, a technique with comparable short measurement times and minimalistic sample preparation, can be disturbed by contaminants on the surface, removing such layers with laser pulses before measurement is easily included in LIBS analysis. Additionally, the sample does not have to be conductive, in contrast to e.g., SEM-EDX or spark spectrometry. Only with extra effort, like analysis in variable pressure mode, non-conductive samples can be characterized with these methods.

Finally, the small analysis volume is an essential benefit of LIBS analysis. The minimally inversive character enables the method's utilization in the analysis of historical artifacts [41,42], in quantity control [43-46], and the analysis of (metallic) scrap [21,39] and particle samples, for example for glass characterization [22] or qualitative TCA particle characterization. [47] Even though LIBS has been suggested in the VDA 19.1 as possible candidate for TCA analysis, quantitative studies have not been published to the point of this dissertation.

Despite all above-mentioned advantages of LIBS, the method has one major drawback: it is strongly impacted by the sample matrix and the measurement environments, like laser parameters and atmospheric conditions. [12,13] The evaporation and plasma generation processes are dependent on the local composition of the sample, due to severe differences in melting and evaporation temperatures of different material classes, like organic and metal samples. Considering the metals as analyte class, even different metals and metal alloys strongly vary in their respective excitation behaviour. [51,86]

As the volume analysed by LIBS is small, the local element composition is also of importance, especially for quantitative analysis. Differences in local matrix change the excitation and plasma generation, hampering the direct correlation of signal intensity and analyte

concentration. Therefore, LIBS generally shows higher LODs and LOQs compared to analytical methods, that minimize such matrix effects (e.g. ICP-OES/-MS, GF-AAS). [12,13]

Still, due to the fast, easy measurement and low preparation effort of LIBS, the method is widely applied (see chapter 1.2). Especially when minimal LODs and LOQs are not the key factor of analysis, as is the case for TCA, the advantages can outweigh the disadvantages.

In the following chapters, the physical basics of LIBS, including ablation, plasma generation and signal emission, are discussed. Describing the occurring disturbances during LIBS measurements, the reader is provided with possible solutions to the respective challenge. Further, the instrumental and process parameters are described.

2.3.1. Physical Basics of LIBS

In LIBS analysis, a high-energy laser generates a plasma and excites the sample's constituents. A schematic overview of the processes on the surface of a solid sample is shown in figure 9. The here described scheme applies to a LIBS measurement in atmospheric pressure.

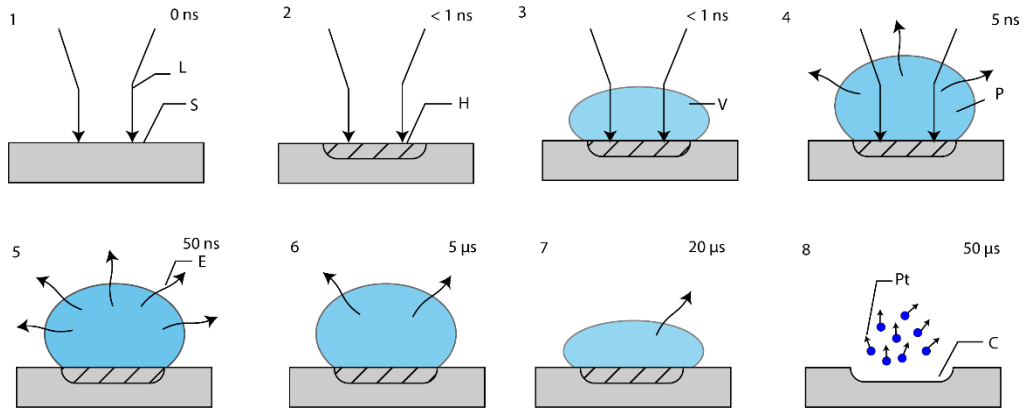

Figure 9: Schematic depiction of LIBS measurement process in atmospheric pressure in phases 1-8. L: laser beam, S: sample, H: region of energy deposition, V: material vapor, P: plasma, E: element-characteristic emission, C: crater, Pt: particles. The provided time scales depict the temporal evolution after the start of the laser pulse. Adapted from [12].

First, the laser beam (L) is focused on the surface (S) (1), transferring energy to the sample. The energy transfer to and the storage in the material is dependent on the optical sample properties, like absorption coefficient and reflectivity. After the energy is shortly locally stored in the material (H) (2) the sample is evaporated, forming a vapor cloud (V) (3). Denoting this process as "evaporation" is a simplification, as no pure transfer from solid to gaseous phases

occurs. Liquid transient phases may also exist depending on measurement parameters like pulse duration and sample properties (e.g. heat conductivity). It has been shown that the ablation process is most effective for short laser pulses and short laser wavelengths. With sufficient energy absorbance the vapor evolves into a plasma (P), consisting of free electrons, non-charged atoms and positively charged atomic bodies in high density (4). The generated plasma now expands (4) due the pressure difference to the atmosphere in form of a shock wave, transferring energy to the ambient gas by thermal conduction, radiative transfer and general heating. [12,87]

After the plasma's internal pressure is similar to the shock wave, the plasma starts cooling down, also called decaying. During plasma decay, element-characteristic emission (E) occurs (5–7). The radiation is collected and separated in a detector to generate spectra carrying qualitative and quantitative information on the plasma's composition. After approximately 50 µs, the plasma has completely decayed, and its constituents have recondensed to particle form (Pt). The ablated material and condensed atoms are removed from the incident location by plasma expansion and, if used in the experimental set-up, external gas flow. The non-evaporated material remains at the measurement location and cools down, forming a crater (C) (8). [12]

The crater depth depends on measurement parameters and material properties like heat conductivity, melting, and evaporation temperature. Materials tending to melt instead of transferring to the gaseous phase tend to have deeper craters, as molten material is ejected from the interaction point in the form of droplets or collars around the crater. [12,51]

In the following, the processes of plasma generation and signal emission are described in detail, to enable an understanding of the most common disturbances in LIBS analysis.

2.3.1.1. Laser-Induced Plasma

Plasmas are induced by means of free electrons absorbing energy via *inverse bremsstrahlung*. How these charge carriers are generated is dependent on the sample properties.

In gaseous samples, electrons are excited via multiphoton or cascade ionization. In multiphoton ionization, multiple photons are absorbed simultaneously to surpass the necessary ionization energy. Cascade ionization describes the avalanche-like generation of ions due to inelastic collisions of strongly oscillating electrons with atoms. In the collision, the electrons transfer the oscillation energy to the atom removing an electron and continuing the

cascade process. [13] In non-conductive solids, electron-hole-pairs must first be generated to form free electrons. [76] Therefore, higher incident energies are necessary to ignite the plasma in such samples compared to conductive materials like metals, where the electrons are located in conductive bands. The electrons in the metal's conductive band can interact more easily with the laser radiation and be excited via *inverse bremsstrahlung*. Due to the absorption, the sample heats up, melts, and evaporates. Therefore, the multiphoton and cascade ionization mechanism to induce plasma is delayed after vaporization. [13]

The induced plasma is generally characterized by plasma temperature and electron density. These parameters can also be used to evaluate the resulting spectra (see e.g., calibration-free (CF-) LIBS, chapter 2.4.1) and explain spectral disturbances. (see chapter 2.3.2)

Assuming *local thermodynamic equilibrium (LTE),* meaning there are no macroscopic changes in locally separated plasma regions, it can be mathematically described by Boltzmann's distribution (equ. 1).

$$\frac{n_j}{n_i} = \frac{g_j}{g_i} \exp\left(-\frac{E_j - E_i}{k_B T}\right) \qquad \text{(equ. 1)}$$

Indices i and j refer to the ionization stage of the species, k_B to the Boltzmann constant ($1.38*10^{-23}$ J/K), T to the plasma temperature, n, E, and g to the population, energy, and the degeneracy of the upper energy level respectively. Transforming the equation yields equ. 2. [88]

$$\ln\left(\frac{\varepsilon_{ij}\lambda_{ij}}{A_{ij}g_j}\right) = -\frac{E_j}{k_B T} + C \qquad \text{(equ. 2)}$$

Here, ε_{ij} is the emission coefficient for the respective transition, directly correlating to the peak intensity in the LIBS spectrum, λ_{ij} is the transitions' wavelength and A_{ij} is the transition probability. C is a constant, summarizing other parameters of the transition. Variables λ_{ij}, A_{ij}, g_{ij}, can be found in the database of the National Institute of Standards and Technologies (NIST). [89]

Plotting $\ln\left(\frac{\varepsilon_{ij}\lambda_{ij}}{A_{ij}g_j}\right)$ against E_j now yields a so-called Boltzmann plot. The straight line's slope corresponds to $-\frac{1}{k_B T}$, so that the plasma temperature can be calculated. [13,88]

Finally, Sahas' equation (equ. 3, equ. 4) can be used to determine the plasmas' electron density, n_e assuming only the first ionization step is significant. [12,90]

$$n_e[cm^3] = \frac{I_Z^*}{I_{Z+1}^*}\ 6.04 * 10^{21} * T^{\frac{2}{3}} * \exp\left(\frac{-E_{j,Z+1} + E_{j,Z} - \chi_Z}{k_B T}\right) \quad \text{(equ. 3)}$$

, with

$$I_Z = \frac{I_Z \lambda_{ij,Z}}{g_{j,Z} A_{ij,Z}} \quad \text{(equ. 4)}$$

Index Z corresponds to the ionization state, I_Z^* to the integral of the studied signal and χ_Z to the ionization energy of Z.

A plasma's electron density and temperature are central figures for LIBS, as they influence the emitted radiation. The higher the density and the temperature, the stronger the resulting signals. Therefore, these parameters directly impact the sensitivity of LIBS measurements. [12,13]

2.3.1.2. Atomic Emission in LIBS

The observed variable in LIBS is the emitted radiation produced by atomic emission. Shortly after a plasma is induced, it starts to decay. During decay, energy is released in the form of heat and electromagnetic radiation. The emission can be divided into unspecific continuous and element-characteristic radiation, whose intensity ratio changes over the lifetime of the plasma (Figure 10).

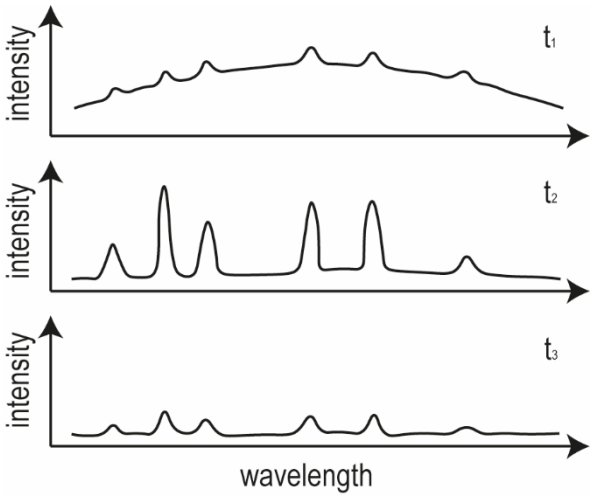

Figure 10: Schematic illustration of emission spectra of LIBS for different delay times. [12]

Shortly after plasma generation (t_1), the non-characteristic continuous emission, caused by free-free transitions of electrons (*bremsstrahlung*), is predominant. This is visible in the elevated baseline, which overlays the distinct element signals, so only their tips are visible. *Bremsstrahlung* is especially strong for plasmas with high electron densities. [12,13]

After a few hundred ns (t_2), the plasma has started to cool down, significantly decreasing the continuum radiation. Now, the atomic emission of discrete and element-characteristic energy levels is predominant. The atomic emission results from the recombination of positively charged atomic bodies with electrons. Initially, the electrons occupy high excited states in the newly recombined neutral atom, from which they relax to lower states. The discrete energy difference between these states is released as electromagnetic radiation and can be used to identify and quantify the emitting atoms. [12,91]

Observing the plasma at later time points (t_3), it has further decreased in temperature, leading to a decrease in overall signal intensity and, therefore signal-to-noise-ratio (SNR). [12] After the delay time of spectra acquisition has exceeded 10 µs, emission of atoms has decreased significantly while emission from simple molecules (e.g. from the condensed atoms or positively charged atomic bodies reacted with the surrounding atmosphere) starts to appear. [13]

2.3.2. Spectral Disturbances in LIBS Measurements

In spectrometric methods, measurement parameters are optimized for intense and narrow signals, with high SNR and without self-absorption or -inversion. This way, more information can be obtained from the spectra, and more valuable results can be achieved.

Considering the theoretic process of atomic emission, the resulting signals would be only limited by Heisenberg's uncertainty principle (*Natural broadening*). However, in reality, emission signals are broadened by *Stark* and *Doppler effect*. Stark effect is defined as the degeneration of energetic states in the presence of strong electric fields. In atomic emission, such degeneracy results in broader signals. [76] In LIBS, powerful electric fields correlate with high electron densities in the plasma, consequently leading to signal broadening. Doppler broadening occurs due to the difference in velocity of studied atoms and observer, in this case, the detector. [76] As the atoms' velocity directly links with the plasma temperature, high temperatures lead to broader signals.

Another spectral disturbance in LIBS is *self-absorption*. Here, part of the emitted radiation is re-absorbed before reaching the detector, decreasing the line intensity in the resulting spectrum. In quantitative analysis, the effect is sometimes visible in a flattening of the calibration curve towards higher analyte concentrations. Self-absorption is especially relevant for plasmas with high particle densities, leading to a higher probability of re-absorption by other atoms. In some cases, self-absorption is visible in the spectrum as a central dip in the emission line (*self-reversal*). Wavelengths corresponding to a highly probable energetic transition of an atom or positively charged atomic body are most likely to be reabsorbed – the more likely the transition, the more likely the re-absorption. Therefore, signals with lower transition probability should be used for quantification. However, for small concentrations or the analysis of trace elements, less intensive signals are often coupled with an increase in the limit of detection (LOD) and quantification (LOQ). [12,87]

2.3.3. Instrumental and Process Parameters

Figure 11 depicts the principle set-up of a LIBS measurement unit. The pulsed LIBS laser is guided via a mirror (M) to a focus lens (L), through a radiation-transparent window (W1), and into the sample chamber (C). Depending on the measurement parameters, the chamber can be flushed with protective gases like argon or alternatively with ambient air (G). The sample is placed on a stage (A) so that the measurement location can be selected, and the sample (S)

can be put into focus. The focused laser induces a plasma (P) on the sample surface, whose emitted radiation is transmitted via fibre optics (FO) to a spectrometer, where it is dispersed and converted to electrical signals to be detected (D). [12]

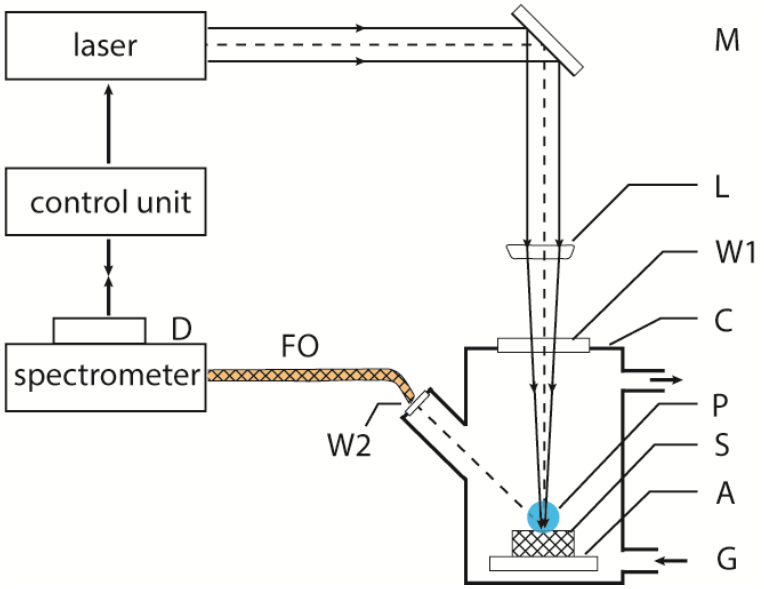

Figure 11: Schematic setup for laser-induced breakdown spectrometry; M: mirror, L: focusing lens, W1: window for laser radiation, C: measurement chamber, P: laser-induced plasma, S: sample, A: sample stage, G: gas fitting, window for measurement radiation, FO: fibre optics, D: detector. Adapted from [12].

The most commonly used lasers in LIBS are Nd:YAG solid-state lasers (1064 nm). Combining them with actively coupled Q-switching leads to narrow and intense laser pulses that are well fit for the application in LIBS analysis. [13,92]

The plasma can be induced using single or double pulsing of the laser. The time difference between the two pulses in double pulsing can vary from 100 ns to several microseconds. Single and double pulsing leads to differences in plasma excitation and expansion, which can be visualized in plasma imaging (figure 12). Three time points are observed after inducing a plasma with a single pulse of 80 mJ (a) and a double pulse of 2 × 40 mJ (b), respectively. [12]

The single pulse (a) plasma is larger initially than the double pulse's (b). However, it decays faster, leaving only a small emitting volume in contact with the surface after 0.5 µs. The double pulse plasma is smaller initially and shows a visible detachment from the sample at 0.15 µs. For a delay of 0.5 µs, the plasma of the double pulse is visibly larger compared to the single pulse, indicating enhanced emission. This enhancement makes the measurement more sensitive to low analyte concentrations, indicating lower LODs and LOQs when using double pulsed excitation. [12]

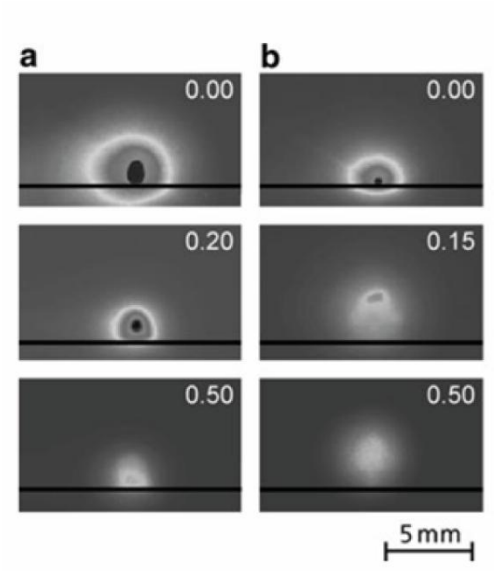

Figure 12: Images of the plasma evolution for (a) a single pulse of 80 mJ and (b) a symmetric double pulse with 2× 40 mJ. The observation time in µs is shown in each image in the upper right corner. [12]

Another tuneable parameter in LIBS measurements is the atmosphere. As the sample is vaporized and a plasma is induced, the density of the surroundings has a significant impact. The measurement can be performed under protective gas atmosphere, like argon or nitrogen, ambient air, or vacuum. Therefore, LIBS is a popular analysis method for space exploration. [18,93]

Still, the most common measurement atmospheres in research and application are ambient air and argon. In an argon atmosphere, the plasma's expansion is decreased, leading to it being more confined. Confined plasmas generally have higher densities and temperatures compared to less confined ones. This leads to stronger emission and therefore improvement of the method's sensitivity (see chapter 2.3.1.1), while at the same time increasing the probability of self-absorption. Further, in an argon surrounding, wavelengths below 200 nm are transmitted better, improving the radiation yield detected in this spectral region. Additionally, the formation of molecules at the end of the plasma decay significantly decreases. Finally, in such a controlled atmosphere, the reproducibility is increased, improving comparability between measurements. [12]

Even though performing LIBS measurements in argon surroundings has advantages regarding the method's sensitivity and comparability, in practical application it also has disadvantages. Using argon, or other protective gases, decreases the analysis speed, as the sample chamber needs to be flushed after every sample change. Therefore, it decreases the convenience of LIBS, while at the same time increasing costs. Considering in-line applications e.g., in quality or process control, the sample cannot be isolated and put into a chamber to be flushed or filled. Also for applications, which are focused on easy application and analysis speed and not on sensitivity in the ppm region, like TCA or material sorting, the use of protective gas is uncommon. [12] In such applications, LIBS measurements are often performed under ambient air, unless the analytical question explicitly requires high sensitivity or protective gas.

Lastly, the sample is an important parameter to consider before measurement. Firstly, the matrix composition at the specific measurement location has a significant impact. The local matrix influences the ablation and excitation due to melting, boiling, and evaporation

temperatures, as well as the optical reflectivity. [12,51] For inhomogeneous samples, e.g., metal alloys, matrix effects can be even more challenging, as the local matrix varies over the sample. This may result in varying spectra for the analysis of the same sample and reduced representativeness of a single measurement for the “whole” bulk material.

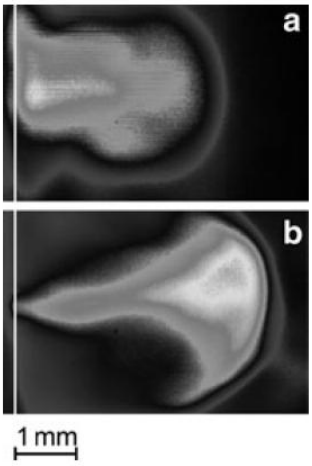

Figure 13: Side-on images of luminous plasma evolving from the sample surface of (a) a flat surface and (b) a crater of preceding laser pulses. Measurement has been performed under ambient air atmosphere and with 160 mJ laser pulse energy. The images have been taken at a delay time of 5 µs. [12]

Additionally to the matrix, the surface topography influences the resulting spectra. Rough surfaces have been shown to yield higher signal intensities than smooth ones, since the roughness leads to a more confined plasma, increasing its respective density. [93] In figure 13, the plasma confinement is clearly visible in the comparison of the plasma of (a) on a flat surface and (b) on a surface with a crater (depth of 0.9 mm) from proceeding laser pulses at the same delay after the laser pulse. The confinement in (b) is clearly visible, with the plasma showing stronger expansion towards the incoming beam and a shift regarding the centre of the plasma compared to the measurement on the flat surface. The confinement changes plasma expansion, and dynamics impacting the resulting emission spectra of each sample. [12]

This dependency on the sample topography is especially challenging for LIBS chemical mapping applications. If the emission depends on the sample topography, which varies over the surface, the intensities alone would not be sufficient to provide information on the element distribution. However, it is possible to overcome or at least minimize this problem by careful data treatment, like normalization and line selection.

2.4. LIBS Data Evaluation

LIBS is a multi-element analysis method that results in complex spectra with a multitude of analyte and matrix signals. The spectra can be used to qualitatively identify the constituents, classify the samples, or quantitatively determine analytes. In the direct analysis of solid and inhomogeneous samples, like metal alloys, the complexity of the spectra is increased even more due to (local) matrix effects. To quantitatively evaluate these highly condensed datasets, different approaches are used.

In the following chapters, different quantification techniques used in LIBS will be described. A special focus will be on partial least squares regression (PLS-regression), as this is the approach used in this work.

2.4.1. Quantification Techniques in LIBS Analysis

The most straightforward approach to quantification is the *univariate* calibration. For calibration model design, a single signal (or its integral) is correlated with the reference analyte concentration. This approach works well for linear correlations of concentration and signal intensity. This is the case for methods with little or no matrix interference, like ICP-OES or when working with small concentration regions of interest, where the matrix effects stay approximately constant. [91] However, this is often not the case for LIBS measurements, especially in the direct analysis of metal alloys. In general, LIBS analysis is hampered by matrix effects due to changes in evaporation and excitation behaviour depending on the local element composition. Additionally, metal alloys show a broad concentration range regarding their alloy components. For example, technically applied iron alloys can vary in their chromium content between zero up to 40 $\%_{wt}$ in chilled cast iron. [75] Therefore, other evaluation techniques than univariate calibration need to be explored.

A more theoretically based approach is *calibration-free (CF)* LIBS. Here, the sample composition is calculated directly from the LIBS spectrum using the physical correlations of plasma emission and concentration. [94] By considering self-absorption effects in the calculations, accuracy can be increased. [95,96] A measurement of reference samples, like in classical calibration, is not necessary, minimizing the measurement effort for quantification. However, several assumptions must be made for CF-LIBS, such as LTE conditions in the plasma and stoichiometric ablation of the sample into the plasma. These assumptions are beyond control in most LIBS practices, leading to less accurate results in applied LIBS – especially for minor or trace elements. [97]

Another group of quantification approaches for LIBS is based on *multivariate data analysis (MDA).* Generally, in MDA, the interpreter algorithm uses multiple features of the provided data to discriminate between or correlate individual samples. A common example for MDA is human face recognition and memory. Without knowing the exact length of the nose or the distance between the eyes, humans can instinctively recognize different faces by considering the overall composition of the face instead of single variables. While human brains normally can

differentiate easily between faces and find patterns here, it is more challenging to identify correlations and covariances in abstract numerical data, like spectra. [98]

For such complex datasets, mathematical algorithms are employed to decipher patterns and identify similarities and differences between samples. The basis of all multivariate methods is the reduction of complex systems to relevant variables that summarize the data in a concentrated fashion. These relevant variables, also called *main* or *principal components* (PCs), are linear combinations of existing variables with individual weighting factors. They are optimized mathematically to maximize the variability between the original variables. [47,98]

One example of quantitative MDA in LIBS is the *least absolute shrinkage and selection operator* (LASSO). In this shrunken regression technique, the values of the regression coefficients are constrained in a multiple linear regression. The sum of all coefficients is restricted to a boundary value β. As the model weights each channel's significance for the respective prediction, insignificant variables are assigned a correlation coefficient of zero after the optimization process. This “hard” feature selection, reducing minor channels to zero, can make the regression more robust against noise compared to other “softer” selection methods. [99,100]

However, the main disadvantage of LASSO is the arbitrarily chosen variables that are evaluated. As the others are discarded, the selected ones are highly impactful. [101] If, e.g., the analyte’s concentration is by chance increasing with another alloyed element, the model could be based on the signal of the other element’s signals instead of that of the analyte. In “softer” selection methods, such effects also occur and hamper evaluation. However, they are not as relevant due to the incomplete exclusion of other variables.

The PLS-regression is an example of such a “soft” selection of relevant variables or spectral regions in the case of LIBS spectra. This method will be described in detail in the following chapter.

2.4.2. Partial-Least-Squares (PLS) Regression

This thesis is mainly based on the quantification and calibration method of *partial least squares regression* (PLS-regression). For clarity, only the general mathematical steps of the methods are highlighted at this point. The reader is referred to the corresponding literature for an in-depth background of MDA and PLS-regression. [56,98]

Assume a data matrix X of m observed variables of n samples with corresponding observed Y-matrix variables. In the case of calibration, X corresponds to the signal intensities and Y to the corresponding element concentration. Linearly correlating X and Y yields a linear calibration model that can quantify analyte concentrations in unknown samples. In univariate calibration, normally, an analyte signal or its integral is used. In PLS-regression, PCs are used to condense the dataset to relevant information. [98]

To calculate the PCs, the data matrices X and Y are first pretreated with *standardization* and *centralization*. Each column has a mean value of zero (centralization) and a deviation of one (standardization). As deviations from a zero value substitute the previously absolute values, initially large deviations from the mean do not dominate the evaluation. Instead, the generally more relevant deviation of the mean is increasing in importance. The standardization converts the variables to the same scale to eliminate arbitrariness in the computing. Afterward, the *correlation matrices* $\mathrm{R_X}$ and $\mathrm{R_Y}$ are calculated independently using equ. 5, showing the connection of the individual variables. Here, $\mathrm{X^T}$ depicts the transformed X-matrix with order n; the calculation of $\mathrm{R_Y}$ is carried out analogously. [98]

$$R_X = X^T * X * (n-1)^{-1} \qquad \text{(equ. 5)}$$

Values in R describe the correlation of different variables. Positive values show a positive correlation, meaning an increase in one variable leads to an increase in the other. Analog negative correlation (and values in R) leads to a decrease of the other variable. A value of zero indicates no correlation between the variables. The matrix diagonal displays the correlation of each variable with itself, meaning its scattering over all objects. [98]

Using equ. 6 and 7, the score *(T, U),* loading *(P, Q),* and residue *(E, F)* matrix can be calculated.

$$X = TP^T * E \qquad \text{(equ. 6)}$$

$$Y = UQ^U * F \qquad \text{(equ. 7)}$$

The scores *(T, U)* display the direction and absolute value of the variable vector in the coordinate system of the PCs. The associated *eigenvalues* describe the PCs all variables have in common and are summarized in the loadings matrix *(P, Q).* It contains the principal components' numerical values and describes the variables' significant common features. In summary, the weight or score matrix contains the individualities of the objects, while the loadings matrix represents the commonalities of all the data. The residual matrices E and F

represent the loss of information associated with the coordinate transformation. [98] This evaluation of PCs is called *principle component analysis* (PCA) and is generally used to identify significant features in the samples or detect outliers. [29,58,59,61,87,101]

In PLS, the PCA is performed for both X and Y. The resulting matrices are correlated in an iterative process, exchanging T and U vectors between the data matrices X and Y. To link X and Y matrices, the covariance of each element of X and Y, respectively, is maximized in an iterative process and exchanged between the matrices. Consequently, the first estimated T_1 corresponds to the U_1 vector. This results in a new loadings matrix W, which contains information of both X and Y. This way, the eigenvector matrices W and Q are iteratively optimized to maximum correlation. [98]

After optimization, a linear relationship between actual and calculated concentration can be specified, corresponding to a calibration curve. The underlying calibration function corresponds to a linear combination that cannot be represented in a simple two-dimensional plot in contrast to univariate calibration. A so-called prediction plot, as shown in figure 14, can be used to visualize the calibration. Here, the concentrations calculated by the PLS-model are plotted against the reference concentrations. If the individual measurements scatter among themselves, they also scatter in the prediction plot. In this way, the homogeneity of the measurement and reference standards can be estimated, and "outliers" can be identified. [98]

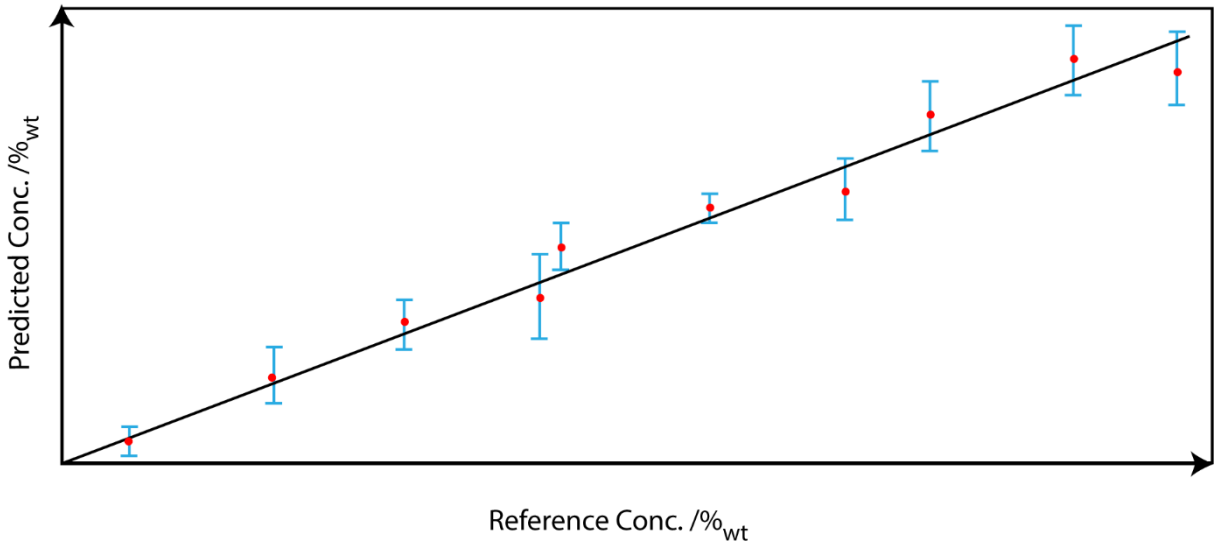

Figure 14: Schematic display of a PLS-regression prediction plot. On the y-axis the values predicted from the PLS-regression model and on the x-axis the reference values are shown.

The quality of the calibration model can be estimated by considering different parameters. The first important parameter is the *coefficient of determination* R^2. It is defined as the ratio of the

explained dispersion of the calculated element contents and the total dispersion of the reference concentrations. As a coefficient of determination of the calibration, it describes the deviation from the linear calibration function. Another important parameter is the *root mean square error of calibration (RMSEC)*, defined as the mean deviation of the measured values from the regression line (equ. 8). Therefore, the RMSEC should be as small as possible for a high-quality calibration. [98]

$$\mathrm{RMSEC} = \sqrt{\frac{\sum_{i=1}^{n}(y_i - \hat{y})^2}{n}} \qquad \text{(equ. 8)}$$

The number of PCs used for the PLS-regression model needs to be optimized individually, as it is essential for the applicability to unknown samples. Most information is summarized in the first PC. The variance explained by the next PCs decreases with an increasing number of PCs until they represent purely the spectral noise. This way, the model increases in accuracy regarding the description of the calibration data, which is visible in low RMSEC and high R^2. However, for samples not part of the calibration, the *overfitted* model will also evaluate the random spectral noise, leading to a loss in accuracy. On the other hand, using too few PCs leads to an *underfitted* model. In this case, relevant information is not included in the evaluation, and the chance of including systematic errors increases. To keep the model flexible for different matrix samples, choosing as many PCs as necessary and as little as possible is advised. [63,98]

The *root mean square error of cross-validation* (RMSECV) can be used for an initial test on under- and overfitting. Here, individual measurements are gradually left out of the calibration and evaluated with the PLS-regression model of the remaining samples as unknown samples. If the RMSECV increases, the system is likely to be overfitted. Considering RMSECV, RMSEC and R^2, the number of PCs can be optimized accordingly not over- or underfitting the quantification model. [63,98]

2.4.3. Importance of Data Treatment in PLS-Regression

The previous chapter established the importance of optimizing the number of PCs used for model development, so the model is neither under- nor overfitted. However, the treatment of the input data also essential for successful and accurate PLS-regression. [63,98]

The PLS-regression models are developed, optimizing on the largest variances in the dataset and weighting the variables accordingly. The stronger the variance, the stronger the respective variable will be weighted. This way, the dimensions are reduced, yielding PCs, and correlations between signals that have previously been considered independently can be identified. Nevertheless, this automated detection and selection of correlations and significant variables, and their correlations poses risks. Assume a set of metal alloy CRMs used for calibration for analyte *A*. Additionally, the CRMs contain analyte *B*, whose concentration, by chance, increases with the one of *A*. Including signals of *A* and *B* in the PLS-regression can lead to the model correlating a high signal intensity of *B* with a high concentration of *A*. However, this correlation might not be based on scientifically relevant information but a random artifact resulting from the CRMs' composition. Knowledge of the real samples and the CRMs is necessary to decide whether the correlation is relevant. If in production of tested samples, the analytes *A* and *B* are being alloyed independently, the correlation needs to be removed from the quantification model to avoid inaccuracies. [63] Only if the correlation is always present due to e.g., specific processing steps, the correlation could be included into the evaluation models.

Removing unwanted correlation can be done, e.g., by adjusting the variables' weighting, comparable to LASSO, or by selecting spectral regions for evaluation. Wang et al. have developed a dominant factor based PLS for this adjustment. Here, dominant factors that carry the main quantitative information are calculated using the plasma dynamics equations and included in the data treatment. Insignificant variables, like noise, are therefore reduced in weight, increasing the regression accuracy. [102] However, with the dominant factor being based on physical plasma principles, challenges similar to CF-LIBS occur, namely the hardly controllable LTE conditions. Additionally, if the dominant factor is based solely on plasma physics, possibly wrong correlations are disregarded.

An alternative approach is the manual selection of signals or spectral areas that carry quantitative information and are free of disturbances. Here, optimizing between including enough information to make the best use of MDA while at the same time minimizing wrong correlations can be tedious work. However, basing the selection on literature, possibly also from other established OES methods, decreases the necessary effort significantly and can increase comparability between individual analytical techniques.

Additionally, data treatment comparable to other analytical techniques can be performed for data preselection. The most common treatments are baseline correction and normalization. In

LIBS analysis, baseline correction is mostly unnecessary if the delay time is long enough, so the continuum radiation has decayed. [63]

On the other hand, normalization greatly impacts PLS-regression results, as using the non-normalized spectra can negatively affect the model. Small changes in the absolute spectral intensity, e.g., due to laser energy fluctuations, strongly impact the variance between the samples. If this variance is falsely integrated into the model, it will decrease the calibration quality significantly. [98]

Commonly used normalization mechanisms are vector normalization and normalization on a reference signal. In both cases, the conjoined scales lead to improved accuracy and the decreased importance of outliers. When using reference signal normalization, the signal should be stable and not vary strongly between the samples. Else the accuracy might be strongly impaired. For different analytes and matrices different normalization techniques might be optimal. However, a comparison of Castro et al. has shown no significant differences between reference signal and vector normalization. [103]

References

[1]: V. Panahi, M. Kargahi, F. Faghih. Control Performance Analysis of Automotive Cyber-Physical Systems: A Study on Efficient Formal Verification. ACM Trans. Cyber-Phys. Syst. 8 (2024), pp. 1–19.

[2]: Korte, D. Concept of a Safety-Related Sensor System for Collaboration Between Human and Automated Guided Vehicles. In: P. Weißgraeber, F. Heieck, C. Ackermann, Advances in Automotive Production Technology – Theory and Application; Springer Berlin Heidelberg, 2021, pp 416–423.

[3]: P. Brag, M. Rochowicz, Safety in Electromobility – Technical Cleanliness Between the Poles of Design Requirements and Efficient Production. In: P. Weißgraeber, Heieck, C. Ackermann, Advances in Automotive Production Technology – Theory and Application; Springer Berlin Heidelberg, 2021, pp 319–326.

[4]: J. Faber, K. Brodzik, M. Nycz,. Understanding Technical Cleanliness: Importance, Assessment, Maintenance. Combustion Engines.186 (2021) pp. 41–50.

[5]: M. Oravec, A. Divoková, P. Lipovský, M. Karásek, R. Janošík. Technical Cleanliness - a Requirement of Precision Manufacturing. Acta Mechanica Slovaca. 23 (2019) pp. 46–51.

[6]: German Association of the Automotive Industry, VDA 19.1 - Inspection of Technical Cleanliness: Particulate contamination of functionally relevant automotive components, VDA Automotive Standard, Berlin, 2015.

[7]: German Association of the Automotive Industry, VDA 19.2 - Technical Cleanliness in Assembly: Environment, Logistics, Personell and Assembly facilities., VDA Automotive Standard, Berlin, 2015.

[8]: Fraunhofer-Gesellschaft. Sauberkeitskontrolle Technische Sauberkeit VDA 19. Sauberkeitskontrolle Technische Sauberkeit VDA 19. https://www.reinigung.fraunhofer.de/de/projekte/vda19.html, last accessed:03.11.2024.

[9]: A. Grabowski, A. Lisiecki, M. Dyzia, J. Łabaj, S. Stano. The Effect of Laser Wavelength on Surface Layer Melting of the AlSi/SiC Composite. Journal of Manufacturing Processes. 75 (2022) pp. 627–636.

[10]: X. Cao, M. Jahazi, J.P. Immarigeon, W. Wallace. A Review of Laser Welding Techniques for Magnesium Alloys. Journal of Materials Processing Technology. 171 (2006) pp. 188–204.

[11]: A. Dzetzit, G. Nagit, Research on Importance of Cleanliness in Manufacturing Reliable Products for Automotive. MATEC Web Conf. 112 (2017) pp. 09017.

[12]: R. Noll, Laser-Induced Breakdown Spectroscopy: Fundamentals and Applications; Springer: Berlin, 2012.

[13]: S. Musazzi, U. Perini, Laser-Induced Breakdown Spectroscopy: Theory and Applications; Springer: Berlin, 2014.

[14]: D. W. Hahn, N. Omenetto, Laser-Induced Breakdown Spectroscopy (LIBS), Part II: Review of Instrumental and Methodological Approaches to Material Analysis and Applications to Different Fields. Applied spectroscopy, 2012, 66, pp. 347–419.

[15]: L. B. Guo, D. Zhang, L. X. Sun, S.C. Yao, L. Zhang, Z.Z. Wang, Q.Q.Wang, H.B. Ding, Y. Lu, Z.Y. Hou, Z. Wang. Development in the Application of Laser-Induced Breakdown Spectroscopy in Recent Years: A Review. Front. Phys. 16 (2021) pp. 22500.

[16]: J.R. Scott, A.J. Effenberger, J.J. Hatch. Influence of Atmospheric Pressure and Composition on LIBS. In: S. Musazzi, U. Perini, Laser-Induced Breakdown Spectroscopy; Springer Series in Optical Sciences; Springer Berlin Heidelberg, 182 (2014), pp. 91–116.

[17]: F. Colao, R. Fantoni, V. Lazic, A. Paolini, F. Fabbri, G.G. Ori, L. Marinangeli, A. Baliva. Investigation of LIBS Feasibility for in Situ Planetary Exploration: An Analysis on Martian Rock Analogues. Planetary and Space Science. 52 (2004) pp. 117–123.

[18]: J. Lasue, R.C. Wiens, S.M. Clegg, D.T. Vaniman, K.H. Joy, S. Humphries, A. Mezzacappa, N. Melikechi, R.E. McInroy, S. Bender. Remote Laser-induced Breakdown Spectroscopy (LIBS) for Lunar Exploration. J. Geophys. Res. 117 (2012).

[19]: H. Rajavelu, N.J. Vasa, S. Seshadri. LIBS Technique Combined with Blow Gas and Vacuum Suction to Remove Particle Cloud and Enhance Emission Intensity during Characterization of Powder Samples. Spectrochimica Acta Part B: Atomic Spectroscopy, 2021, 181, pp. 106215.

[20]: M. Imran, L. Sun, P. Liu, H. Sattar, D. Zhao, Z. Mu, H. Ding. Depth Profiling of Tungsten Coating Layer on CuCrZr Alloy Using LIBS Approach. Surface & Interface Analysis, 2019, 51, pp. 210–218.

[21]: S. Merk, C. Scholz, S. Florek, D. Mory. Increased Identification Rate of Scrap Metal Using Laser Induced Breakdown Spectroscopy Echelle Spectra. Spectrochimica Acta Part B: Atomic Spectroscopy, 2015, 112, pp 10–15.

[22]: V. Merk, D. Huber, L. Pfeifer, S. Damaske, S. Merk, W. Werncke, M. Schuster. Discrimination of Automotive Glass by Conjoint Raman and Laser-Induced Breakdown Spectroscopy and Multivariate Data Analysis. Spectrochimica Acta Part B: Atomic Spectroscopy, 2021, 180, pp. 106198.

[23]: S. Xie, T. Xu, X. Han, Q. Lin, Y. Duan. Accuracy Improvement of Quantitative LIBS Analysis Using Wavelet Threshold De-Noising. Journal of Analytical Atomic Spectrometry, 2017, 32, pp. 629–637.

[24]: V. C. Costa, F. W. B. Aquino, C. M. Paranhos, E. R. Pereira-Filho. Identification and Classification of Polymer E-Waste Using Laser-Induced Breakdown Spectroscopy (LIBS) and Chemometric Tools. Polymer Testing, 2017, 59, pp. 390–395.

[25]: Z. Gajarska, L. Brunnbauer, H. Lohninger, A. Limbeck. Identification of 20 Polymer Types by Means of Laser-Induced Breakdown Spectroscopy (LIBS) and Chemometrics. Anal Bioanal Chem 2021, 413, pp. 6581–6594.

[26]: M. Vahid Dastjerdi, S. J. Mousavi, M. Soltanolkotabi, A. Nezarati Zadeh. Identification and Sorting of PVC Polymer in Recycling Process by Laser-Induced Breakdown Spectroscopy (LIBS) Combined with Support Vector Machine (SVM) Model. Iran J Sci Technol Trans Sci. 2018, 42, pp. 959–965.

[27]: P. Devangad, V. K. Unnikrishnan, M. M. Tamboli, K. M. M. Shameem, R. Nayak, K. S. Choudhari, C. Santhosh. Quantification of Mn in Glass Matrices Using Laser Induced

Breakdown Spectroscopy (LIBS) Combined with Chemometric Approaches. Anal. Methods. 2016, 8, pp. 7177–7184.

[28]: A. V. Skalny, T. V. Korobeinikova, M. Aschner, O. V. Baranova, E. G. Barbounis, A. Tsatsakis, A. A. Tinkov. Medical Application of Laser-Induced Breakdown Spectroscopy (LIBS) for Assessment of Trace Element and Mineral in Biosamples: Laboratory and Clinical Validity of the Method. Journal of Trace Elements in Medicine and Biology. 2023, 79, pp. 127241.

[29]: Y. Zhao, Q. Wang, X. Cui, G. Teng, K. Wei, H. Liu. Discrimination of Hazardous Bacteria with Combination Laser-Induced Breakdown Spectroscopy and Statistical Methods. Appl. Opt. 2020, 59, pp. 1329.

[30]: B. B. S. Jaswal, V. K. Singh. Analytical Assessments of Gallstones and Urinary Stones: A Comprehensive Review of the Development from Laser to LIBS. Applied Spectroscopy Reviews. 2015, 50, pp. 473–498.

[31]: B. Sezer, S. Durna, G. Bilge, A. Berkkan, A. Yetisemiyen, I. H. Boyaci. Identification of Milk Fraud Using Laser-Induced Breakdown Spectroscopy (LIBS). International Dairy Journal. 2018, 81, pp. 1–7.

[32]: T. V. Silva, S. Z. Hubinger, J. A. Gomes Neto, D. M. B. P. Milori, E. J. Ferreira, E. C. Ferreira. Potential of Laser Induced Breakdown Spectroscopy for Analyzing the Quality of Unroasted and Ground Coffee. Spectrochimica Acta Part B: Atomic Spectroscopy. 2017, 135, pp. 29–33.

[33]: S. Beldjilali, D. Borivent, L. Mercadier, E. Mothe, G. Clair, J. Hermann. Evaluation of Minor Element Concentrations in Potatoes Using Laser-Induced Breakdown Spectroscopy. Spectrochimica Acta Part B: Atomic Spectroscopy. 2010, 65, pp. 727–733.

[34]: M. Markiewicz-Keszycka, R. Cama-Moncunill, M. Pietat Casado-Gavalda, C. Sullivan, P. J. Cullen. Laser-Induced Breakdown Spectroscopy for Food Authentication. Current Opinion in Food Science. 2019, 28, pp. 96–103.

[35]: G. S. Senesi, J. Cabral, C. R. Menegatti, B. Marangoni, G. Nicolodelli. Recent Advances and Future Trends in LIBS Applications to Agricultural Materials and Their Food Derivatives: An Overview of Developments in the Last Decade (2010–2019). Part II. Crop Plants and Their Food Derivatives. TrAC Trends in Analytical Chemistry. 2019, 118, pp. 453–469.

[36]: V. Gupta, A. K. Rai, T. Kumar, R. Junjuri, G. M. Kumar, A. K. Rai. Chemical and Physical Studies of Metallic Alloy-Based Old Indian Coins with LIBS Coupled with Multivariate Analysis. Plasma Sci. Technol. 2023, 25, pp. 095501.

[37]: S. W. Hudson, J. Craparo, R. De Saro, D. Apelian. Applications of Laser-Induced Breakdown Spectroscopy (LIBS) in Molten Metal Processing. Metall Mater Trans B 2017, 48, pp. 2731–2742.

[38]: R. Noll, C. Fricke-Begemann, F. Schreckenberg. Laser-Induced Breakdown Spectroscopy as Enabling Key Methodology for Inverse Production of End-of-Life Electronics. Spectrochimica Acta Part B: Atomic Spectroscopy. 2021, 181, pp. 106213.

[39]: P. Werheit, C. Fricke-Begemann, M. Gesing, R. Noll. Fast Single Piece Identification with a 3D Scanning LIBS for Aluminium Cast and Wrought Alloys Recycling. Journal of Analytical Atomic Spectrometry. 2011, 26, pp. 2166.

[40]: S. V. Den Eynde, D. J. Diaz-Romero, B. Engelen, I. Zaplana, J. R. Peeters. Assessing the Efficiency of Laser-Induced Breakdown Spectroscopy (LIBS) Based Sorting of Post-Consumer Aluminium Scrap. Procedia CIRP. 2022, 105, pp. 278–283.

[41]: S. Awasthi, R. Kumar, G. K. Rai, A. K. Rai. Study of Archaeological Coins of Different Dynasties Using Libs Coupled with Multivariate Analysis. Optics and Lasers in Engineering. 2016, 79, pp. 29–38.

[42]: A. Khedr, H. Sadek, O. Aied Nassef, M. Abdelhamid, M. A. Harith. Discrimination between the Authentic and Fake Egyptian Funerary Figurines “Ushabtis” via Laser-Induced Breakdown Spectroscopy. Journal of Cultural Heritage. 2019, 40, pp. 25–33.

[43]: L. Peter, V. Sturm, R. Noll. Liquid Steel Analysis with Laser-Induced Breakdown Spectrometry in the Vacuum Ultraviolet. Appl. Opt. 2003, 42, pp. 6199.

[44]: A. K. Myakalwar, C. Sandoval, M. Velásquez, D. Sbarbaro, B. Sepúlveda, J. Yáñez. LIBS as a Spectral Sensor for Monitoring Metallic Molten Phase in Metallurgical Applications—A Review. Minerals. 2021, 11, pp. 1073.

[45]: S. H. Gudmundsson, J. Matthiasson, B. M. Björnsson, H. Gudmundsson, K. Leosson. Quantitative In-Situ Analysis of Impurity Elements in Primary Aluminum Processing Using Laser-Induced Breakdown Spectroscopy. Spectrochimica Acta Part B: Atomic Spectroscopy 2019, 158, pp. 105646.

[46]: G. Hubmer, R. Kitzberger, K. Mörwald. Application of LIBS to the In-Line Process Control of Liquid High-Alloy Steel under Pressure. Anal Bioanal Chem. 2006, 385, pp. 219–224.

[47]: D. Huber, M. Schuster. Development of a Composite Analysis Process with Laser-Induced Plasma Spectrometry and Multivariate Data Evaluation for Characterizing Particles in the Field of Technical Cleanliness Analysis. Dissertation, Technical University Munich, 2021.

[48]: R. W. Cahn, P. Haasen, E. J. Kramer, Processings of Metals and Alloys; Materials science and technology; VCH: Weinheim New York, 1991.

[49]: Fraunhofer-Gesellschaft. Eigenspannungen in Aluminium-Silizium-Gusslegierungen. https://www.itwm.fraunhofer.de/de/abteilungen/sms/leichtbau-und-daemmstoffe/eigenspannungen-in-aluminium-silizium-gusslegierungen.html (last accessed: 21.11.2024).

[50]: V. C. Costa, M. L. Mello, D. V. de; Babos, J. P. Castro, E. R. Pereira-Filho. Calibration Strategies for Determination of Pb Content in Recycled Polypropylene from Car Batteries Using Laser-Induced Breakdown Spectroscopy (LIBS). Microchemical Journal, 2020, 159, pp105558.

[51]: D. Bleiner, Z. Chen, D. Autrique, A. Bogaerts. Role of Laser-Induced Melting and Vaporization of Metals during ICP-MS and LIBS Analysis, Investigated with Computer Simulations and Experiments. Journal of Analytical Atomic Spectrometry, 2006, 21, pp. 910.

[52]: J. Nölte. ICP Emission Spectrometry: A Practical Guide; Wiley-VCH: Weinheim, 2003; p 267.

[53]: A. P. Thorne, U. Litzén, S. Johansson. Spectrophysics: Principles and Applications; Springer: Berlin ; New York, 1999.

[54]: M. V. Belkov, D. A. Borisevich, K. Y. Catsalap, M. A. Khodasevich. Multivariate Calibration of Concentrations of C, Mn, Si, Cr, Ni, and Cu in Low-Alloy Steels from Raw Low-Resolution Spectra Obtained By Laser-Induced Breakdown Spectroscopy. Journal of Applied Spectroscopy, 2021, 88, pp. 970–974.

[55]: Y. Dai, C. Song, X. Gao, A. Chen, Z. Hao, J. Lin. Quantitative Determination of Al–Cu–Mg–Fe–Ni Aluminum Alloy Using Laser-Induced Breakdown Spectroscopy Combined with LASSO–LSSVM Regression. Journal of Analytical Atomic Spectrometry, 2021, 36, pp. 1634–1642.

[56]: C. Dutouquet, G. Gallou, O. Le Bihan, J. B. Sirven, A. Dermigny, B. Torralba, E. Frejafon. Monitoring of Heavy Metal Particle Emission in the Exhaust Duct of a Foundry Using LIBS. Talanta, 2014, 127, pp. 75–81.

[57]: D. Girón, T. Delgado, J. Ruiz, L. M. Cabalín, J. J. Laserna. In-Situ Monitoring and Characterization of Airborne Solid Particles in the Hostile Environment of a Steel Industry Using Stand-off LIBS. Measurement. 2018, 115, pp. 1–10.

[58]: M. A. Sperança, D. F. Andrade, J. P. Castro, E. R. Pereira-Filho. Univariate and Multivariate Calibration Strategies in Combination with Laser-Induced Breakdown Spectroscopy (LIBS) to Determine Ti on Sunscreen: A Different Sample Preparation Procedure. Optics & Laser Technology, 2019, 109, pp. 648–653.

[59]: P. Yaroshchyk, D. L. Death, S. J. Spencer. Comparison of Principal Components Regression, Partial Least Squares Regression, Multi-Block Partial Least Squares Regression, and Serial Partial Least Squares Regression Algorithms for the Analysis of Fe in Iron Ore Using LIBS. Journal of Analytical Atomic Spectrometry, 2012, 27, pp. 92–98.

[60]: L. Gómez-Nubla, J. Aramendia, S. Fdez-Ortiz de Vallejuelo, J. M. Madariaga. Analytical Methodology to Elemental Quantification of Weathered Terrestrial Analogues to Meteorites Using a Portable Laser-Induced Breakdown Spectroscopy (LIBS) Instrument and Partial Least Squares (PLS) as Multivariate Calibration Technique. Microchemical Journal, 2018, 137, pp. 392–401.

[61]: T. Takahashi, B. Thornton, T. Sato, T. Ohki, K. Ohki, T. Sakka. Temperature Based Segmentation for Spectral Data of Laser-Induced Plasmas for Quantitative Compositional Analysis of Brass Alloys Submerged in Water. Spectrochimica Acta Part B: Atomic Spectroscopy, 2016, 124, pp. 87–93.

[62]: C. R. Ytsma, C. A. Knudson, M. D. Dyar, A. C. McAdam, D. D. Michaud; L. M. Rollosson. Accuracies and Detection Limits of Major, Minor, and Trace Element Quantification in Rocks by Portable Laser-Induced Breakdown Spectroscopy. Spectrochimica Acta Part B: Atomic Spectroscopy, 2020, 171, pp. 105946.

[63]: K. Backhaus, B. Erichson, W. Plinke, R. Weiber. Multivariate Analysemethoden, Springer Gabler Berlin, Heidelberg, 14th Edition, 2016.

[64]: ISO 16232:2018-12, Straßenfahrzeuge - Sauberkeit von Komponenten Für Fluidsysteme; Deutsche Fassung. https://www.dinmedia.de/de/norm/iso-16232/300157067.

[65]: C. Pedrosa, N. M. Almeida, F. Pereira, C. M. Reis, P. Braga. Impact of Metallic Particle Contamination in Relation to Product Requirements in the Automotive Industry (Case Study)—Part 1. In Occupational and Environmental Safety and Health IV; Arezes, P. M., Baptista, J.

S., Melo, R. B., Castelo Branco, J., Carneiro, P., Colim, A., Costa, N., Costa, S., Duarte, J., Guedes, J. C., Perestrelo, G., Eds.; Studies in Systems, Decision and Control; Springer International Publishing: Cham, 2023; Vol. 449, pp 99–109.

[66]: D. Schulz. Strategien gegen Partikel: Bauteilsauberkeit von der Konstruktion bis zur Montage. J Oberfl Techn 2010, 50, pp. 46–49.

[67]: F. H. Rögner, M. Pfeilschifter. Markt- und Trendanalyse in der Industriellen Teilereinigung 2020; F. H. Rögner, Ed.; Fraunhofer-Institut für Organische Elektronik, Elektronenstrahl- und Plasmatechnik FEP: Dresden, 2021.

[68]: CleanControlling GmbH. Particle stamp https://www.cleancontrolling.com/en/technical/products-services/products/particle-monitoring/particle-stamp (last accessed 21.11.2024).

[69]: CleanControlling GmbH. C|PS2 - Das Kompaktsystem für die Partikelsaugextraktion. https://www.cleancontrolling.com/technical/produkte-leistungen/produkte/cps2-kompaktsystem (last accessed 21.11.2024).

[70]: JOMESA HFD: Metall - Nichtmetall Unterscheidung. https://www.jomesa.com/german/filter_analysis/Metall_Nichtmetall.html (last accessed 21.11.2024).

[71]: D. A. Skoog, J. J. Leary. Raman-Spektroskopie. Instrumentelle Analytik, Springer-Verlag Berlin Heidelberg 1996, pp. 321–334.

[72]: A. Douglas, J. J. L. Skoog. Oberflächenanalyse in Elektronenstrahlen. In Instrumentelle Analytik; Skoog, D. A., Leary, J. J., Eds.; Springer-Lehrbuch; Springer Berlin Heidelberg: Berlin, Heidelberg, 1996; pp. 415–433.

[73]: D. A. Scott, R. Schwab. Metallography in Archaeology and Art; Cultural Heritage Science; Springer International Publishing: Cham, 2019.

[74]: E. Roos, K. Maile. Werkstoffkunde für Ingenieure: Grundlagen, Anwendung, Prüfung, 5th Edition.; Springer Vieweg: Berlin, 2015; pp. 421.

[75]: H. J. Bargel, G. Schulze. Grundlagen der Metall- und Legierungskunde. In Werkstoffkunde; Bargel, H.-J., Schulze, G., Eds.; Springer Berlin Heidelberg: Berlin, Heidelberg, 2008; pp 1–66.

[76]: P. W. Atkins, J. De Paula, J. Keeler. Atkins' Physical Chemistry, 12th edition.; Oxford University Press: New York, NY, 2023.

[77]: A. Hofmann. Physical Chemistry Essentials, 1st edition. 2018.; Springer International Publishing : Imprint: Springer: Cham, 2018.

[78]: H. J. Bargel, G. Schulze. Werkstoffkunde: jetzt mit Aufgaben und Lösungen, 11th edition, Eds.; Springer-Lehrbuch; Springer Vieweg: Berlin Heidelberg, 2012.

[79]: G. Benkißer, T. Bernthaler, K. Cyrener. Aluminium Und Aluminiumlegierungen. In Metallografie; Oettel, H., Schumann, H., Eds.; Master; Wiley-VCH Verlag GmbH & Co. KGaA: Weinheim, 2016; pp 815–833.

[80]: K. Schiebold. Zerstörende Werkstoffprüfung: Metallographische Werkstoffprüfung und Dokumentation der Prüfergebnisse; Springer Vieweg: Berlin, Heidelberg, 2018.

[81]: G. Benkißer, T. Bernthaler, K. Cyrener. Metallografie: Mit einer Einführung in die Keramografie, 15th edition, Wiley-VCH Verlag GmbH & Co. KGaA: Weinheim, 2016.

[82]: E. Hornbogen, H. Warlimont, B. Skrotzki. Metalle: Struktur und Eigenschaften der Metalle und Legierungen, 7th edition, Springer Vieweg: Berlin, 2019.

[83]: DIN EN ISO 16120-2: Walzdraht aus unlegiertem Stahl zum Ziehen - Teil 2: Besondere Anforderungen an Walzdraht für allgemeine Verwendung, Beuth Verlag GmbH, Berlin, 2017.

[84]: C. Kammer. Weiterverarbeitung und Anwendung, 17th edition, Aluminium Taschenbuch; Beuth: Berlin; Wien; Zürich, 2014.

[85]: E. Hornbogen, B. Skrotzki. Mikro- und Nanoskopie der Werkstoffe; Springer Berlin Heidelberg: Berlin, Heidelberg, 2009.

[86]: T. A. Labutin, A. M. Popov, V. N. Lednev, N. B. Zorov. Correlation between Properties of a Solid Sample and Laser-Induced Plasma Parameters. Spectrochimica Acta Part B: Atomic Spectroscopy 2009, 64, pp. 938–949.

[87]: D. A. Cremers, L. J. Radziemski. Handbook of Laser-Induced Breakdown Spectroscopy, 2nd edition.; Wiley, A John Wiley & Sons, 2013.

[88]: V. K. Unnikrishnan, K. Alti, V. B. Kartha, C. Santhosh, G. P. Gupta, B. M. Suri. Measurements of Plasma Temperature and Electron Density in Laser-Induced Copper Plasma by Time-Resolved Spectroscopy of Neutral Atom and Ion Emissions. Pramana - J Phys 2010, 74, pp. 983–993.

[89]: A. Kramida, Y. Ralchenko. NIST Atomic Spectra Database, NIST Standard Reference Database 78, 1999.

[90]: W. Lochte-Holtgreven. Plasma Diagnostics; American Vacuum Society classics; AIP Press: New York, 1995.

[91]: D. C. Harris, D. C. Harris. Lehrbuch der quantitativen Analyse, 2nd edition, Springer Spektrum: Berlin Heidelberg, 2014.

[92]: J. D. Pedarnig, S. Trautner, S. Grünberger, N. Giannakaris, S. Eschlböck-Fuchs, J. Hofstadler. Review of Element Analysis of Industrial Materials by In-Line Laser—Induced Breakdown Spectroscopy (LIBS). Applied Sciences 2021, 11, pp. 9274.

[93]: J. P: Grotzinger, S. Gupta, M. C. Malin, D. M. Rubin, J. Schieber, K. Siebach, D. Y. Sumner, K. M. Stack, A. R. Vasavada, R. E. Arvidson, F. Calef, L. Edgar, W. F. Fischer, J. A. Grant, J. Griffes, L. C. Kah, M. P. Lamb, K. W. Lewis, N. Mangold, M. E. Minitti, M. Palucis, M. Rice, R. M. E. Williams, R. A. Yingst, D. Blake, D. Blaney, P. Conrad, J. Crisp, W. E. Dietrich, G. Dromart, K. S. Edgett, R. C. Ewing, R. Gellert, J. A. Hurowitz, G. Kocurek, P. Mahaffy, M. J. McBride, S. M. McLennan, M. Mischna, D. Ming, R. Milliken, H. Newsom, D. Oehler, T. J. Parker, D. Vaniman, R. C. Wiens, S. A. Wilson. Deposition, Exhumation, and Paleoclimate of an Ancient Lake Deposit, Gale Crater, Mars. Science 2015, 350.

[94]: A. Ciucci, M. Corsi , V. Palleschi , S. Rastelli , A. Salvetti , and E. Tognoni . New procedure for quantitative elemental analysis by laser-induced plasma spectroscopy. Appl. Spectrosc. 53, 1999, pp. 960 – 964.

[95]: D. Bulajic, M. Corsi, G. Cristoforetti, S. Legnaioli, V. Palleschi, A. Salvetti, E. A. Tognoni. Procedure for Correcting Self-Absorption in Calibration Free-Laser Induced Breakdown Spectroscopy. Spectrochimica Acta Part B: Atomic Spectroscopy 2002, 57, pp. 339–353.

[96]: F. Rezaei, G. Cristoforetti, E. Tognoni, S. Legnaioli, V. Palleschi, A. Safi. A Review of the Current Analytical Approaches for Evaluating, Compensating and Exploiting Self-Absorption in Laser Induced Breakdown Spectroscopy. Spectrochimica Acta Part B: Atomic Spectroscopy 2020, 169, pp. 105878.

[97]: Z. Q. Hao, L. Liu, R. Zhou, Y. W. Ma, X. Y. Li, L. B. Guo, Y. Lu, X. Y. Zeng. One-Point and Multi-Line Calibration Method in Laser-Induced Breakdown Spectroscopy. Optics Express, 2018, 26, pp. 22926–22933.

[98]: R. Henrion, G. Henrion. Multivariate Datenanalyse: Methodik und Anwendung in der Chemie und verwandten Gebieten; Springer: Berlin Heidelberg New York London Paris Tokyo Hong Kong Barcelona Budapest, 1995.

[99]: M. D. Dyar, M. L. Carmosino, E. A. Breves, M. V. Ozanne, S. M. Clegg, R. C. Wiens. Comparison of Partial Least Squares and Lasso Regression Techniques as Applied to Laser-Induced Breakdown Spectroscopy of Geological Samples. Spectrochimica Acta Part B: Atomic Spectroscopy, 2012, 70, pp. 51–67.

[100]: T. F. Boucher, M. V. Ozanne, M. L. Carmosino, M. D. Dyar, S. Mahadevan, E. A. Breves, K. H. Lepore, S. M. Clegg. A Study of Machine Learning Regression Methods for Major Elemental Analysis of Rocks Using Laser-Induced Breakdown Spectroscopy. Spectrochimica Acta Part B: Atomic Spectroscopy 2015, 107, pp. 1–10.

[101]: S. Moncayo, S. Manzoor, J. D. Rosales, J. Anzano, J. O. Caceres. Qualitative and Quantitative Analysis of Milk for the Detection of Adulteration by Laser Induced Breakdown Spectroscopy (LIBS). Food Chemistry 2017, 232, pp. 322–328.

[102]: Z. Wang, J. Feng, L. Li, W. Ni, Z. Li. A Multivariate Model Based on Dominant Factor for Laser-Induced Breakdown Spectroscopy Measurements. Journal of Analytical Atomic Spectrometry, 2011, 26, pp. 2289.

[103]: J. P. Castro, E. R. Pereira-Filho. Twelve Different Types of Data Normalization for the Proposition of Classification, Univariate and Multivariate Regression Models for the Direct Analyses of Alloys by Laser-Induced Breakdown Spectroscopy (LIBS). J. Anal. At. Spectrom. 2016, 31, pp. 2005–2014.

3. Results and Discussion

3.1. Chapter 1:
Development of Laser-Induced Breakdown Spectroscopy-Methods for Rapid Element Quantification in Alloy Particles in Technical Cleanliness Analysis

Maria Lanzinger[a,b], Dominik Huber[a], Virginia Merk[c], Stephanie Kaufmann[a], Michael Schuster[b], Natalia Ivleva[b]

[a]BMW AG, 80809 Munich, Germany

[b]Department of Chemistry, Technical University of Munich, 85748 Munich, Germany

[c]LTB Lasertechnik Berlin GmbH, 12489 Berlin, Germany

3.1.1. Declaration of Contribution and Summary

Maria Lanzinger, Dominik Huber, Virginia Merk, Stephanie Kaufmann, Michael Schuster, Natalia P. Ivleva

Spectrochimica Acta Part B: Atomic Spectroscopy **2023,** 205, 106691, DOI: 10.1016/j.sab.2023.106691

This work studies the representativeness of in-house generated Al alloy particles for their respective bulk material using LIBS. Multivariate PLS-regression models have been developed, optimized, and validated to assess representativeness for ten common aluminium alloy elements, specifically for the use in particle characterization.

ML planned and executed the LIBS measurements for training and validation. For PLS-regression, the spectra are baseline corrected and normalized to a matrix (Al) signal. Additionally, dominant regions are selected, and the models are divided into sub-calibrations, when favourable. ML optimized and developed the models as well as implemented the Matlab® code. SK, VM and DH contributed to their conception and optimization. The models are successfully validated using bulk CRMs both included and not included into calibration. This way, the functionality and applicability of the developed algorithms are also shown for matrices unknown to the respective PLS-regression models.

ML performed in-house generation of reference particles by first turning four validation CRMs collecting the shavings. Afterwards the scrapes were hand-grinded and sieving according to five different size classes of 45 -- 100 µm, 100 -- 250 µm, 250 -- 500 µm, 500 -- 1000 µm and > 1000 µm. The sieve discriminates the particles according to their width.

ML and SK performed microstructure analysis of the particles to find a homogeneous distribution of crystal phases and no damage to specific structures in the samples. This finding was supported by the following LIBS analysis of ten particles from each size class, performed by ML, as no correlation has been found between particle size and bulk material.

The study concluded that all particle size classes have a high representativeness for their bulk material after being treated with mechanical force. This result allows for improved transferability between particle and bulk material, enabling direct contamination source identification. These results also present an easy and cheap way to generate in-house

reference particles of different chemical compositions. All authors contributed in discussion and interpretation of the results.

NI, MS and SK supervised and reviewed the work.

3.1.2. Abstract

In today's industrial production, technical cleanliness with respect to eliminating particle contamination is a major factor in guaranteeing safe and high-quality products. Metal particles need to be avoided in particular, due to their hard and conductive nature. By characterizing the particle composition as accurately as possible, the corresponding source material is more likely to be identified, in order to target the origin of the contamination efficiently.

If particles are generated through mechanical processes the microstructure can be damaged, possibly changing the sample composition and consequently hampering the identification of the source material. Therefore, we studied the representativeness of in-house generated aluminium reference particles to their source bulk material applying quantitative element analysis. The used multivariate quantification models for ten aluminium alloy elements were specially designed for particle characterization.

Validation and limit of quantification calculations showed the functionality and applicability in the calibrated alloy element concentration ranges for particles down to a size of 45 µm.

In this study the representativeness of particle samples to their bulk material could be shown for the entire size range analysed (> 1000 – 45 µm) using laser-induced breakdown spectroscopy (LIBS). The LIBS measurements were complemented by microstructure analysis of the investigated materials, showing no damage to specific phases. The combination of these analyses enables an improved transferability of particle analysis to the possible bulk material as well as the easy in-house generation of internal reference particles of different chemical composition.

Highlights:

- Application of LIBS in modern technical cleanliness analysis.
- Development of PLS quantification models optimized for particle characterization.
- Discussion of impact of microstructure features on element quantification.
- Representativeness of particles for bulk is studied for five particle size classes.

Keywords: Laser-induced breakdown spectroscopy (LIBS), Technical cleanliness analysis (TCA), multivariate calibration, particle characterization, aluminium alloy.

3.1.3. Introduction

Technical cleanliness analysis (TCA) and measures have been known in the automotive sector for over a decade to ensure high-quality products. Both a process and product can be disturbed or damaged when surfaces or components are contaminated by, depending on the process, liquids (e.g. oil, solvents) or solids (metallic, non-metallic particles). While, in general, liquid contaminations disturb processes like chemical resistance and adhesiveness, solid particles can cause damages to the components due to their abrasiveness, hardness and electrical conductivity [1-3].

TCA measures are aimed at preventing contamination in the production environment by the optimization of logistics, handling and mechanical processes. Naturally, most mechanical processes (e.g. drilling, milling) can produce particles of both the processed component and the used tool. Some of these particles can remain on the component despite careful handling and in-state cleaning processes, potentially harming the resulting product. To identify and eliminate such particle sources, it is necessary to characterize the samples' material as accurately as possible. In standard TCA, surface impurities on particle contaminations, like oil residue or other organic matter, is not of importance, as they do not provide additional information about the particles' origin.

Due to sustainability regulations and the resulting shift to propulsion systems without fossil fuels e.g. from the EU government [4], most automotive companies have recently expanded their product portfolio to electrically driven vehicles. Critical functional areas in the systems involved (e.g. electric engines, high-voltage storages (HVS)) are vulnerable to particle contaminations, since particles can lead e.g. to short-circuits which can result in thermal events. Therefore, TCA measures are increasingly implemented in most production steps to ensure high-quality and safe products [1,2].

In TCA, metal particles are of special interest due to their capability to cause mechanical damage (wear of mechanically moving components) and electrical conductivity [1,2]. Identifying the origin of such metallic particles can be challenging due to multiple reasons: Firstly, the inherent inhomogeneity of the bulk material (in the sense of whole components) [5-7] should be mentioned. Generally, the inhomogeneity of element distribution can be partly compensated by analyzing a sufficiently large sample volume. Since this is not possible for small subsamples, like particles, the inhomogeneity of the original material might not be compensated for. This in turn can reduce the representativity of the particles of their original material.

Secondly, the high variety of quantitative element compositions in alloys can be challenging. Considering all aluminum alloys used in industrial production, their composition range is rather broad, e.g. covering silicon concentrations of 0 to roughly 17 $\%_{wt}$. This variety of alloy compositions should therefore be considered in the development of calibration models for industrial use, meaning they need to cover a broad concentration range with different microstructures.

Thirdly, alloy materials with similar applications often show highly similar element compositions, hampering differentiation of individual alloys. Some alloy compositions can only be differentiated by element quantification methods, for example AlSi9Cu3(Fe) and AlSi9Cu3(Fe)(Zn), whose compositions only differ in their zinc concentration.

For the analysis of TCA relevant particles laser-induced breakdown spectroscopy (LIBS) is a suitable method since it is highly sensitive, fast in measurement, needs only minimal sample preparation and consumes little of the sample [7-9]. LIBS has already been successfully used for analyzing the elemental composition of various samples like soil [10,11], polymers [12,13] and metals [14-19]. Particles have been characterized with LIBS qualitatively in the context of environmental analysis [10,11,16] and industrial processes, like sorting [17,18] or quality control [19].

In contrast to the exemplary named industrial processes of sorting and quality control, which generally implement a qualitative classification of metal alloys, TCA additionally needs quantitative information for detailed characterization [20]. Also, the sample size differs for the named applications. While in industrial sorting, larger scraps of 1 – 30 mm [17, 18] are analyzed, particles down to the size of 45 µm are of interest in TCA [1]. In this special application of quantitative element analysis of metal alloy particles, to the best of our knowledge, studies have not been published yet.

While LIBS is well established for the qualitative analysis of large samples, the quantification of elements in particles via LIBS is still challenging due to the influence of sample inhomogeneity and matrix effects [21].

There are several studies for the development of LIBS quantification models using partial least square (PLS) regression [22-25] or principal component analysis (PCA) [20,24,26,27]; especially for complex matrices the named multivariate approaches are already established [21,28], but up to this point they have not been optimized for the quantitative analysis of small particles.

The scope of this work is the development and optimization of PLS regression models for ten different elements in aluminium alloys which can be applied to the quantitative analysis of small particles. The applicability of the models for analysing different in-house generated particle size classes down to 45 µm is discussed. The results are used to assess the impact of particle size on their representativity for the corresponding origin material and the comparability of different size classes.

3.1.4. Material and Methods

Samples

For the development of calibration models for ten different elements in aluminium alloy particles, a set of 51 disc shaped certified reference materials (CRMs) was used. Out of those 51 CRMs, nine were picked as validation materials. Additionally, eight CRMs not included into calibration were used for validation. Detailed information about the used CRM is shown in the supporting information (Table S1). An overview over the covered concentration ranges as well as the number of CRMs used for each element is displayed in Table S2.

The studied particles were generated in-house by lathing of bulk CRMs (Table S1, Appendix). To minimize surface impurities, the CRMs' surface was previously cleaned by removing 1-2 mm of the surface layer. To generate particles with adequate morphology, material and size representing particles which can be found in TCA, the chips resulting from lathing were ground in a mortar. To divide into individual size classes, the ground samples were sieved (AS 200, Retsch Maschinen GmbH, Setzingen, Germany) for 10 min at an amplitude of 0.5 mm in size classes 45-100 µm (a), 100-250 µm (b), 250-500 µm (c), 500-1000 µm (d), >1000 µm (upper limit approx.: 5000 µm) (e). Below a size of 45 µm metal particles are not relevant for TCA applications. Therefore, they were not considered in this work.

The results of this in-house particle generation and size classification were validated by light microscopy (HFD, JOMESA, Munich, Germany). Validation results regarding size distribution and particle morphology can be found in the supporting information in Fig. S1 (Appendix). The microscopic size measurements are calibrated with respective particle norms provided by the producer.

For LIBS measurements particles are fixed on an adhesive carbon tab (25 mm, PLANO, Wetzlar, Germany).

Experimental Procedure

LIBS measurements are performed using a coupled LIBS / Raman device (CORALIS, LTB Lasertechnik Berlin, Germany). With the built-in imaging system particles can be displayed with a magnification of 10× using the overview lens and of 80× using the detail lens. Optical and laser focus are on the sample surface with focal lengths of 70 mm for the collector optics and 100 mm for the laser focus optics. The device uses a pulsed Nd:YAG laser at 1064 nm with continuously variable laser energy up to 50 mJ for LIBS analysis. Using the described focal length, the resulting laser spot has a diameter of about 20 µm which enables the analysis of small particles. The used Echelle spectrometer Aryelle Butterfly (LTB Lasertechnik Berlin, Germany) covers a wavelength range of 190 -- 25 nm with a spectral resolution of 15000 ($\lambda/\Delta\lambda$).

Measurement parameters used in this work were 5 mJ laser pulse energy, gain of the EM-CCD-camera of 200 and a delay time between laser pulse and measurement of 1.4 µs for all samples. In our preliminary studies of Al-alloys, these parameters showed a good signal-to-noise-ratio for several selected elemental lines. In the calibration each CRM is represented by 100 measurements at different locations with seven laser pulses averaged on each location.

Validation measurements were done independently of the calibration measurements. For validation, LIBS measurements were performed at 40 different locations, also with seven pulses at each location. Ten spectra were averaged resulting in four analyses for each validation CRM.

For each size class and each material ten randomly picked particles were analysed by performing three measurements at different locations with seven laser pulses at each measurement point. Some particles disappeared or were “shot through” at the laser-sample interaction point after the measurement, which results in an increased carbon signal due to the used carbon tab for immobilization of the particles. Such spectra are not included in the evaluation.

For microstructure analysis, particles from size class (c) (250 -- 500 µm) are embedded in Technovit 2000LC (Kulzer GmbH, Hanau, Germany), sanded (15 µm, 6 µm) and polished (3 µm, 1 µm) before optical microscopy on a Polyvar Met 66 (Leica Microsystems GmbH, formally Reichert-Jung, Wetzlar, Germany) was conducted.

Data Treatment

For assignment of the individual emission lines in the LIBS spectra, the NIST atomic spectra database [29] was used.

In this work, quantification models for ten elements (Si, Cu, Mn, Ti, Fe, Zn, Mg, Ni, Pb, Cr) were developed using PLS regression. Development and validation of calibration models was carried out using in-house written Matlab® (2021a edition, Mathworks, Natick, MA, USA) programs. The spectra were processed in the following manner:

First, baseline correction using the Matlab®function *msbackadj* and normalization were performed on each spectrum. The spectra were normalized to the signal intensity of the aluminium line at 266.04 nm, as it does not show self-reversal or overlaps with other signals. Furthermore, for the creation of quantification models of each element only parts of the spectra (wavelength sections) are used. The regions are chosen in such a way, that mainly non-disturbed element lines are included, in contrast to evaluating the whole spectral range. This way, the impact on the PLS of signals from other sources, which have no correlation with the analyte concentration, is reduced. This approach is similar to the dominant factor based PLS by Wang et al., in which the most important analyte signals are chosen and more strongly weighted [30]. An exception to this is the calibration of silicon in concentrations above 4 $\%_{wt}$, where the whole spectral range is evaluated, as the relevant signals are detected very well by the algorithm.

The chosen spectral regions for PLS regression are shown in the supporting information (Table S3, Appendix).

The quality of the developed quantification models is assessed by conducting validation measurements and calculating the coefficient of determination (R^2). To validate the developed quantification models, the absolute deviation of the calculated and the reference concentration is determined. Additionally, the validation results are visualized using boxplots.

LOQ Approximation

In this study we were aiming to build stable models to be used in industrial TCA. Therefore, for us, stability of the models is more important than sensitivity. In literature, different approaches are described to assess limit of detection (LOD) and limit of quantification (LOQ) for multivariate calibration models. Most of them extend the calculation of univariate figures to

multivariate systems [31-33] or use a univariate surrogate function [34-36]. In this work, the latter method is used to approximate LOQ by identifying an analyte signal for each calibration, which is strongly weighted in the PLS and one of the first signals to disappear in the noise for low analyte concentrations. This signal will not be distinguishable from the noise and therefore cannot provide information for the PLS evaluation. Since the signal is strongly weighted, its disappearance will strongly decrease the quantification accuracy, which makes it possible to use this signal as indicator for LOQ.

A univariate calibration is performed using the chosen signal as a surrogate function. Afterwards LOQ are calculated using the confidence interval resulting from the calibration curve (Fig. S2, Appendix). This analytically proven method considers the linear range of the calibration and is therefore related more closely to the calibration curve itself, compared to using the deviation of the background signal.

After calculating the intercept of upper confidence interval with the y-axis, a horizontal line is drawn until it intercepts the lower confidence interval. The analyte concentration at this interception point corresponds to the LOQ for this univariate calibration [36]. To decrease the risk of underestimating LOQ it is rounded up. Therefore, it is subsequently addressed as LOQ_{approx}.

3.1.5. Results and Discussion

Regression Model Design

The calibration models developed in this work are designed to characterize industrially used aluminium alloys. Since the industrially used aluminium alloys show a high variation in composition, the models need to cover large concentration ranges with various microstructures. The LIBS-laser interacts differently with the microstructures, impacting the plasma and therefore, impacting the resulting spectra and the performance of the quantification models. In this study, these changes in sample matrix over a large concentration range are tackled by splitting the quantification models.

This approach and its limits will be discussed in the following section in detail using the silicon calibration model covering concentrations of 0 - 12.7 $\%_{wt}$. For setting up the calibration models, 49 CRMs are used, nine of which are additionally used for validation. Furthermore, eight CRMs

not part of the calibration are used for validation. The CRMs' details are summarized in Tables S1-S2 (Appendix).

In Fig. 15 the recovery plots of the developed silicon calibrations are shown. The x-axis shows the reference concentration of the sample, while on the y-axis the calculated values are displayed. In dark blue, a 45-degree line is displayed to show the deviation of found and certified concentrations.

In Fig. 15, A, a 'global' calibration covering the whole concentration range (0 -- 12.7 $\%_{wt}$), with a mismatch between calculated and certified concentrations can be seen. To approximate the data using a linear fit, two separate functions with different slopes are needed (Fig. 1, A). We therefore generated three different calibration models: A 'global' calibration over the whole concentration range (Fig. 1, A), which is used for a rough determination of the concentration, and two 'sub-calibrations' covering high and low concentrations respectively. These yield a detailed assessment of the composition depending on the result of the global quantification (Fig 15, B, C).

For the sub-calibrations, different spectral regions (see chapter 2.3) were used since not all lines are suitable for the different concentration ranges. While, for instance, for low concentrations, intense signals can be used, the same lines could be affected by self-reversal or other disturbances for high concentrations. Therefore, they were not included in these sub-calibrations.

In the gap between 2 and 6 $\%_{wt}$ of silicon concentration no CRMs were available, which is why the calibration is expected to show less accurate results in this region. But since most aluminium alloys which are of interest in TCA analysis have either high (> 6 $\%_{wt}$) or low (< 2 $\%_{wt}$) silicon concentrations [37], inaccuracy in this concentration region is acceptable.

In addition to the silicon model, calibration models of zinc and magnesium were split into sub-calibrations at 4 and 3 $\%_{wt}$ respectively. The splitting point was selected as explained above for silicon, according to the slope of the recovery fit plot. The corresponding concentration and evaluated spectral ranges are displayed in Table S3 (Appendix).

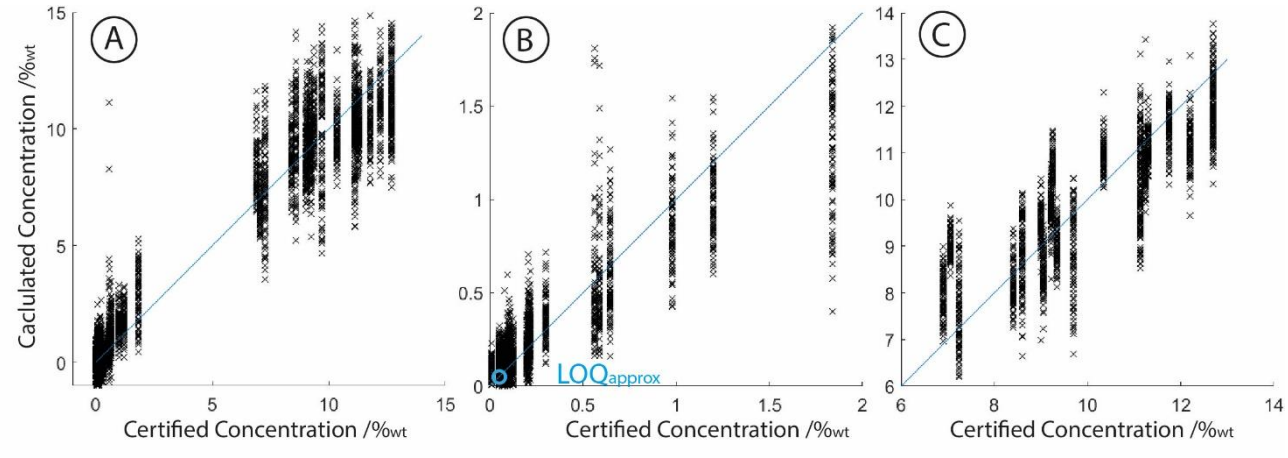

Figure 15: Recovery plots of silicon-PLS-calibration. (A): Global calibration and sub-calibrations for low (B) and high (C) concentration regions to increase the accuracy of the quantification model. In (B) LOQ_{approx} is indicated in blue.

Regression Model Performance

To assess the performance of the developed quantification models, the limit of quantification (LOQ_{approx}) for each element was approximated and validation measurements were performed. The results are summarized in Table S4 (Appendix). Here, the signals used for univariate calibration ($line_{uv}$), the LOQ_{approx}, the R^2 value for the multivariate calibration models as well as the absolute deviation of the reference concentration are displayed. The results of the validation measurements are shown using the absolute value of the absolute deviations (d_{abs}) from the reference concentration (above the respective $LOQ_{approx.}$). Additionally, the validation results are visualized using boxplots. In Fig. 16 the silicon, manganese and magnesium are displayed; Plots of the remaining alloy elements can be found in the supporting information (Fig. S2, Appendix). In black, the reference concentration is shown, while the blue boxes summarize the results of four independent validation measurements. CRMs not used for calibration are marked with a green star.

Except for copper ($LOQ_{approx.}$: 0.10 %$_{wt}$), the LOQ was approximated to 0.05 %$_{wt}$ for all calibrated elements. This is adequately small for TCA analysis since the commonly used aluminium alloys have concentration norms way above 0.05 %$_{wt}$ or even 0.1 %$_{wt}$. This is visible e.g., for the EN-AW-AlCu6BiPb alloy, whose normed silicon concentration range is between 0-0.40 %$_{wt}$ [37].

The analysis of silicon in CRM 121 (d_{abs} = 2.1 %$_{wt}$) and CRM 3047-2 (d_{abs} = 1.1 %$_{wt}$) as well as the quantification of magnesium in CRM 565 (d_{abs} = 1.81 %$_{wt}$) showed deviations above

1 $\%_{wt}$. These samples possess analyte contents that are less well defined by the quantification models – meaning they are in regions close to the upper or lower limits of the quantification models (CRM 3047-2, CRM 565), or in regions that are not represented well (CRM 121, see Fig. 15 A). Using the developed methods, one must be aware of these limitations and consider them when interpreting the results.

Regarding accuracy, there is no difference visible between CRMs which were used for calibration and those which were not. All generally show low absolute deviations of 0.5 down to 0.002 $\%_{wt}$, implying the stability and accuracy of the developed calibrations for the quantification in aluminium matrices, both known and unknown for the multivariate models.

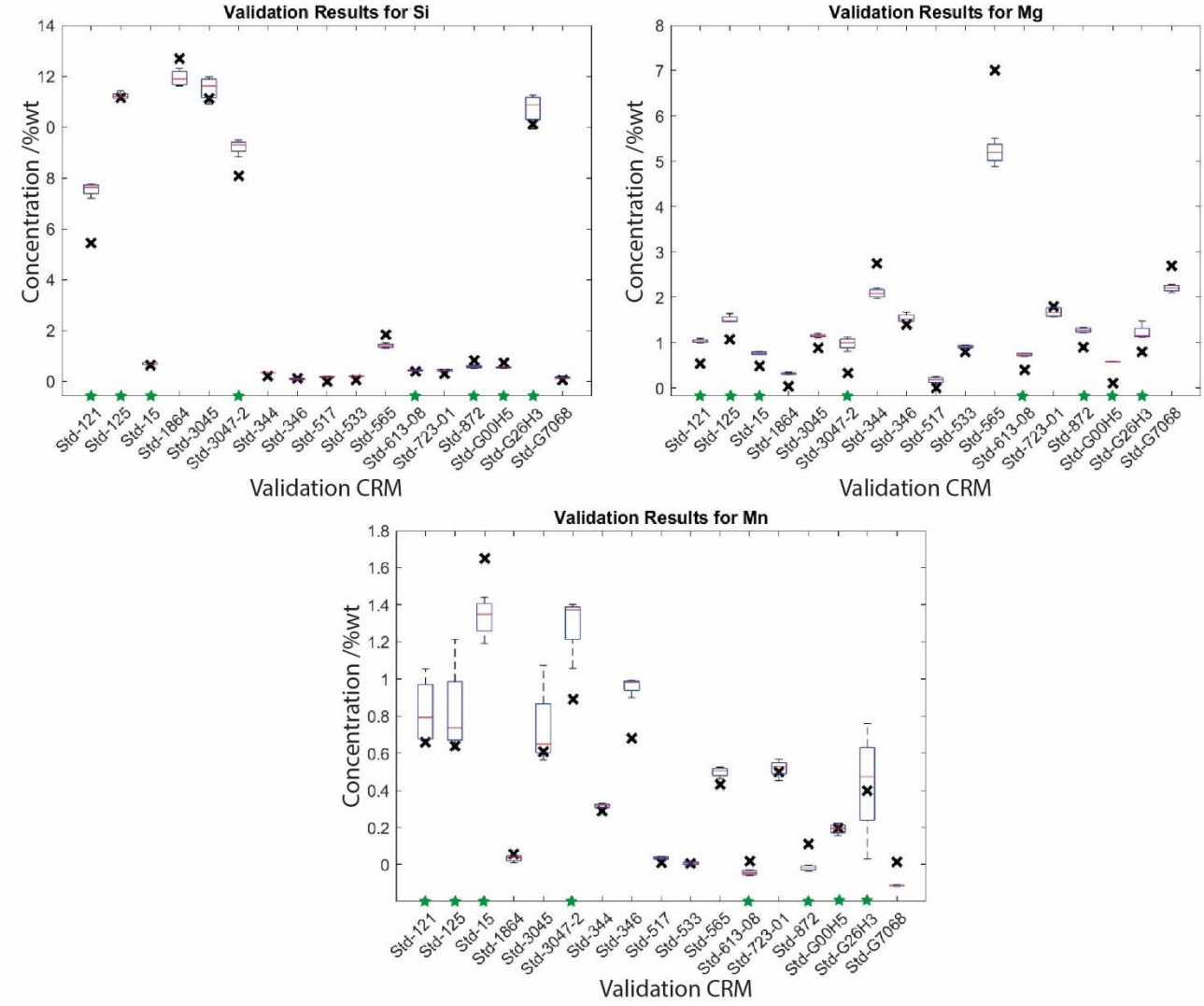

Figure 16: Visualization of validation for calibration models of silicon (top left), magnesium (top right) and manganese (bottom). The black cross shows the reference concentration, while the boxes summarize the quantification results of four individual validation measurements. CRMs marked with green stars are not part of the calibration.

Quantitative Particle Characterization

The developed quantification models optimized for aluminium alloy particle characterization, were shown to be valid for different matrices by analysing bulk CRMs. In the following they are applied for the quantification of particle composition to gain insight into the representativeness for the material they have originated from. This was done by comparing the composition of particulate material to their respective origin material. Additionally, the particles' size was taken into account by studying the representativeness of different particle size classes.

Particles of interest in TCA are predominantly found in production – mostly after investigating irregularities in the production system. By the time the particles are isolated, they have usually been subjected to high forces due to mechanical stress, milling or high temperatures. These high forces might change the elemental composition of the sample by melting, or by causing certain phases to break out of the microstructure (Fig. S7, S8, Appendix).

To study how representative a particle composition is with respect to the bulk material, particles generated from six CRMs were analysed regarding their microstructure, as well as their elemental composition. For the sake of clarity only the results for three selected alloy elements, namely silicon, manganese, magnesium and two of the six materials – one cast and one wrought aluminium alloy – are discussed at this point. The results for the other analysed materials can be found in the supporting information (Microstructure: Fig. S5, Boxplots: Fig. S6, Appendix).

Silicon was chosen since it is the most prominent element in cast structures. Manganese and magnesium form two of the most common intermetallic phases in combination with aluminium, enabling an analogy regarding the phase distribution achieved by the microstructure analysis and element quantification.

Fig. Figure 3 shows the microstructure of the cast (D) and wrought aluminium alloy (E). In the microstructure of the alloy D, white α-aluminium dendrites and grey eutectic aluminium-silicon phases are evident; other intermetallic phases are not visible (Figure 3 D). The dendritic structures are spread inhomogeneously over the sample with varying forms and sizes. Their maximum diameter varies between approximately 10 µm and 50 µm. Damage to specific phases of the microstructure like breakouts is not observable. As a reference, damaged particle microstructures are shown in the supporting information (Fig. S7, S8, Appendix).

In the wrought alloy (E) no dendrites are present (Figure 17 E). The grey areas represent intermetallic phases, which are spread homogeneously throughout the white aluminium matrix.

The intermetallic phases are visibly small in size (<10 µm) but differ in morphology; some are formed like slim bands, while other show a more spot-like shape. The exact character of the intermetallic phases cannot be determined from the image alone, but most probably they consist of manganese or magnesium intermetallic phases, since those are most common intermetallic phases in aluminium-wrought alloys [38].

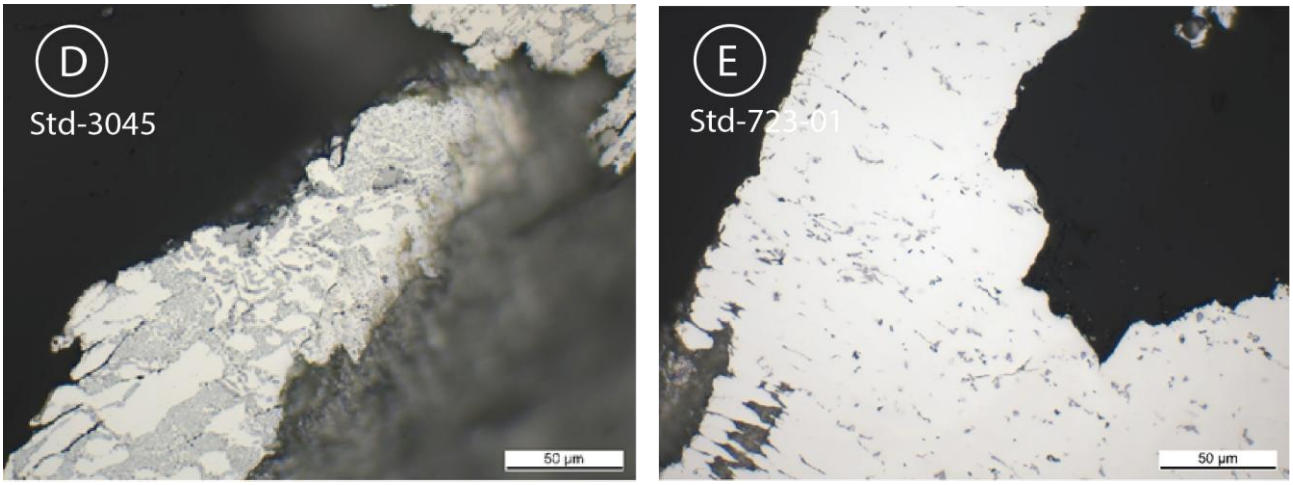

Figure 17: Microstructure analysis of particles (250 -- 500 µm) of a cast (D) and wrought aluminium alloy (E).

Since there is no phase-specific damage to the microstructure visible in the analysed samples, a high representativeness for the bulk material is expected. But the possible effects of sample size cannot be approximated by microstructure alone.

To assess these, LIBS measurements were performed on particles from different size classes and compared to their respective bulk element quantification values. For each size class (a: 45 -- 100 µm, b: 100 -- 250 µm, c: 250 -- 500 µm, d: 500 -- 100 µm, e: > 1000 µm) ten particles were randomly picked and analysed by performing three LIBS measurements at different locations on each particle. The results are shown in the boxplots (Fig. 18). Outliers are defined as values larger or smaller than 1.5 times the 75 %- or 25 %-interquartile, respectively and marked in the plot by red crosses. The blue line denotes the reference concentration given in the CRMs' certificates. The green area represents the results of the bulks' compositions determined by LIBS and is limited by the highest and lowest concentration determined from four bulk analyses.

If the certificate value and the results from the bulk measurements do not overlap, an inaccuracy of the quantification model due to e.g., local matrix effects, is indicated. In this case, a comparison of the results of the particle measurements to the certificate value does not make sense, since the bulk measurements themselves did not yield the certified value; a comparison to the results of the bulk measurements is, therefore, preferred. This procedure is also in

accordance with TCA analytics, as for real samples the identification and, therefore, the representativeness towards the bulk material is of importance, not reaching a theoretical reference value.

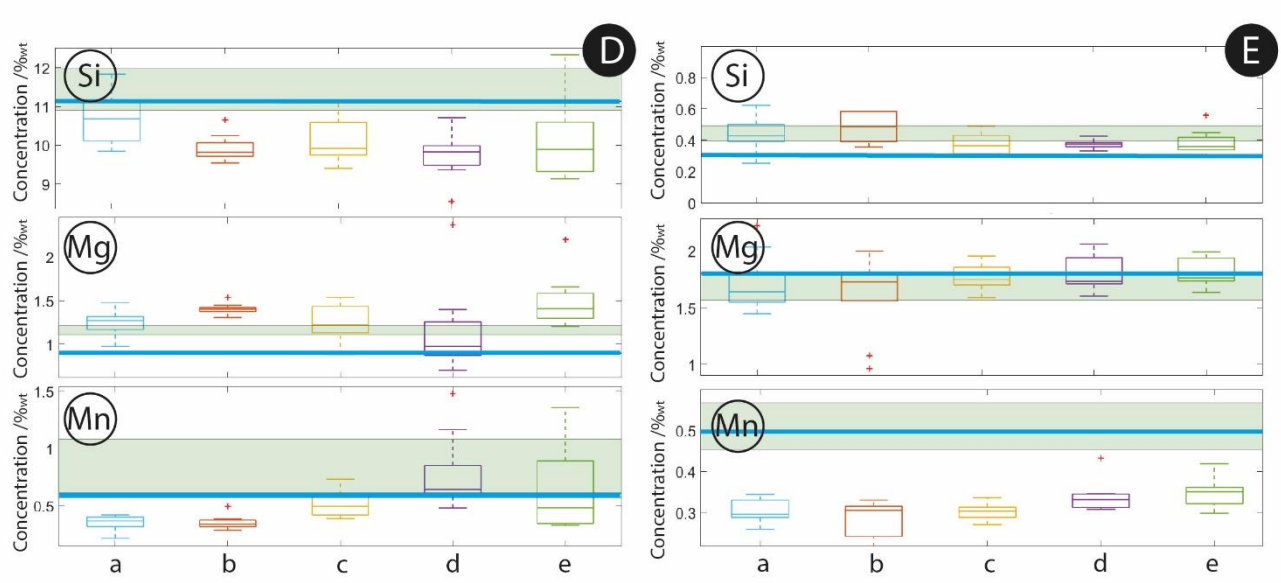

Figure 18: Results of element quantification of particles of different size classes (45 -- 100 µm (a), 100 -- 250 µm (b), 250 -- 500 µm (c), 500 -- 1000 µm (d), > 1000 µm (e)) of the cast (D) and wrought (E) alloy for the elements silicon, magnesium and manganese. The green areas display the range of the quantification results of bulk measurements. The reference concentration specified in the certificate is shown by the blue line.

For the silicon quantification in alloy (E) and magnesium in both alloys, the particles represent the bulk measurements well, independent of their respective size. The distributions of quantification results of all size classes are highly similar to each other and the reference bulk measurements. Therefore, a high representativeness of the particles for the bulk material is demonstrated.

In the cast alloy (D), particle measurements show an underestimation and a rather broad distribution in silicon concentration of up to 2.5 $\%_{wt}$. The latter observation can be assigned to the presence of the aluminium-silicon mixed crystal and α-aluminium dendrites seen in the microstructure and their difference in silicon content. While the eutectic has 11.7 $\%_{wt}$ of silicon, the solubility of this analyte in the dendrites and therefore its concentration is very low [39]. Especially with the small analysis volumes in LIBS, the chance of analysing parts of the sample that are not representative for the bulk composition increases, as only a fracture of the inhomogeneous structure can be represented. We assume, this is the reason for the broad spread in the silicon quantifications in the particulate samples. The general trend to underestimate the silicon content can also be an effect of a local concentration difference in

the samples, for example by breaking out of certain phases. But since such break-outs are not observable in the microstructure analysis, and single particles from classes (a) and (c) also correspond well with the bulk, this is unlikely. Rather we assume macro-segregation in the bulk, hampering the particle generation process or effects of changed sample properties like heat transfer and plasma generation.

Regarding the manganese composition, similar broadening of the boxes for larger size classes can be observed in alloy (D). The manganese distribution cannot be assessed by microstructure analysis, but according to literature its solubility in aluminium is high [39], indicating a homogeneous distribution in the α-aluminium dendrites. Therefore, the argument described for silicon also applies here.

In alloy (E), manganese quantification shows a slight offset of about 0.2 $\%_{wt}$ for particle measurements. As explained above, damage to the microstructure of selective phases is unlikely, concluding effects of macro-segregation. For the application in TCA, the offset is not problematic, due to the generally broad concentration norms (see chapter *Regression model design*).

In both alloys, manganese quantification results show a slight dependency on sample volume: for larger particle size classes, the deviation from the bulk measurements decreases. Due to the lack of observable microstructure damage and the expected homogeneous distribution of manganese, we assume the behaviour is an artifact from the selection of measurement location. On larger particles, the measurement points can be spread over a larger surface, increasing the chance of including multiple phases. This in turn can increase the representativity for the bulk, as we see in this case.

3.1.6. Conclusions

In this study, multivariate quantification models for ten elements in Al-alloys were developed and validated by LIBS using CRMs. The models were successfully validated using CRMs., that have been included into the calibration, as well as CRMs that have not. The low absolute deviations display the high stability of the developed models for unknown matrices with different compositions. By in-house generating particles of five different size classes (size range >1000 – 45 µm) the applicability of the developed LIBS PLS-regression models for the quantification of the elemental composition of the particles was demonstrated. Additionally, an optical analysis of the microstructure was performed by light microscopy.

Comparison of the elemental composition of particles of different size classes from cast and wrought aluminium alloys and the bulk material, showed no systematic correlation between particle size and representativeness for the bulk material. This result is in accordance with optical analysis of the microstructure, as phases were seen to be distributed homogeneously with no damage to specific phases.

In single cases a slight offset with increasing representativeness for larger particle sizes were observed. The offset can be assigned to effects of macro-segregation and the small analysis volume of each particle. Since for larger samples the user has a larger volume to spread the locations over, the chance of including different phases into the analysis increases; in turn increasing the representation of the “mean” bulk concentration.

Generally, these offsets and slight changes in representativity are not significant in the context of TCA, resulting in the particles representing their bulk material well, independent of their size class. On the one hand this opens the possibility for any laboratory working in TCA to easily generate particles in-house, e.g., for use as internal reference standards. Most of the necessary equipment is usually already present in the laboratories or can be cheaply bought. Matrix and element composition can be adjusted individually for different applications while staying consistent with the source material. On the other hand, this finding makes it possible to directly correlate the composition found in an unknown particle to bulk materials, to identify the correct source material.

Of course, the microstructure of the sample is still of high importance and needs to be studied in detail before interpreting the results. Comparing the results of LIBS to established methods, like EDX can facilitate more insight into this topic.

Author contributions

Maria Lanzinger performed conceptualization, experimental execution, data curation, writing of the original draft and editing. PD Dr. Natalia Ivleva, Prof. Dr. Michael Schuster and Dr. Stephanie Kaufmann performed supervision and writing – review and editing. Dr. Dominik Huber and Dr. Virginia Merk performed review and editing.

Conflict of Competing Interest

The project was funded by BMW Group.

Data Availability Statement

Data will be made available on request.

Acknowledgements

We would like to thank Daniela Cipolla (BMW AG Munich) for the preparation and visualization of the microstructures, Alexander Thomas (BMW AG Munich) and Dr. Lutz Pfeiffer (Laser Technik Berlin) for advisory activity.

Appendix A: Supplementary Data

Supplementary data to this article can be found online at https://doi.org/10.1016/j.sab.2023.106691.

3.1.7. References

[1] German Association of the Automotive Industry, VDA 19.1 - Inspection of Technical Cleanliness: Particulate contamination of functionally relevant automotive components, VDA Automotive Standard, Berlin, 2015.

[2] P. Brag, M. Rochowicz, Safety in Electromobility – Technical Cleanliness Between the Poles of Design Requirements and Efficient Production, in: P. Weißgraeber, F. Heieck, C. Ackermann, Advances in Automotive Production Technology – Theory and Application: Stuttgart Conference on Automotive Production, Springer Berlin, Berlin, 2021; pp 319–326.

[3] M. Oravec, A. Divoková, P. Lipovský, M. Karásek; R. Janošík, Technical Cleanliness - a Requirement of Precision Manufacturing, Acta Mechanica Slov., 23, 2019, 46–51.

[4] European Commission. European Green Deal: Commission proposes transformation of EU economy and society to meet climate ambitions, Brussels, 2021.

[5] S. Jantzi, V. Motto-Ros, F. Trichard, Y. Markushin, N. Melikechi, A. Giacomo, Sample treatment and preparation for laser-induced breakdown spectroscopy, Spectrochimica Acta Part B: Atomic Spectroscopy, 115 (2016) 52–63.

[6] K. Danzer, Comparison of sampling procedures for investigation of chemical homogeneity of solids by spark emission spectrography, Spectrochimica Acta Part B: Atomic Spectroscopy, 39 (1984) 949–954.

[7] R. Noll, Eds. Laser-induced breakdown spectroscopy: Fundamentals and applications, Springer, Berlin, 2012.

[8] S. Musazzi, U. Perini, Eds. Laser-induced breakdown spectroscopy: Theory and applications, Springer, Berlin, 2014.

[9] V. Costa, D. Babos, J. Castro, D. Andrade, R. Gamela, R. Machado, M. Sperança, A. Araújo, J. Garcia, E. Pereira-Filho, Calibration strategies applied to laser-induced breakdown spectroscopy: A critical review of advances and challenges, J. Braz. Chem. Soc., 31 (2020) 2439-2451.

[10] X. T. Yan, K.M. Donaldson, C. M. Davidson, Y. Gao, H. Wu, A. M. Houston, A. Kisdi, Effects of sample pretreatment and particle size on the determination of nitrogen in soil by portable LIBS and potential use on robotic-borne remote Martian and agricultural soil analysis systems, RSC Adv. 8 (2018) 36886–36894.

[11] S. C. Jantzi, J. R. Almirall, Characterization and forensic analysis of soil samples using laser-induced breakdown spectroscopy (LIBS), Anal. Bioanal. Chem. 400 (2011) 3341–3351.

[12] S. Grégoire, M. Boudinet, F. Pelascini, F. Surma, V. Detalle, Y. Holl, Laser-induced breakdown spectroscopy for polymer identification. Anal. Bioanal. Chem. 400 (2011) 3331–3340.

[13] V. C. Costa, F. W. B. Aquino, C. M. Paranhos, E. R. Pereira-Filho, Identification and classification of polymer e-waste using laser-induced breakdown spectroscopy (LIBS) and chemometric tools, Polymer Testing. 59 (2017) 390–395.

[14] Y. Dai, C. Song, X. Gao, A. Chen, Z. Hao, J. Lin, Quantitative determination of Al–Cu–Mg–Fe–Ni aluminum alloy using laser-induced breakdown spectroscopy combined with LASSO–LSSVM regression, J. Anal. At. Spectrom. 36 (2021) 1634–1642.

[15] C. Chen, Q. Shi, S. Wang, Q. Lin, Y. Duan, A novel method for metallic element analysis in particle samples using a laser-induced breakdown spectroscopy technique. J. Anal. At. Spectrom. 31 (2016) 1527–1533.

[16] C. Dutouquet, G. Gallou, O. Le Bihan, J. B. Sirven, A. Dermigny, B. Torralba, E. Frejafon, Monitoring of heavy metal particle emission in the exhaust duct of a foundry using LIBS, Talanta. 127 (2017) 75–81.

[17] S. Merk, C. Scholz, S. Florek, D. Mory, Increased identification rate of scrap metal using Laser Induced Breakdown Spectroscopy Echelle spectra, Spectrochimica Acta Part B: Atomic Spectroscopy. 112 (2015) 10–15.

[18] P. Werheit, C. Fricke-Begemann, M. Gesing, R. Noll, Fast single piece identification with a 3D scanning LIBS for aluminium cast and wrought alloys recycling, J. Anal. At. Spectrom. 26 (2018) 2166.

[19] F. Boué-Bigne, Laser-induced breakdown spectroscopy and multivariate statistics for the rapid identification of oxide inclusions in steel products, Spectrochimica Acta Part B: Atomic Spectroscopy. 119 (2016) 25–35.

[20] D. Huber, Development of a composite analysis process with laser-induced plasma spectrometry and multivariate data evaluation for characterizing particles in the field of technical cleanliness analysis [doctoral dissertation, Technical University of Munich, Munich]. mediaTUM.

[21] V. Costa, D. Babos, J. Castro, D. Andrade, R. Gamela, R. Machado, M. Sperança, A. Araújo, J. Garcia, E. Pereira-Filho, Calibration Strategies Applied to Laser-Induced Breakdown Spectroscopy: A Critical Review of Advances and Challenges, J. Braz. Chem. Soc. 31 (2020) 2439-2451.

[22] M. V. Belkov, D. A. Borisevich, K. Y. Catsalap, M. A. Khodasevich, Multivariate Calibration of Concentrations of C, Mn, Si, Cr, Ni, and Cu in Low-Alloy Steels from Raw Low-Resolution Spectra Obtained By Laser-Induced Breakdown Spectroscopy, J. Appl. Spectrosc. 88 (2021) 970–974.

[23] L. Gómez-Nubla, J. Aramendia, S. Fdez-Ortiz de Vallejuelo, J. M. Madariaga, Analytical methodology to elemental quantification of weathered terrestrial analogues to meteorites using a portable Laser-Induced Breakdown Spectroscopy (LIBS) instrument and Partial Least Squares (PLS) as multivariate calibration technique, Microchemical Journal 137 (2018) 392–401.

[24] T. Takahashi, B. Thornton, T. Sato, T. Ohki, K. Ohki, T. Sakka, Temperature based segmentation for spectral data of laser-induced plasmas for quantitative compositional analysis of brass alloys submerged in water, Spectrochimica Acta Part B: Atomic Spectroscopy. 124 (2016) 87–93.

[25] C. R. Ytsma, C. A. Knudson, M. D. Dyar, A. C. McAdam, D. D. Michaud, L. M. Rollosson, Accuracies and detection limits of major, minor, and trace element quantification in rocks by portable laser-induced breakdown spectroscopy, Spectrochimica Acta Part B: Atomic Spectroscopy. 171 (2020) 105946.

[26] M. A. Sperança, D. F. Andrade, J. P. Castro, E. R. Pereira-Filho, Univariate and multivariate calibration strategies in combination with laser-induced breakdown spectroscopy (LIBS) to determine Ti on sunscreen: A different sample preparation procedure, Optics & Laser Technology. 27 (2019) 648–653.

[27] P. Yaroshchyk, D. L. Death, S. J. Spencer, Comparison of principal components regression, partial least squares regression, multi-block partial least squares regression, and serial partial least squares regression algorithms for the analysis of Fe in iron ore using LIBS, J. Anal. At. Spectrom. 27 (2012) 92–98.

[28] A. Safi, B. Campanella, E. Grifoni, S. Legnaioli, G. Lorenzetti, S. Pagnotta, F. Poggialini, L. Ripoll-Seguer, M. Hidalgo, V. Palleschi, Multivariate calibration in Laser-Induced

Breakdown Spectroscopy quantitative analysis: The dangers of a ‘black box’ approach and how to avoid them, Spectrochimica Acta Part B: Atomic Spectroscopy. 144 (2018) 46-54.

[29] A. Kramida, Y. Ralchenko, NIST Atomic Spectra Database, NIST Standard Reference Database 78, 1999.

[30] Z. Wang, J. Feng, L. Li, W. Ni, Z. Li, A multivariate model based on dominant factor for laser-induced breakdown spectroscopy measurements, J. Anal. At. Spectrom. 26 (2011) 2289.

[31] R. Boqué, N. M. Faber, F. Rius, Detection limits in classical multivariate calibration models. Analytica Chimica Acta. 423 (2000) 41–49.

[32] M. Ostra, C. Ubide, M. Vidal, J. Zuriarrain, Detection limit estimator for multivariate calibration by an extension of the IUPAC recommendations for univariate methods, Analyst. 133 (2008) 532–539.

[33] F. Allegrini, A. C. Olivieri, IUPAC-consistent approach to the limit of detection in partial least-squares calibration, Anal. Chem. 86 (2014) 7858–7866.

[34] H. C. Goicoechea, A. C. Olivieri, A new family of genetic algorithms for wavelength interval selection in multivariate analytical spectroscopy, J. Chemometrics. 17 (2003) 338–345.

[35] C. D. Brown, Discordance between net analyte signal theory and practical multivariate calibration, Anal. Chem. 76 (2004) 4364–4373.

[36] J. Vogelgesang, J. Hädrich, Limits of detection, identification and determination: a statistical approach for practitioners, Accreditation and Quality Assurance. 3 (1998) 242–255.

[37] DIN EN 573-3 Aluminium and aluminium alloys - Chemical composition and form of wrought products - Part 3: Chemical composition and form of products, Beuth Verlag GmbH, Berlin, 2022.

[38] G. Benkißer, T. Bernthaler, K. Cyrener, Aluminium und Aluminiumlegierungen, in H. Oettel, H. Schumann (Eds.), Metallografie: Mit einer Einführung in die Keramografie, Wiley-VCH Verlag GmbH & Co. KGaA, Weinheim, 2016, 815–833.

3.2. Chapter 2:
LIBS as a Fast and Reliable Alternative to µXRF and SEM EDX for Quantitative Analysis of Aluminium Alloy Particles in Technical Cleanliness Analysis

Maria Lanzinger[a,b,c], Stephanie Kaufmann[b], Michael Schuster[c], Natalia P. Ivleva[a]

[a]Chair of Analytical Chemistry & Water Chemistry, TUM School of Natural Sciences (NAT, Dep. Chemistry), Technical University of Munich, 85748 Garching, Germany

[b]BMW AG, 80809 Munich, Germany

[c]Division of Analytical Chemistry, TUM School of Natural Sciences (NAT, Dep. Chemistry), Technical University of Munich, 85748 Garching, Germany

3.2.1. Declaration of Contribution and Summary

Maria Lanzinger, Stephanie Kaufmann, Michael Schuster, Natalia P. Ivleva

Microchemical Journal **2024,** 207, 111782, DOI: 10.1016/j.microc.2024.111782.

This work studies the comparability of LIBS to established metal particle characterization methods SEM-EDX and µXRF regarding precision and accuracy in element quantification in metal alloy particles. By consecutively analysing different samples with these methods, direct comparability is possible. By considering measurement effort and analysed volume a holistic view and comparison between the analysis techniques is enabled.

ML planned the experimental and evaluation procedure of the studied methods. ML performed the measurements using SEM-EDX and LIBS. The particle CRMs were selected in such a way, that they represent different aluminium alloys commonly used in industrial applications (Al-Mg, Al-Si, Al-Cu, Al-Zn). Since the CRMs are certified in their particle form, they are not mechanically processed further, to not impact their element composition. The analysis methods µXRF, SEM-EDX and LIBS performed consecutively on the same CRM particles and compared regarding their quantitative results for analytes Si, Mg, Mn, Cu, Zn and Fe. The results are compared using statistical t-testing methods between particles of the same CRM using the same method and between methods.

ML and SK performed microstructure analysis of the particles' matrix to find a homogeneous distribution of crystal phases. Additionally, an in-house developed Matlab® algorithm (ML) is used to visualize the effect of matrix inhomogeneity on the quantitative results: For accurate results, a sufficiently large amount of area needs to be analysed. Including less area, increases the chance of seeing only part (and possibly inaccurate) part of the whole picture.

ML performed the analysis volume approximation. The approximation for the chosen measurement parameters concluded, that LIBS analysis volume was smaller, than SEM-EDX analysis volume, but larger than the one from µXRF. Therefore, inaccuracies of individual methods could be seen and evaluated in this context.

This study concluded that LIBS is indeed a reliable and fast alternative or addition to SEM-EDX and µXRF analysis of metal alloy particles. T-test of both the particles among each, as well as LIBS to the X-ray-based methods showed high comparability. Only for single samples LIBS showed disadvantages regarding LOQ. However, considering the strong advantage of LIBS

regarding fast measurement and easy sample preparation, as well the opportunity to analyse light elements link Be and Li, this study opens the possibility to use LIBS as a valuable addition to standard methods of metal particle characterization.

All authors contributed to discussion and interpretation of the results.

NI, MS and SK supervised and reviewed the work.

3.2.2. Abstract

The characterization of metal alloy (particle) characterization is a vital tool in today's high-tech applications for quality and process control in industry, especially for applications in technical cleanliness analysis (TCA). Here, metal alloy fragments down to sizes of 200 µm need to be quantitatively characterized as accurate as possible. Laser-induced breakdown spectroscopy (LIBS) offers several advantages due to its easy use, short measurements times, and high sensitivity.

To enable the application of LIBS in this context, the method must yield adequately accurate results. Therefore, in this study we assess the performance of LIBS by comparison with well-established methods – scanning electron microscopy coupled with energy-dispersive X-ray spectroscopy (SEM-EDX) and µ-X-ray fluorescence (µXRF). We analyse particulate certified reference materials consecutively with non-destructive and destructive methods on the quantitative composition regarding the key elements necessary for distinguishing aluminium alloys: Si, Zn, Mn, Mg, Cu and Fe. Sample inhomogeneity and the effect of sampling location and area is shown via microstructure analysis and combined with an assessment of the analysis volume for each used method. By evaluating the data statistically and by comparing quantitative results achieved with different methods, we can postulate a high agreement between LIBS and the studied reference methods, providing a basis for the use of LIBS in industrial analysis of metal alloy particles.

Highlights:

- Quantitative characterization of metal particle composition to enable alloy identification comparing results of LIBS to SEM-EDX and µXRF.
- Comparability between individual reference particles is shown.
- High correspondence of LIBS to established particle characterization methods (SEM-EDX, µXRF).

Keywords: Laser-induced breakdown spectroscopy (LIBS), Particle characterization, Metal alloy, µ-X-ray fluorescence (µXRF), Scanning electron microscopy coupled with energy-dispersive X-ray spectroscopy (SEM-EDX).

3.2.3. Introduction

The analysis of metal alloys is essential in various industries and applications for quality and process control, ranging from steel production [1, 2] over recycling [3, 4] to technical cleanliness analysis. [5] While in production and recycling often large material volumes are analysed, in TCA it is necessary to draw conclusions from a small sample to its origin by identifying contaminations from different sources.

TCA summarizes the methods to assess the risk potential of (particle) contamination components or the production environment, e.g., in car or aircraft production, including the type and degree of the contamination. The most critical contaminants in automotive production are metallic particles, which can originate from mechanical processes like abrasion or shaving, as well as physical processes, like welding. Therefore, the metallic contaminants of interest to TCA are mainly industrially used metal alloys, like Al-, Fe- and Cu-alloys, in various compositions. The characterization of such metallic particles is fundamental in TCA, as the engine and connected mechanical and electrical components can be damaged by their hard, abrasive and/or electrically conductive nature – both during production and in use. Depending on the criticality, design and delicacy of the component(s), different particle sizes can be of interest to TCA. However, generally, particles larger than 200 µm are critical in this context as they can severely hamper production and the quality and safety of the resulting product. [5-7]

As many industrially used alloys are highly similar regarding their elemental composition, they can only be differentiated by detailed characterization, like element quantification. [5] The quantitative characterization of metallic materials can be performed, depending on the size and volume of the sample, by widely established methods like inductively-coupled plasma optical emission spectroscopy (ICP-OES) for larger quantities of sample material, scanning electron microscopy coupled with energy-dispersive X-ray spectroscopy (SEM-EDX) or µ-X-ray fluorescence (µXRF) for quick analysis of small particles.

However, for these methods to be used in quantitative analysis, measurement in a vacuum atmosphere is often necessary, increasing the analysis time and effort. With time being a valuable resource in industrial production and analysis, another method has been applied recently to metal particle characterization and shows promising results: laser-induced breakdown spectroscopy (LIBS).

LIBS is highly sensitive and suitable for the analysis of small volumes while at the same time requiring minimal sample preparation and measurement time. [4, 8, 9] The application of LIBS in solid state analysis ranges from the analysis of soils [10-12], and polymers [13, 14] to metals

[15, 16], with industrial applications in process control [17, 18], sorting[3, 4, 8, 19] and TCA. [5, 6, 20, 21] The technique can be used for qualitative [20, 22, 23], and quantitative analysis [21, 24, 25] of large (bulk) samples down to very small sample volumes, including particles in aerosols [26-29], and powders. [30-31]

Since this is a measurement in a solid matrix that cannot be changed in contrast to e.g. ICP, massive matrix effects can massively influence the ideally linear correlation between signal and analyte concentration, thus hampering calibration and characterisation of the sample material. To tackle the impact of these matrix effects, multivariate approaches, including multiple variables, like signals or spectral areas, are commonly applied, to improve the calibration accuracy. Common multivariate methods for element quantification using LIBS include principal component analysis (PCA) [20, 32-34], and partial least square (PLS) regression. [21, 25, 35-37]

One of the main challenges in the analysis of the metal alloy samples in a size range of roughly 200 µm to a few millimetres, is the sample inhomogeneity. Metal alloys are principally inhomogeneous due to the crystallization process during cooldown and the formation of mixed crystal phases, resulting in micro- and macro-segregations (inhomogeneities on a micro- or macro-scale). Therefore, the analysed volume is essential, if the result should be representative for a larger, origin material – especially for quantitative characterization. For large-volume or bulk samples, the analysed volume can be increased over the whole sample, in turn also increasing the chance of representing the composition of the whole material. Very small particles close to the nanometre range often contain only one phase due to their small volume, making them homogeneous by approximation. However, for samples in between nanometre range and bulk volume, such approximations often do not hold: The volume is too small to assume homogeneity by averaging over the whole sample and at the same time too large to assume homogeneity as has been described for nanometre samples. Therefore, the question of representativeness of quantification results for the origin material composition is often unanswered.

In the presented study we are offering a way to assess matrix homogeneity and, therefore, representativity, for such metal alloy samples by microstructure analysis and transfer the knowledge to quantitative element analysis. This work is based on our previous publication[102] and uses the PLS-regression models developed and described there. The models have been shown to be fit for metal alloy characterization of particles in size ranges of 50 µm to above 1 mm with low deviation. In the presented work, we compare the results additionally to established metal alloy analysis methods: SEM-EDX and µXRF. For this purpose, four Al-alloy

certified reference materials (CRMs) in particulate form are analysed regarding their element concentration of some of the most common alloy elements (Si, Mg, Mn, Fe, Cu, Zn) present in Al-alloys. [38]

The CRMs have been selected so that four different matrices are presented, making the results applicable to a broad audience. They outline the aluminium alloys most used in industry (A: Al-Cu, B: Al-Si, C: Al-Mg, D: Al-Zn-Si). The particle analysis methods were evaluated using automated algorithms for all techniques to simulate a real-life analysis in an industrial context.

3.2.4. Material and Methods

In this study four certified reference materials in particle form are analysed consecutively by µXRF, SEM-EDX and LIBS to determine the fitness of the novel LIBS as a reliable alternative to the established X-ray-based methods in particle characterization.

The data of the used certified reference material, including name, producer and country is displayed in table 1. Their respective certified concentration of analytes Si, Fe, Mn, Mg, Cu, and Zn is displayed in table 2.

The used sample preparation and analysis equipment are summarized in table 3 and 4, respectively. Their use and parameters are described when describing the experimental procedure.

Table 1: Certified reference materials (A-D) used in this study. BAS: ger: Bundesanstalt für Materialforschung und -Prüfung, NIST: National Institute of Science and Technology, VAW: VAW: formerly: ger.: Vereinigte Aluminiumwerke, now: Norsk Hydro.

Sample	Naming	Company	Country
A	216/3	BAS	Germany
B	87a	NIST	USA
C	565/3	ALUSUISSE	Switzerland
D	3402	VAW	Germany

Table 2: Used samples and their certified element concentration of Si, Fe, Mn, Mg, Cu, and Zn.

Sample	Si /%$_{wt}$	Fe /%$_{wt}$	Mn /%$_{wt}$	Mg /%$_{wt}$	Cu /%$_{wt}$	Zn /%$_{wt}$
A	0.74	0.77	0.76	0.76	5.45	0.214
B	6.24	0.61	0.26	0.36	0.30	0.16
C	1.84	0.50	0.43	7.01	0.05	0.031
D	9.24	0.4	0.027	0.38	0.04	10.35

Table 3: Sample preparation equipment used in this study.

Preparation Equipment	Company	Country
Carbon tabs (25 mm)	Plano GmbH	Wetzlar, Germany
Technovit® 2000LC	Kulzer GmbH	Hanau, Germany

Table 4: Analysis equipment used in this study.

Analysis Equipment	Company	Country
Polyvar Met 66	Leica Microsystems GmbH	Wetzlar, Germany
VHX-7000	Keyence Deutschland GmbH	Neu-Isenburg, Germany
M4 Tornado Plus	Bruker Nano GmbH	Berlin, Germany
ZEISS EVO10	ZEISS	Oberkochen, Germany
CORALIS	LTB Lasertechnik Berlin	Berlin, Germany

Samples

This study analysed four aluminium alloy CRMs in particle form using different particle analysis methods (LIBS, SEM-EDX, and µXRF). CRMs serve as a measure and comparative value in measurement procedures. As their element composition is known, they are commonly used for comparative studies and calibration. The particle sizes range from approximately 250 µm – 3 mm, provided in the respective certificate. To maintain the certified element composition, the particles were not further treated to alter their size. To increase comparability between the analysis methods, the same particles are consecutively analysed using µXRF, SEM-EDX and LIBS consecutively in this order.

The Si, Fe, Mn, Mg, Cu, and Zn concentrations were quantified to compare the methods. The CRMs' element concentrations for the specific analytes are displayed in table 2.

All analyte concentrations are shown and quantified using the *mass fraction in percent* also known as *weight percent* (*%wt*). The mass fraction is, according to DIN EN ISO 80000-9, a unit to quantitatively describe the composition of phase or material mixtures. For calculation, the mass of the analyte is related to the sum of masses of all mixture components (equ. 10). [39]

$$\%_{wt} = \frac{m_i}{m_{tot}} * 100\% \qquad \text{equ. 10}$$

To ensure comparable results, five single particles were picked randomly, labelled, and analysed consecutively by µXRF, SEM-EDX, and LIBS in this order. Microstructure analysis of the particles was performed to gain complementary information on alloy element distribution. Additionally, the images were used to estimate the minimal area necessary to generate results with decreased effects due to inhomogeneity and compare it to the area analysed by the respective analysis method.

For µXRF, the samples were prepared on a cuvette covered with a Mylar® sheet using adhesive tape to reduce background signals. It was analysed before sample measurements to exclude additional analyte signals from the tape. For the following SEM-EDX and LIBS measurements, the particles were fixed on an adhesive carbon tab (25 mm, PLANO GmbH, Wetzlar, Germany).

Experimental Procedure

For microstructure analysis and assessment of minimal sub-sampling area, particles from all samples were embedded in Technovit® 2000LC (Kulzer GmbH, Hanau, Germany), sanded (15 µm, 6 µm), polished (3 µm, 1 µm), and visualized by optical microscopy (Polyvar Met 66, Leica Microsystems GmbH, formally Reichert-Jung, Wetzlar, Germany).

Six alloy elements (Si, Mg, Mn, Fe, Cu, Zn) were quantified with three analysis methods (SEM-EDX, µXRF, LIBS) on five particles from each CRM. Each particle was analysed five times with each technique. In this context, one analysis means one measurement for µXRF and SEM-EDX and the average of ten measurements on different locations for LIBS, to even out the smaller analysis volume of LIBS compared to the other techniques (with the chosen

parameters). The measurement locations have been placed randomly on the surface, in such a way, that they would not overlap. First, the non-destructive methods µXRF and SEM-EDX were conducted, followed by micro-destructive LIBS analyses.

This study performed the µXRF analysis (M4 Tornado Plus, Bruker Nano GmbH, Berlin, Germany) with a spot size of 20 µm with measurement parameters of 60 s, 50 kV/300 µA, and two mbar. The SEM-EDX analysis (ZEISS EVO10, Zeiss, Oberkochen, Germany) was performed by focusing on the sample surface and scanning (4 min, 20 kV/1 nA) the whole imaged surface at a magnification of 200× (~ 247 448 μm^2).

The LIBS device (CORALIS, LTB Lasertechnik Berlin, Berlin, Germany) uses a pulsed Nd:YAG laser at 1064 nm with continuously variable laser energy for LIBS analysis. The laser spot has a diameter of about 20 µm. The instrument covers a wavelength range of 200 -- 680 nm with a spectral resolution of 15000 ($\lambda/\Delta\lambda$). Measurement parameters used in this work were optimized to 5 mJ of laser power, 7 laser pulses on each location, and a delay time between measurement and laser pulse of 1.4 µs as described in our previous publication on the quantitative analysis of aluminium alloys. [21]

Data Treatment and Evaluation

Microstructure analysis was performed to assess sample inhomogeneity of the used CRMs by calculating the surface coverage of the visibly distinguishable phases. The phases were differentiated visually by colour gradient using Matlab® (2022 edition, Mathworks, Natick, MA, USA). For better visibility, they were additionally coloured with Photoshop (2022 edition, Adobe Inc., Dublin, Ireland).

To assess sample homogeneity, the surface coverage of each visibly differentiable phase over the whole image was used as a reference and compared to the coverage of n circular sub-sampling areas (r = 30 µm). The coverage in the respective sub-sampling areas for different n was calculated 30 times for each n. The results are visualized in boxplots.

The analysis volume of µXRF and SEM-EDX is calculated using the spot size (spot size: 20 µm) and imaged area (247 448 μm^2), and the excitation energy (µXRF: 20 kV, SEM-EDX: 50 kV), respectively. Following Castaing's formular [40, 41] penetration depth is approximated for pure Al-matrices. The analysed volume with is typically displayed as a pear shape for EDX methods, is approximated as a cylinder for µXRF and cuboid for SEM-EDX in this case to decrease complexity. The calculation results in $6*10^3$ μm^3 (µXRF) and $1010*10^3$ μm^3 (SEM-EDX) for one analysis.

In the assessment of the volume analysed in LIBS, ten craters on Al-alloy bulk CRM using the same experimental parameters are analysed via digital 3D-microscopy (VHX-7000, Keyence Deutschland GmbH, Neu-Isenburg, Germany) by generating depth profiles of the craters. Four profiles at angels 0°, 45°, 90°, 135° are determined to account for asymmetrical crater morphology. Using Python, the depth profiles are tilt and baseline corrected and fitted using a polynomial function (figure 19). The areas of the crater and the piled-up material on its edges are integrated and subtracted. This resulting "interaction area" averaged for the four measured profiles for each crater (291 ± 25 μm^2). Using the mean determined depth (6.82 ± 0.75 µm) and the analysis volume of one crater can be approximated to a cone volume of 1305 μm^3. Consequently, the total analysed volume of one LIBS analysis, consisting of ten craters in this study, corresponds to $13*10^3$ μm^3.

The particles' composition is determined using automated evaluation algorithms to simulate real-life analysis. In µXRF analysis, the studied elements were quantified using a fundamental parameter (FP-) method provided by Bruker Nano GmbH. In SEM-EDX analysis, the elements to be studied were selected manually for evaluation. The quantification was conducted using ESPRIT© software by Bruker Nano GmbH. Visible carbon and oxygen signals were not included in the assessment. To check the system settings, the position of the K_α-Cu signal of a highly pure Cu CRM is tested each measurement day.

LIBS data was evaluated using in-house developed PLS-regression quantification models in Matlab® described in our prior publication. [21] The algorithm includes normalization on matrix signals and the selection of dominant regions of the respective analyte and the matrix element for calibration. They cover broad analyte concentrations and were optimized and validated for the characterization of metal alloy particles. For more details on the quantification models, like the evaluated spectral lines, the reader is referred to the respective publication. [21]

A 2-sided t-test (α=0.05) is used to detect significant differences in calculated element concentrations of particles of the same reference material and significant differences between studied analysis methods. To assess the overall comparability of the studied analytical methods, the composition of each material is summarized in bar plots using OriginPro® (2022b edition, OriginLab Corporation, Northampton, MA, USA).

Additionally, the relative deviation (d_{rel}) from the certified reference value is calculated (equ. 11). It is calculated as the absolute value of the difference of calculated (c_{calc}) and reference (c_{ref}) concentration, related to the reference concentration (c_{ref}) times 100 %.

$$d_{rel} = \frac{|c_{calc} - c_{ref}|}{c_{ref}} * 100\% \qquad \text{equ. 11}$$

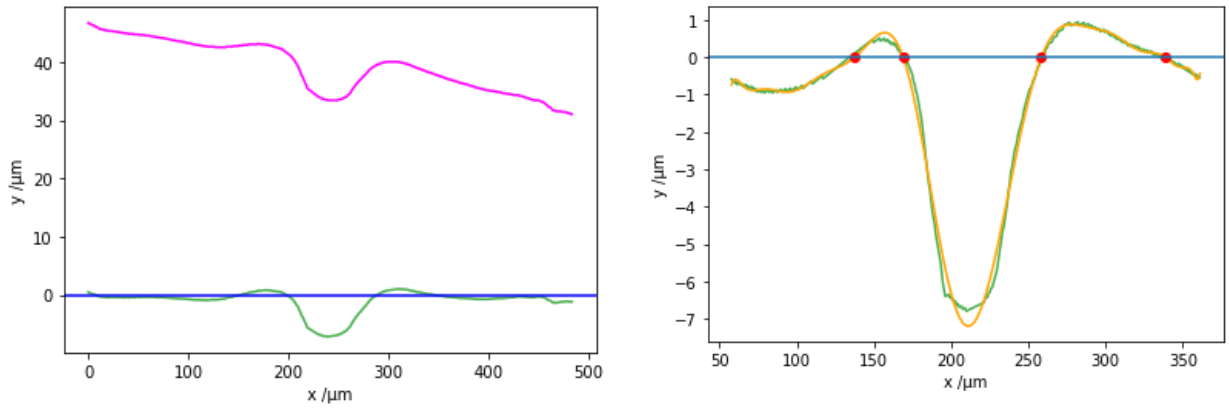

Figure 19: Visualization of LIBS crater depth profile analysis. Left: effect of tilt and baseline correction; pink: untreated profile; green: after correction, blue: baseline. Right: Curve fitting of corrected profile (green) to obtain fitted orange line. Intercepts with y=0 are marked with red dots to visualize the areas integrated.

3.2.5. Results and Discussion

Microstructure Analysis

Particle analysis methods, by design, analyse a small sample volume, which increases the impact of inhomogeneous analyte distributions on the quantification results. Since the metal alloys used in this study are realistically complex matrices, consisting of multiple crystal structures and intermetallic phases, the sample inhomogeneity is first assessed using microstructure analysis before conducting element quantification. The microstructures of CRMs A-D are visualized in figure 20. The certified element concentrations for each CRM of Si, Mg, Mn, Fe, Cu, and Zn are shown in table 1.

The white regions correspond to α-Al phases in all samples, with aluminium being the main element.

The microstructure of sample A (Al-Cu-alloy) shows finely distributed light grey structures, which most likely correspond to AlCu eutectic phases, as copper is the main alloy element. The eutectics are visible as thin (~1 µm), outstretched (~20 -- 100 µm) lines on the surface. The slightly darker grey, point like regions of the microstructure can be assigned to FeMn intermetallic phases (~1 µm). They are primarily located at the edges of the AlCu phases with

a higher density on the right side of the imaged surface, indicating the possibility of macro-segregations and inhomogeneous distributions on a macro-scale. [42]

Sample B (Al-Si-alloy) possesses a Si concentration of 6.24 $\%_{wt}$, so one would expect eutectic AlSi phases in the microstructure. Nevertheless, instead of the AlSi phases, homogeneously distributed grey-blue flakes (~5-15 µm) are observable. The colour and shape indicate the character of these phases being α-Si. Additionally, light grey intermetallic phases (~1 µm) are noticeable, which can be assigned to AlCu and FeMn mixed crystals. [42]

In the microstructure of sample C (Al-Mg-alloy), multiple phases can be observed: blue, finely structured AlMg (~5 -- 10 µm) and light grey AlSi (~10 -- 50 µm) phases, as well as slightly darker grey FeMn intermetallic structures are present (~2 µm). A grey plate-like structure (~30 µm) is also visible in the lower left corner, which can also be assigned to AlSi crystals. [42] Lastly, slight brown phases are observable (marked in blue circles). They cannot be classified with the information from the microstructure image but are assumed to be defects due to sample preparation and not features relevant to microstructure analysis.

The microstructure of sample D (Al-Zn-Si) shows a typical dendritic structure with white α-Al phases surrounded by light grey eutectic phases. Compared to sample A, the light white α-Al dendrites in the microstructure are thinner (~5 -- 10 µm) and more tightly branched. This soft grey area is probably a mixture of AlSi and AlZn eutectic phases, considering both alloy elements' concentrations (Si: 9.24 $\%_{wt}$, Zn: 10.35 $\%_{wt}$). [42]

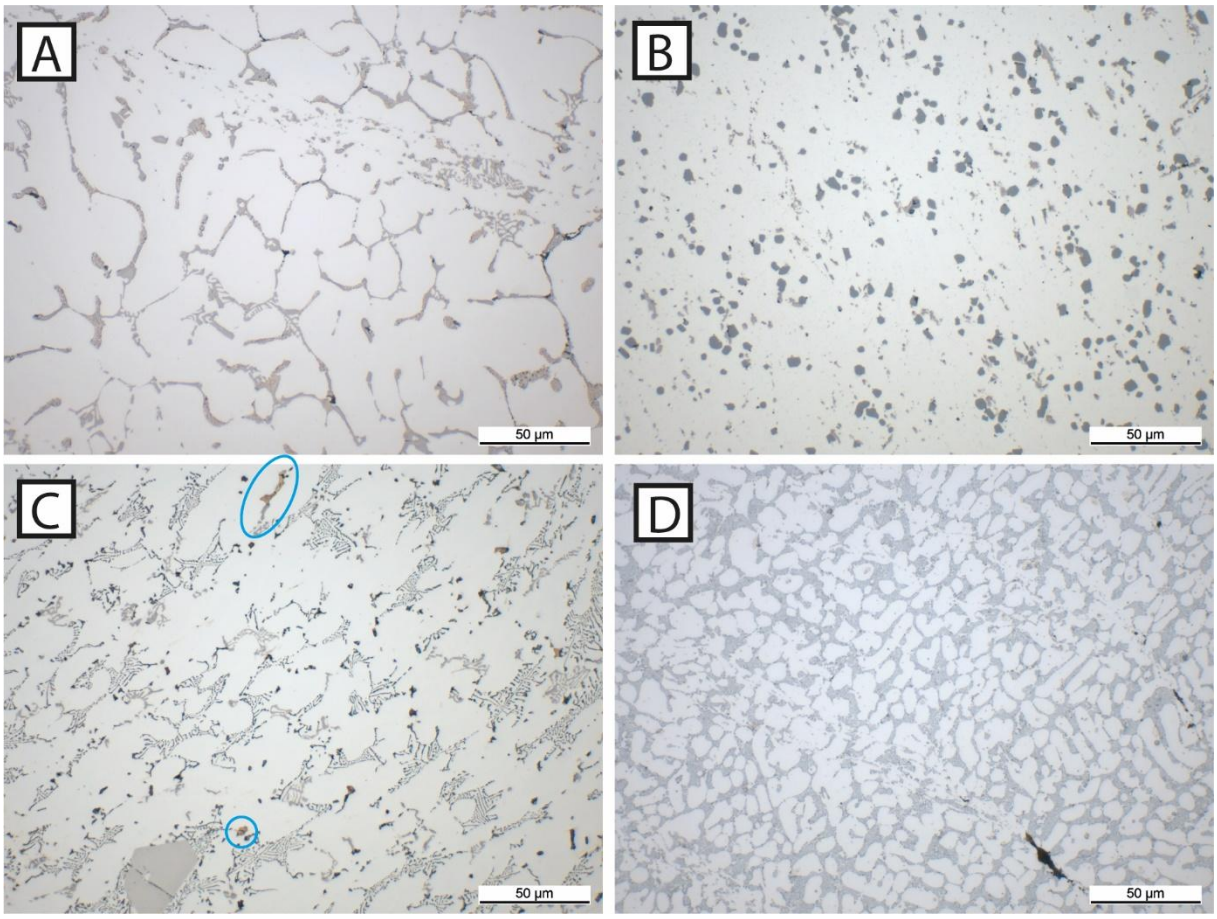

Figure 20: Microstructure images of CRMs A (Al-Cu alloy), B (Al-Si alloy), C (Al-Mg alloy), and D (Al-Zn alloy). Blue marked areas in C: Defects in the microstructure due to preparation – not relevant for the microstructure analysis. The CRMS's composition can be found in table 1.

To assess the sample matrix in more detail, the surface coverage of the visibly distinguishable phases is calculated for different simulated sampling areas (*n* circles of a diameter of 20 µm, each). The surface coverage of the crystal phases in the sampling areas is then compared to the respective coverage over the whole image to visualize the sample inhomogeneity. For better visibility, the phases are artificially coloured. Since the results are comparable for all studied materials, only one is described at this point.

In figure 21, left the artificially coloured microstructure of CRM A is shown. In orange, the previously described AlCu-phase is displayed. The circular sampling area (blue) is schematically demonstrated on the bottom right. In figure 3, right, the results for n = 1, 3, 5, 11, 25, and 101 are visualized using boxplots, with the green line corresponding to the coverage over the whole image. The red lines in each box represents its data's mean and the red crosses respective the outliers.

As expected, due to the large number of repetitions displayed in each box (30), the mean of all boxes is in good correspondence with the reference value. This already shows that a larger

sampling area increases the chance of representativity for the whole material. This finding is also supported due to the decreased variance between sampling datapoints for larger n. While small n e.g., n = 1, are strongly affected by inhomogeneities and high chance of misinterpreting the results, larger sampling areas decrease such effects, until for n = 51 and 101, the variance is almost neglectable. However, the decrease of variance is not linear, but stagnating. While the decrease from n = 1 to 3 is apparent, the difference between, e.g., n = 3, 5, and 11 is slighter. An improvement from n = 25 to n = 101 finally is hardly visible.

In conclusion we see, that a certain area needs to be analysed to be representative for the area coverage for the whole material. As the crystal phases correspond to the element distribution in the sample, this finding can be transferred to element quantification. Only if a large enough sample volume is analysed, the result will be representative for the whole material.

In case of micro-segregations, as visualized in the microstructure images, analysing only small areas of the sample holds the chance of low representativity for the whole sample. This makes it necessary to sample a larger volume to represent the bulk. Considering inhomogeneities over the whole bulk material (makro-segregations) the sampling areas should additionally be spread over a large or the whole volume. This way differences between edges and planes, the surface and the core would be included in the evaluation, possibly increasing the representativeness of the analysis for the bulk material.

However, in individual particle analysis, this course of ideal sampling is not possible. Firstly, the particles are generated from one location in the bulk, making their composition prone to makro-segregations. Therefore, they only display a certain fraction of the whole bulk composition. Secondly, if they are in a size relevant in this study, they will display multiple crystal phases with different element compositions. Therefore, the sampling or measurement location on the sample also will have an impact on the representativeness of the result.

All these considerations make it hard to directly compare different analysis methods, with different sampling volumes. Only by approximating the analysis volumes before interpreting the quantification results, the actual accuracy of the individual analysis method can be assessed; this will be done in the next chapter for the used analysis method LIBS as well as the reference methods µXRF and SEM-EDX.

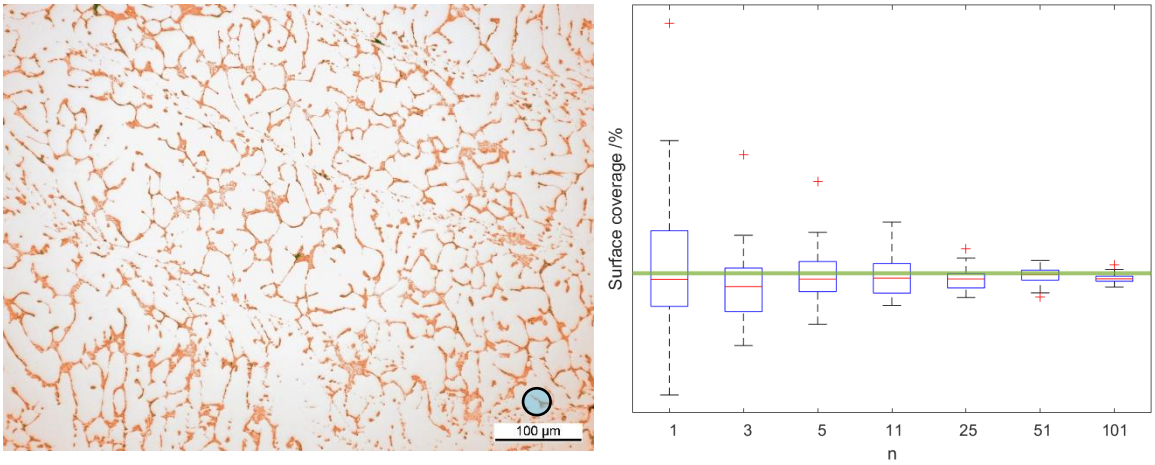

Figure 21: Left: Artificially coloured microstructure of CRM A (Al-Cu alloy); AlCu eutectic has been coloured orange. The blue circle schematically shows the size of a sub-sampling area. Right: surface coverage of AlCu phases n randomly placed circles on the microstructure. Each box is representing the results of 30 repetitions. In the boxplots the red line visualizes the mean value and red crosses indicate outliers. The green line shows the surface coverage over the whole image.

Assessment of Analysed Volume

Due to the previously described inhomogeneity in metal alloys (see figures 20 and 21), the quantified element content will be highly dependent on the analysed sample volume. To compare the performance of different analysis methods, it is, therefore, essential to first indicate their analysed volume. At this point only the results are presented, for a detailed description of the calculation and its background, the reader is referred to chapter *Experimental procedure*.

The analysed volume for LIBS craters is assessed by analysis via the resulting crater. Assuming, that all evaporated and analysed material is removed from the laser-sample interaction location and the molten material will form the crater rim, the analysed volume can be calculated from the microscopic analysis. The volume of one LIBS analysis in this study is approximated to $13*10^3$ µm^3. The determined approximated volume is comparable to findings in literature under ambient air pressure. [43, 44] This comparison considers the influence of sample matrix and measurement parameters, such as the number of laser pulses and laser pulse energy. Previous studies have demonstrated that these parameters have a significant impact on crater formation and ablated volume. [45, 46]

The computation of the analysis volume of X-ray-based methods is highly complex, as the penetration depth of the electrons and the backscattering in the material, impact the analysed volume. As an approximation, the penetration depth in pure Al is calculated using Castaing's

formula [40, 41] resulting in a penetration depth of roughly 4 µm (SEM-EDX, 20 kV) and 19 µm (µXRF, 50 kV) for the studied methods. Combining the area or spot size with the penetration depth yields analysed volumes of roughly $6*10^3$ µm^3 and $1010*10^3$ µm^3 for µXRF and SEM-EDX, respectively. Taking the previously assessed inhomogeneities into account, all analysis methods study a volume larger than observed inclusions in the microstructure.

In summary, the analysis volume of LIBS is found to be between the approximated volume for µXRF and SEM-EDX. This means that any possible inaccuracies in LIBS, which are not found in the reference methods, are unlikely to be caused by inhomogeneity effects. Instead, they are inaccuracies in the evaluation process. Therefore, calculating the analysis volumes helps to make a better comparison of the performance of LIBS with the established metal characterization techniques µXRF and SEM-EDX.

Comparison of Analysis Methods

Up to this point, we have set the stage for comparing LIBS to established particle analysis methods SEM-EDX and µXRF by assessing the sample homogeneity and the estimated volume. As we have seen that the analysis volume of LIBS is between the ones from the reference methods, we can now evaluate the quantitative results for the analytes (Si, Mg, Mn, Fe, Cu, and Zn) using five particles of each of the four CRM.

First, the reproducibility between the studied particles is assessed for each analysis method individually by performing a 2-sided t-test ($\alpha = 0.05$) on all particle results. This way we can detect significant differences between individual particles. Since we study CRMs with defined compositions, we can assess the precision of studied particle characterization methods this way. After the statistical precision has been assessed, we compare the methods to each other, again by t-testing ($\alpha = 0.05$). A more detailed description of the t-test and examples of calculated t-values are shown in the Appendix (table S1-S2).

The t-test results regarding reproducibility are summarized graphically in table 5: G (green) indicates no significant differences between all particles, Y (yellow) indicates significant differences between one particle to at least one other, and U (blue) significant differences between two or three particles to at least one other. Fields marked with “-“ (grey) indicate that no quantitative values have been obtained for this element with the corresponding method. This is the case for Mg and Si values in most measurements using X-ray-based methods due to strong signal overlap with Al and concentrations below the limit of quantification (LOQ), e.g., Zn in B, C for LIBS.

Table 5: The t-test results for individual particle analysis comparing the analyte concentrations (Zn, Mg, Mn, Cu, Si, Fe) in reference materials A-D using LIBS, SEM-EDX, and µXRF. Five particles of each CRM are included. G (green): no significant differences between all samples; Y (yellow): significant differences between one particle and others; U (blue): significant differences between two or three particles and others. – (grey): no quantitative values were obtained in the analysis.

	A			B			C			D		
	LIBS	SEM -EDX	µXRF	LIBS	SEM -EDX	µXRF	LIBS	SEM -EDX	µXRF	LIBS	SEM -EDX	µXRF
Zn	Y	Y	Y	-	G	Y	-	G	G	Y	Y	G
Mg	Y	-	-	Y	-	-	Y	-	G	U	-	-
Mn	G	G	G	G	Y	Y	G	G	Y	G	G	G
Cu	U	Y	Y	Y	Y	Y	G	G	Y	U	-	G
Si	Y	-	-	G	-	Y	Y	-	G	G	-	G
Fe	G	G	G	G	Y	Y	Y	G	G	Y	-	G

We found a high agreement between particle samples with the most studied CRMs, showing no significant difference or only one particle being significantly different for all methods. Only in three cases in LIBS analysis (A: Cu, D: Mg, Cu) did more than one particle differ significantly from the others.

The distribution of single particles differing significantly from at least one other (Y) does not follow a visible pattern in the analytes or the tested materials, with also the established methods SEM-EDX and µXRF often showing significant differences between samples. We, therefore, can assume a similar precision for established techniques SEM-EDX and µXRF. Using LIBS, significant differences between multiple sample particles (U) are found in three instances, indicating lower precision, especially for Cu quantification.

Secondly, the analytical methods are compared to each other regarding the determined element concentration using a 2-sided t-test ($\alpha = 0.05$). Results are again summarized in matrices, G (green) indicating no significant difference and Y (yellow) showing significant differences. For example, the matrix of **CRM A** is shown in table 6. As the strong signal overlap in the spectra of Si and Mg with Al led to no quantitative results for the X-ray-based methods, they are not included. The results for the other materials are displayed in the Appendix (table S3-S5). As they all yield highly similar results to CRM A, they are not discussed at this point.

Table 6: T-test results for comparing the analyte concentrations (Zn, Mn, Cu, Fe) determined in CRM A using LIBS, SEM-EDX and µXRF. G (green): no significant differences between the methods' results; Y (yellow): significant differences between the methods' results. No values using µXRF and SEM-EDX for analytes Si and Mg were obtained, making it redundant to compare the methods.

Zn	LIBS	SEM-EDX	µXRF
LIBS		G	G
SEM-EDX	G		Y
µXRF	G	Y	
Mn	LIBS	SEM-EDX	µXRF
LIBS		G	Y
SEM-EDX	G		G
µXRF	Y	G	
Cu	LIBS	SEM-EDX	µXRF
LIBS		G	Y
SEM-EDX	G		Y
µXRF	Y	Y	
Fe	LIBS	SEM-EDX	µXRF
LIBS		Y	Y
SEM-EDX	Y		Y
µXRF	Y	Y	

We see that LIBS shows no significant differences to at least one of the reference methods for analytes Zn, Mn and Cu. Especially SEM-EDX and LIBS results are highly comparable according to t-testing, as these methods do not show significant differences for the named analytes. This might be an effect of the analysed volume, as in this experiment SEM-EDX and LIBS analyse larger volumes compared to µXRF. As we have shown in chapter 3.1, a small increase of volume can have a large impact on the representativeness for the whole sample.

For the quantification of Fe in CRM A, all methods showed significant differences to each other in their quantitative results, independent of their volume. However, comparing the results for particle analysis using the different methods, no statistical differences have been found for all studied methods. Therefore, the detected significant difference between the techniques might me a statistical effect.

When the deviation between the t-tested values is minimal, even small differences can result in statistically significant differences. However, when comparing quantitatively, these differences may be considered insignificant. Therefore, in the next chapter, we will assess the quantitative results of each studied analysis method regarding their quantification of Si, Mg, Mn, Fe, Cu and Zn.

Results of Quantitative Analysis

In the previous chapter we have assessed the statistical comparability between LIBS and reference methods SEM-EDX and µXRF in metal alloy particle characterization. Now their results will be summarized and compared quantitatively to (1) each other and (2) the certified reference value to show the quantitative performance of the four methods, providing information on their applicability in real-life analysis.

The combined quantification results of six analytes in all studied CRMs (5 particles each) of each analysis method are shown in figure 22; on the left, an overview, and on the right, a zoom-in is displayed, presenting the lower weight percentages in more detail. For this evaluation, all sample measurements are included – five analyses on each of the five CRM particles. The calculated values are compared to the certified values.

As briefly described in chapter *Comparison of analysis methods*, quantifying **Si** and **Mg** was hardly possible using µXRF and SEM-EDX due to the substantial overlap of matrix (Al) and analyte signal. Though the analyte signals were mostly identifiable qualitatively, the automated evaluation algorithms did not yield results.

SEM-EDX analysis did not produce quantitative values for **Si**. Using µXRF, only Si concentrations of 6 $\%_{wt}$ (B) and 9 $\%_{wt}$ (D) could be quantified with low relative deviations of (d_{rel}: 11 % and 4 %, respectively) – the Si content of CRM C was strongly underestimated and while a value for A could not be determined. Using LIBS, Si concentrations of all samples were successfully quantified with d_{rel} between 5 % and 37 %. The highest d_{rel} of 37 % for material B can be attributed to an inaccuracy of the automated LIBS quantification algorithm in this concentration region, described in detail by Lanzinger et al.[102] The quantification model of Si was not built with reference CRMs in the concentration region of 6 $\%_{wt}$, leading to decreased accuracy for quantifying such concentrations.

Similarly to Si, the concentration of **Mg** could not be quantified using the automated SEM-EDX evaluation algorithms. Using µXRF, low concentrations of Mg (0.3 $\%_{wt}$: A, B, D) could also not be quantified. Higher Mg content in C of 7.01 $\%_{wt}$ was determined with d_{rel} of 22 %. For

material C, LIBS yielded a slightly lower d_{rel} of 15 %. In CRMS, A, B and D the Mg content, which µXRF or SEM-EDX could not determine, was overestimated by LIBS with d_{rel} of 36 %, 119 %, and 196 %, respectively. The d_{rel}-values above 100 % refer to an absolute deviation of 0.44 %$_{wt}$ and 0.07 %$_{wt}$, which is low enough to identify metal alloys inside their respective material norm. For example, the Mg concentration in materials defined in EN-AW-6063 [47] can range from 0.45 – 0.90 %$_{wt}$. In this concentration range, the respective alloy norm is still in specification.

The increased variation in Mg quantification using LIBS was already observed in the single particle analysis (chapter 3.3), which showed significant differences between the individual samples. Assuming homogeneous element distribution due to sufficient sampling, we conclude an increased inaccuracy of the LIBS quantification algorithm for this matrix. Including this and other similar matrices in the quantification models could improve the models' performance. As the scope of this paper was only to showcase the strengths and weaknesses of studied automated evaluation methods, their optimization is not included here but is a mere recommendation.

Mn and **Fe** were quantified with high accuracy and precision with all methods (d_{rel}: 0-28 %), excluding Fe quantification in CRM D. This analyte was not quantifiable using SEM-EDX, assumingly due to the concentration falling below the method's LOQ.

The **Cu** determination for material A (5.45 %$_{wt}$) was similarly accurate for all studied methods with d_{rel} between 15 % and 20 %. Analysis of CRM B (0.3 %$_{wt}$) yielded more accurate results for the X-ray-based methods (d_{rel}(EDX): 1 %, d_{rel}(µXRF): 0.3 %) compared to LIBS (d_{rel}: 97 %). Lower concentrations in C (0.05 %$_{wt}$) and D (0.04 %$_{wt}$) were quantified with the highest accuracy for µXRF (C: 6 %, D: 27 %), followed by LIBS (C: 26 %, D: 172 %). SEM-EDX yielded overestimated results for material C (d_{rel}: 145 %) and no quantitative results for material D. Samples B through D again showed small reference concentrations translating the high d_{rel} of LIBS and SEM-EDX to low absolute deviations.

The quantification of **Zn** yielded accurate results for materials A through C using all methods, with LIBS being the least accurate of the studied techniques. For CRM D, the Zn content is underestimated by SEM-EDX (d_{rel}: 31 %) and overestimated by µXRF (d_{rel}: 9 %) and LIBS (d_{rel}: 27 %).

In summary, comparing the methods' results to the reference values, the used X-ray based methods showed decreased performance for Si and Mg, due to signal overlap with the matrix, while LIBS yielded more accurate results. Considering Cu, LIBS showed the largest deviations

from the reference value; however the X-ray based methods also how similar deviations here. In the quantification of Mn, Fe and Zn concentration all methods performed similarly well.

Comparing the analysis methods to each other, we see similar results for quantifying Fe, Mn, Cu, and Zn in Al-alloy particles using LIBS and the widely established methods μXRF and SEM-EDX. A comparison to Si and Mg values between LIBS and the X-ray based techniques was not possible using the automated quantification algorithms. However, comparing the results from LIBS to the certified reference value yielded appropriately small deviations. These results enable using all studied methods, established and novel, in particle characterization for alloy identification in the context of particle characterisation in TCA.

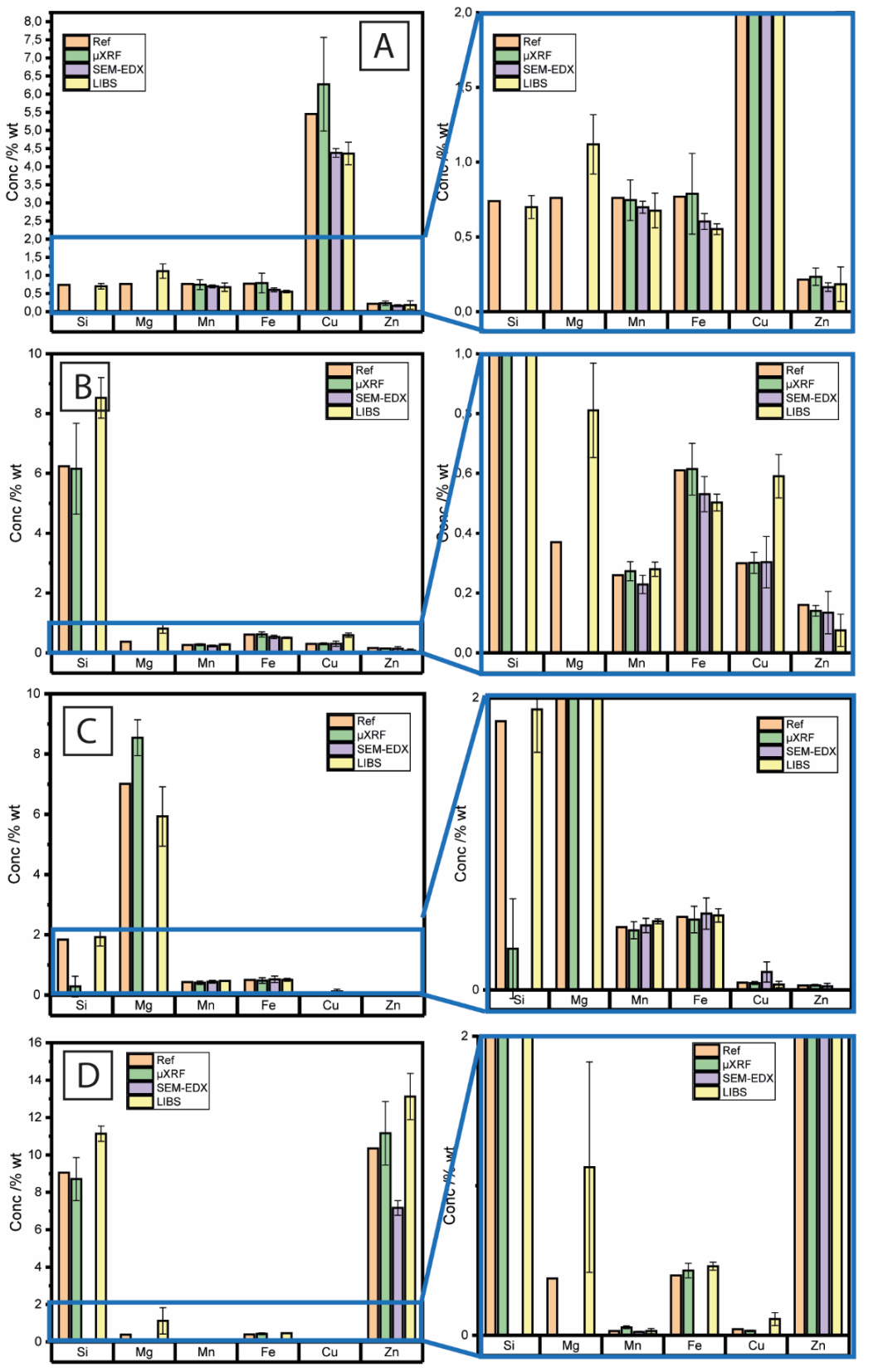

Figure 22: Element quantification results of CRMs A-D from the certificate (orange), µXRF (green), SEM-EDX (purple) and LIBS (yellow).

3.2.6. Conclusion and Outlook

In this study, particles of four CRMs for Al alloys have been analysed consecutively by particle analysis methods µXRF, SEM-EDX, and LIBS, to quantify their respective Si, Mg, Mn, Fe, Cu, and Zn content and compare their results. To assess phase distribution and homogeneity microstructure analysis was performed and the surface coverage was calculated. After the analysis volume for each technique was calculated, the quantitative results were compared.

In the microstructure analysis, micro-segregations and different crystal phases have been visualized. Even though the phases were homogeneously distributed over the samples, a strong effect of the sampling area and location on representativeness was shown. This is particularly important for the analysis of inhomogeneous particles, such as metal alloys, as these samples are affected by both micro and macro-segregations and can only be examined to a limited extent due to their size and presence. Therefore, in the characterization of such samples, the analysed measurement-volume and sample homogeneity is approximated before conducting the evaluation, to ensure representative results.

The approximation of analysis volume showed, that, with the chosen measurement parameters, the volume of LIBS was between µXRF and SEM-EDX. With this information, an improved interpretation of the quantitative results is possible, as the impact of sample inhomogeneity can be assessed more clearly.

In the subsequent evaluation of the representativeness between the CRM particles, significant differences are observed only for single particles within a sample series of each CRM, indicating high comparability between individual particles. As also the reference methods show such differences, we have seen comparable precisions for all studied particle analysis methods. T-testing the methods against each other also showed high comparability between the LIBS and the X-ray-based methods. Generally, LIBS showed no significant differences to at least one of the reference methods for all analytes. In case of significant differences to both reference methods, these techniques showed significantly different results to each other as well.

Comparing the quantitative results of the studied particle analysis methods for all analytes showed advantages and disadvantages for individual techniques. Generally, the X-ray-based methods yielded less accurate or no results for Si and Mg contents using the automated evaluation due to matrix and analyte signal overlap. Even though the analyte could be visually identified (qualitative analysis), the automated assessment did not provide meaningful results. Adjusting the quantification algorithm and optimizing it to fit an Al-matrix would make

quantification possible – but this was beyond the scope of this study. Quantification of Mn and Fe was similarly accurate for all studied particle analysis methods. LIBS showed a higher LOQ compared to µXRF and SEM-EDX for Zn, while SEM-EDX did the same for Fe in CRM D (c(Fe): 0.4 $\%_{wt}$) and Cu in sample C (c(Cu): 0.04 $\%_{wt}$).

In summary, LIBS, a novel method for quantitatively analysing particle materials, showed results comparable to the widely established methods of µXRF and SEM-EDX for quantitative alloy particle characterization. We saw similar accuracy for Mn, Fe, Cu, and Zn, with only slight decreases for LIBS compared to the reference methods. The automatically evaluated X-ray-based methods hardly yielded results for Mg and Si due to signal overlap with the Al-matrix. Here, further optimization would be necessary to quantify these analytes in such matrices.

With LIBS's advantages, such as short preparation time and effort and the opportunity to measure under ambient air, this method is an excellent alternative or addition to µXRF and SEM-EDX analysis. This is especially true for industrial applications, which need fast and easy analysis of metallic samples, like TCA. Considering achieving the results presented here, conducting one measurement of LIBS took only about 5 s, measurement times in the reference methods were significantly higher (SEM-EDX: 4 min, µXRF: 1 min). Another advantage of LIBS is the analysis of light elements such as Be and Li, an important element for rechargeable batteries, which cannot be measured with the X-ray-based methods µXRF and SEM-EDX. With the results presented in this work, the basis for an application of LIBS in metal alloy particle analysis is provided.

Funding

The authors received no financial support for the research, authorship, and/or publication of this article.

CRediT Authorship Contribution Statement

Maria Lanzinger: Writing – review & editing, Writing – original draft, Project administration, Formal analysis, Data curation, Conceptualization. **Stephanie Kaufmann:** Writing – review & editing,Supervision, Project administration, Conceptualization. **Michael Schuster:** Writing – review & editing, Supervision, Project administration, Conceptualization. **Natalia P. Ivleva:** Writing – review & editing, supervision, Project administration, Conceptualization.

Declaration of Competing Interests

The authors declare that they have no known competing financial or personal relationships that could have appeared to influence the work reported in this paper.

Data Availability

Data will be made available on request.

Acknowledgements

We want to thank Stefanie Hengstberger (BMW AG Munich) for the preparation and visualization of the microstructures and Thomas Glabik (BMW AG Munich) for the preparation and performing of the µXRF measurements. Additionally, we would like to thank Alexander Thomas (Technical University of Munich, TUM) and Dr. Dominik Huber (BMW AG Munich) for their advisory activity.

Appendix A. Supplementary Data

Supplementary data to this article can be found online at https://doi.org/10.1016/j.microc.2024.111782.

3.2.7. References

[1] P. Marcus, V. Maurice, Passivity of metals and alloys, in: R. W. Cahn, P. Haasen, E. J. Kramer (Hg.), Materials Science and Technology: A comprehensive treatment, Wiley-VCH Verlag GmbH, Weinheim, Germany, 2000, pp. 131-169.

[2] H. Bargel, G. Schulze, Einwirkung von Herstellung und Weiterverarbeitung auf die Eigenschaften von Metallen in: H. Bargel, G. Schulze, Werkstoffkunde, Springer Berlin, Heidelberg, 2008, pp. 67-96.

[3] P. Werheit, C. Fricke-Begemann, M. Gesing, R. Noll, Fast single piece identification with a 3D scanning LIBS for aluminium cast and wrought alloys recycling, J. Anal. At. Spectrom. 26 (2011) pp. 2166.

[4] R. Noll, C. Fricke-Begemann, S. Connemann, C. Meinhardt, V. Sturm, LIBS Analyses for Industrial Applications – an Overview of Developments from 2014 to 2018, J. Anal. At. Spectrom. 33 (2018) pp. 945–956.

[5] German Association of the Automotive Industry, VDA 19.1 - Inspection of Technical Cleanliness: Particulate Contamination of Functionally Relevant Automotive Components, VDA Automotive Standard, Berlin, 2015.

[6] J. Faber, K. Brodzik, M. Nycz, Understanding Technical Cleanliness: Importance, Assessment, Maintenance. Combust. Engines. 186 (2021) pp. 41–50.

[7] M. Oravec, A. Divoková, P. Lipovský, M. Karásek, R. Janošík, Technical Cleanliness - a Requirement of Precision Manufacturing. Acta Mechanica Slovaca. 23 (2019) pp. 46–51.

[8] R. Noll, Laser-Induced Breakdown Spectroscopy: Fundamentals and Applications, Springer, Berlin, 2012.

[9] S. Musazzi, U. Perini, Laser-Induced Breakdown Spectroscopy: Theory and Applications, Springer, Berlin, 2014.

[10] X. T. Yan, K. M. Donaldson, C. M. Davidson, Y. Gao, H. Wu, A. M. Houston, A. Kisdi, Effects of Sample Pretreatment and Particle Size on the Determination of Nitrogen in Soil by Portable LIBS and Potential Use on Robotic-Borne Remote Martian and Agricultural Soil Analysis Systems. RSC Advances. 8 (2018) pp. 36886–36894.

[11] S. C. Jantzi, V. Motto-Ros, F. Trichard, Y. Markushin, N. Melikechi, A. Giacomo, Sample Treatment and Preparation for Laser-Induced Breakdown Spectroscopy. Spectrochimica Acta Part B: Atomic Spectroscopy 115 (2016) pp. 52–63.

[12] R.S. Bricklemyer, D. J. Brown, P. J. Turk, S.M. Clegg, Improved Intact Soil-Core Carbon Determination Applying Regression Shrinkage and Variable Selection Techniques to Complete Spectrum Laser-Induced Breakdown Spectroscopy (LIBS). Appl. Spectrosc. 2013, 67 (10), pp. 1185–1199.

[13] S. Grégoire, M. Boudinet, F. Pelascini, F. Surma, V. Detalle, Y. Holl, Laser-Induced Breakdown Spectroscopy for Polymer Identification. Anal. and Bioanal. Chem. 400 (2011) pp. 3331–3340.

[14] V. C. Costa, F. W. B. Aquino, C. M. Paranhos, E. R. Pereira-Filho, Identification and classification of polymer e-waste using laser-induced breakdown spectroscopy (LIBS) and chemometric tools, Polymer Testing. 59 (2017) pp. 390–395.

[15] Y. Dai, C. Song, X. Gao, A. Chen, Z. Hao, J. Lin, Quantitative determination of Al–Cu–Mg–Fe–Ni aluminum alloy using laser-induced breakdown spectroscopy combined with LASSO–LSSVM regression, J. Anal. At. Spectrom. 36 (2021) pp. 1634–1642.

[16] C. Chen, Q. Shi, S. Wang, Q. Lin, Y. Duan, A novel method for metallic element analysis in particle samples using a laser-induced breakdown spectroscopy technique. J. Anal. At. Spectrom. 31 (2016) pp. 1527–1533.

[17] A. K. Myakalwar, C. Sandoval, M. Velásquez, D. Sbarbaro, B. Sepúlveda, J. Yáñez, LIBS as a Spectral Sensor for Monitoring Metallic Molten Phase in Metallurgical Applications—A Review. Minerals. 11 (2021) 1073.

[18] L. Peter, V. Sturm, R. Noll, Liquid Steel Analysis with Laser-Induced Breakdown Spectrometry in the Vacuum Ultraviolet. Appl. Opt. 42 (2003), 6199.

[19] S. Merk, C. Scholz, S. Florek, D. Mory, Increased identification rate of scrap metal using Laser Induced Breakdown Spectroscopy Echelle spectra, Spectrochim. Acta Part B At. Spectrosc. 112 (2015) pp. 10–15.

[20] D. Huber, Development of a composite analysis process with laser-induced plasma spectrometry and multivariate data evaluation for characterizing particles in the field of

technical cleanliness analysis [Ph.D. Thesis, Technical University of Munich, Munich]. mediaTUM.

[21] M. Lanzinger, D. Huber, V. Merk, S. Kaufmann, M. Schuster, N. Ivleva, Development of Laser-Induced Breakdown Spectroscopy-Methods for Rapid Element Quantification in Alloy Particles in Technical Cleanliness Analysis, Spectrochim. Acta Part B At. Spectrosc. 205 (2023) 106691.

[22] D. J. Díaz-Romero, S. Van Den Eynde, W. Sterkens, A. Eckert, I. Zaplana, T. Goedemé, J. Peeters, Real-Time Classification of Aluminum Metal Scrap with Laser-Induced Breakdown Spectroscopy Using Deep and Other Machine Learning Approaches. Spectrochim. Acta Part B At. Spectrosc. 196 (2022) 106519.

[23] E. Srivastava, H. Kim, J. Lee, S. Shin, S. Jeong, E. Hwang, Adversarial Data Augmentation and Transfer Net for Scrap Metal Identification Using Laser-Induced Breakdown Spectroscopy Measurement of Standard Reference Materials. Appl Spectrosc 77 (2023), pp. 603–615.

[24] S. Van Den Eynde, D. J. Díaz-Romero, I. Zaplana, J. Peeters, Deep Learning Regression for Quantitative LIBS Analysis. Spectrochim. Acta Part B At. Spectrosc. 202 (2023) 106634.

[25] P. Devangad, V. K. Unnikrishnan, M. M. Tamboli, K. M. M. Shameem, R. Nayak, K. S. Choudhari, C. Santhosh, Quantification of Mn in Glass Matrices Using Laser Induced Breakdown Spectroscopy (LIBS) Combined with Chemometric Approaches. Anal. Methods. 8 (2016) pp. 7177–7184.

[26] D. Hahn, W. L. Flower, K. R. Hencken, Discrete Particle Detection and Metal Emissions Monitoring Using Laser-Induced Breakdown Spectroscopy. Appl Spectrosc 51 (1997) pp. 1836–1844.

[27] C. Dutouquet, G. Gallou, O. Le Bihan, J. B. Sirven, A. Dermigny, B. Torralba, E. Frejafon, Monitoring of Heavy Metal Particle Emission in the Exhaust Duct of a Foundry Using LIBS. Talanta. 127 (2014), pp. 75–81.

[28] C. Niu, X. Cheng, T. Zhang, X. Wang, B. He, W. Zhang, Y. Feng, J. Bai, H. Li, Novel Method Based on Hollow Laser Trapping-LIBS-Machine Learning for Simultaneous

Quantitative Analysis of Multiple Metal Elements in a Single Microsized Particle in Air. Analytical Chemistry. 93 (2021) pp. 2281–2290.

[29] D. Diaz, D. Hahn, U. Panne, LIBS for Aerosol Analysis. In Laser-Induced Breakdown Spectroscopy; Elsevier, (2020) pp. 499–535.

[30] H. Rajavelu, N. J. Vasa, S. Seshadri, LIBS Technique Combined with Blow Gas and Vacuum Suction to Remove Particle Cloud and Enhance Emission Intensity during Characterization of Powder Samples. Spectrochimica Acta Part B: Atomic Spectroscopy. 181 (2021) 106215.

[31] I. B. Gornushkin, A. Ruíz-Medina, J. M. Anzano, B. W. Smith, J. D. Winefordner, Identification of Particulate Materials by Correlation Analysis Using a Microscopic Laser Induced Breakdown Spectrometer. J Anal Spectrom 15 (2000) pp. 581–586.

[32] T. Takahashi, B. Thornton, T. Sato, T. Ohki, K. Ohki, T. Sakka, Temperature based segmentation for spectral data of laser-induced plasmas for quantitative compositional analysis of brass alloys submerged in water, Spectrochim. Acta Part B At. Spectrosc. 124 (2016) pp. 87–93.

[33] M. A. Sperança, D. F. Andrade, J. P. Castro, E. R. Pereira-Filho, Univariate and multivariate calibration strategies in combination with laser-induced breakdown spectroscopy (LIBS) to determine Ti on sunscreen: A different sample preparation procedure, Optics & Laser Technology. 27 (2019) pp. 648–653.

[34] P. Yaroshchyk, D. L. Death, S. J. Spencer, Comparison of principal components regression, partial least squares regression, multi-block partial least squares regression, and serial partial least squares regression algorithms for the analysis of Fe in iron ore using LIBS, J. Anal. At. Spectrom. 27 (2012) pp. 92–98.

[35] M. V. Belkov, D. A. Borisevich, K. Y. Catsalap, M. A. Khodasevich, Multivariate Calibration of Concentrations of C, Mn, Si, Cr, Ni, and Cu in Low-Alloy Steels from Raw Low-Resolution Spectra Obtained By Laser-Induced Breakdown Spectroscopy, J. Appl. Spectrosc. 88 (2021) pp. 970–974.

[36] L. Gómez-Nubla, J. Aramendia, S. Fdez-Ortiz de Vallejuelo, J. M. Madariaga, Analytical methodology to elemental quantification of weathered terrestrial analogues to meteorites using a portable Laser-Induced Breakdown Spectroscopy (LIBS) instrument and Partial

Least Squares (PLS) as multivariate calibration technique, Microchemical Journal 137 (2018) pp. 392–401.

[37] C. R. Ytsma, C. A. Knudson, M. D. Dyar, A. C. McAdam, D. D. Michaud, L. M. Rollosson, Accuracies and detection limits of major, minor, and trace element quantification in rocks by portable laser-induced breakdown spectroscopy. Spectrochim. Acta Part B At. Spectrosc. 171 (2020) 105946.

[38] DIN EN ISO 17034:2017-04: Allgemeine Anforderungen an Die Kompetenz von Referenzmaterialherstellern; Beuth Verlag GmbH, Berlin, 2017.

[39] DIN EN ISO 80000-9:2020-02: Größen und Einheiten -Teil 9: Physikalische Chemie und Molekularphysik; DIN Media GmbH, Berlin 2020.

[40] R. Castaing, Application of Electron Probes to Local Chemical and Crystallographic Analysis. Ph.D Thesis, University of Paris, Paris, 1951.

[41] J. I. Goldstein, D. E. Newbury, J. R. Michael, N. W. M. Ritchie, J. H. J. Scott, D. C. Joy. Scanning Electron Microscopy and X-Ray Microanalysis; Springer New York: New York, NY, 2018.

[42] G. Benkißer, T. Bernthaler, K. Cyrener, Aluminium und Aluminiumlegierungen, in H. Oettel, H. Schumann (Eds.), Metallografie: Mit einer Einführung in die Keramografie, Wiley-VCH, Weinheim, 2016, pp. 815–833.

[43] K. Zhang, W. Song, Z. Hou, Effect of ambient pressures on laser-induced breakdown spectroscopy signals. Front. Phys. 19 (2024) 42203.

[44] F. Bencherif, S. A. Beldjilali, T. Baba-Hamed, A. Belasri, Experimental study of the effect of pressure and laser fluency on laser ablation craters and LIBS emission features of brass sample, Optik. 224 (2020) 165573.

[45] J. Hermann, M. Benfarah, G. Coustillier, S. Bruneau, E. Axente, J.F. Guillemoles, M. Sentis, P. Alloncle, T. Itina, Selective ablation of thin films with short and ultrashort laser pulses, Appl. Surface Science, 252 (2006) pp. 4814-4818.

[46] T.A. Labutin, A.M. Popov, V.N. Lednev, N.B. Zorov, Correlation between properties of a solid sample and laser-induced plasma parameters. Spectrochim. Acta Part B At. Spectrosc. 64 (2009) pp. 938-949.

[47]: DIN EN 573-3:2022-09, Aluminium und Aluminiumlegierungen_- Chemische Zusammensetzung und Form von Halbzeug_- Teil_3: Chemische Zusammensetzung und Erzeugnisformen; Beuth Verlag GmbH, Berlin, 2022.

4. Summary and Outlook

In the automotive industry, TCA is becoming increasingly important to reduce quality related costs, enable the use of highly performance-optimized materials and components as well as produce safe and long-living goods. In this dissertation, LIBS has been studied as a fast and reliable method for analyte quantification in metal alloy particles for the purpose of contamination source identification in TCA. LIBS is a versatile method, applied in various industrial and academical contexts for rapid qualitative and quantitative analysis with little to no necessary sample preparation. [1] Qualitative LIBS has shown promising results for the material classification in the context of TCA [2], however quantitative LIBS, to the point of this dissertation, has not been applied to sample types and sizes relevant in this framework.

Therefore, this dissertation studied the applicability of quantitative LIBS to TCA, developing multivariate calibration models for Al-alloy samples, validating them on TCA (reference) particles and finally comparing the generated results to established particle analysis methods. As in TCA the focus is on easy, fast and possibly automated analysis, the LIBS set-up and measuring procedure was kept as simplistic as possible; no protective gas nor specific sample preparation were used prior to the LIBS measurement.

A general challenge using direct quantitative analysis methods, including LIBS, are matrix effects, impairing the direct correlation of signal and analyte concentration. To reduce such effects the in literature commonly referenced multivariate calibration PLS-R is used for the development of the LIBS quantification models. The training data consists of 49 Al-alloy CRMs covering a range of analyte concentration and alloy matrices. Quantification models for ten analytes common for Al-alloys (Si, Cu, Mn, Ti, Fe, Zn, Mg, Ni, Pb, Cr) are developed, in the cases of Si, Mn, Mg and Zn by implementing a two-step evaluation. In the first of the two steps the rough analyte content is determined, followed by the in-detail quantification over a smaller concentration range. This way, the accuracy of the models is increased. By validating the developed calibrations with CRMs, that have not been used as training data, additional to cross-validation, their robustness against variable sample matrices is showcased. Depending on the analyte absolute deviations between 0.002 - 0.5 $\%_{wt}$ and approximated LOQs of 0.1 $\%_{wt}$ are achieved, showcasing the possibilities of applying LIBS in TCA for particle characterization.

The developed models are additionally applied to validate a method of TCA reference particle generation, that is rapid, easy and can be used for various materials. Using mortar and pestle on e.g. metal alloy shavings, particles in different size classes can be generated, that have

been exposed to mechanical stress, simulating conditions similar to what TCA particles are subjected to in production processes.

Using a sieve, or sieve tower, size classes that are of interest for the individual application can be separated and classified. The aluminium alloy samples tested here show no significant correlation between particle size and analyte concentration, meaning the size does not have an impact on element composition. The result is in accordance with performed microstructure analysis, which does not display damage to specific parts of the microstructure.

However, other matrices, e.g. aluminium with above 17%$_{wt}$ of silicon can be damaged by mechanical force and thereby change their composition during the particle generation. Therefore, using this particle generation process the impact of pressure and stress on particles generated and “processed” in the engine before they are extracted and analysed can also be assessed.

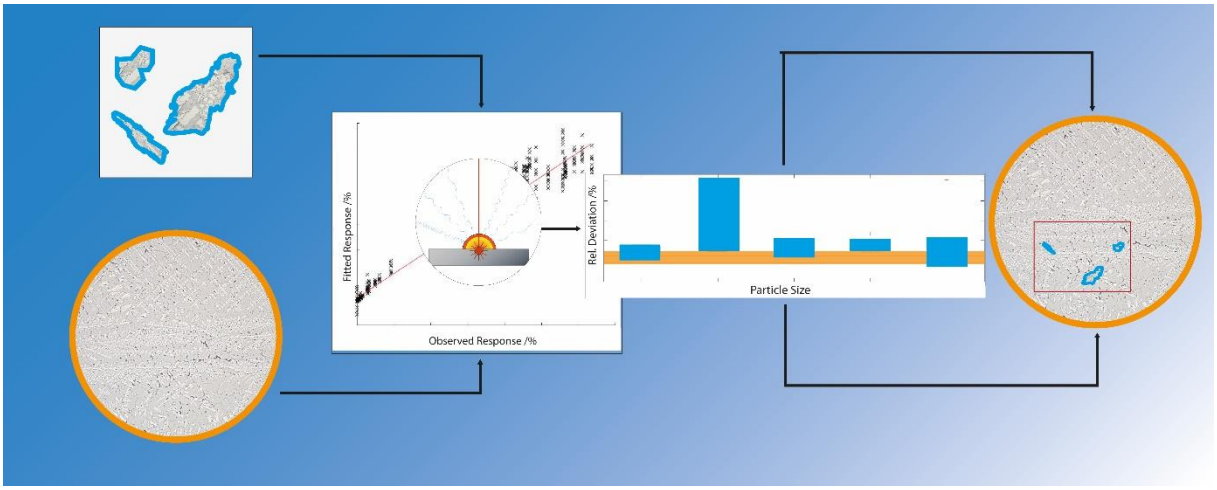

Figure 23: Development of Laser-Induced Breakdown Spectroscopy-Methods for Rapid Element Quantification in Alloy Particles in Technical Cleanliness Analysis. [3]

Developing a novel method or evaluation model always opens discussions regarding the performance compared to other, already established procedures. In the case of the analysis of metal alloy particles, commonly used methods are SEM-EDX and µXRF. Compared to these methods, LIBS offers significant advantages in the context of TCA, especially regarding the effort for sample preparation and general measurement time. While a single quantitative analysis in non-automated SEM-EDX and µXRF takes at least 60 s, not even considering time

to e.g. prepare the sample and generate a vacuum in the sample chamber, a LIBS measurement requires only a fraction of a second.

Keeping in mind, that one TCA sample can include up to 50 particles, that need to be characterized, and multiple filters need to be analysed each day in a TC laboratory, the manual X-ray-based methods are not feasible in this context. However, the micro-destructiveness of LIBS needs to be considered, especially for small volumes and possible follow-up analyses.

Therefore, to use LIBS as a supplement or in some cases alternative to SEM-EDX and µXRF, their comparability needs to be shown, which is done in this dissertation using a comparative study of the three methods. The comparative study is designed by studying four CRMs in particle form subsequently with µXRF, SEM-EDX and LIBS in this order. Five particles of each CRM are analysed three times at different positions on the sample. The analytes Si, Mn, Mg, Cu, Fe and Zn are evaluated using the studied methods. All evaluation is done automatically by either the built-in algorithms (µXRF, SEM-EDX) or the previously developed and described quantification models (LIBS). This simulates the real-life analysis of TC particles of unknown origin.

One of the decisive arguments in comparing direct analysis of metal alloys, is the inhomogeneity of the samples itself. Depending on the amount of sample volume, that is analysed, results will differ from each other as well as from the reference concentration of the bulk material. Using microstructure analysis, the minimal necessary sampling area to generate representative results is estimated.

Additionally, an assessment of the analysis volume is performed. For the X-ray-based methods theoretical calculations are already established, that can be used to approximate the analysed volume. For LIBS the approximation is done by analysing the residual crater, assuming the difference between crater eject and crater volume below the surface results in the volume, that has been transferred into plasma state. Previous tests and literature [2,4] shows, that different matrix elements will impact the LIBS crater depth significantly, so such calculations and experiments will need to be repeated for other base materials than aluminium. These calculations concluded that the analysis volume of LIBS was in between µXRF (smaller) and SEM-EDX (larger) for the chosen parameters, proving the interpretation of the following quantitative results is possible.

Evaluation of the quantitative results revealed advantages and disadvantages for all methods. The X-ray-based methods were not able to accurately quantify Si and Mg using the automated algorithms, due to a signal overlap between the matrix element Al and these analytes. In these

cases, adjustments or optimization of the provided quantification models would be necessary – which was out of scope for this dissertation. Using T-testing to compare the results of LIBS to the ones of SEM-EDX and µXRF, high comparability between LIBS and the established methods is shown, especially for Fe and Mn. In the analysis of Zn, LIBS showed a higher LOQ than µXRF and SEM, while SEM-EDX showed this behaviour for Cu and Fe for low element concentrations.

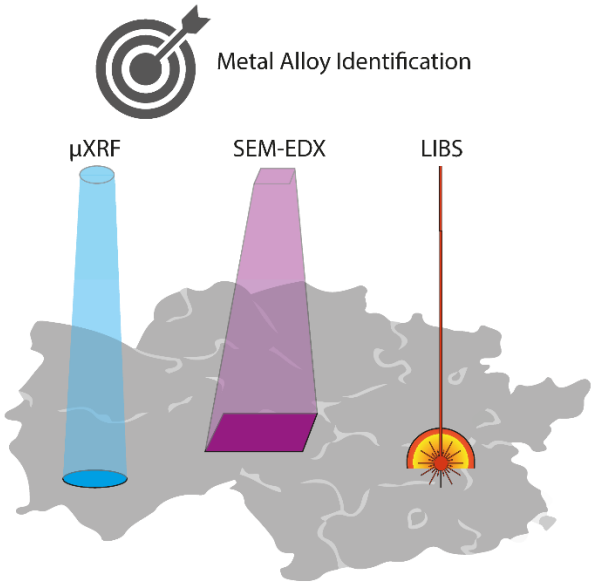

Figure 25: LIBS as a fast and reliable alternative to µXRF and SEM EDX for quantitative analysis of aluminium alloy particles in technical cleanliness analysis. [5]

Concluding this dissertation, a generation process for TC reference particles has been described, which can be done in-house with minimal necessary equipment investment. These particles can be generated from different alloy materials and desired size class, depending on the respective use case. Possible uses, additional to the previously described application in quantification experiments, could be validation for optical particle detection systems, or TC "misuse" experiments to determine critical limits by manually introducing particles of known characteristics into a product or process.

The focus of this dissertation, however, was the development of LIBS quantification models for metal alloy particles in context of TCA. It has been presented, that the developed PLS-R models yield accurate analysis results for bulk materials as well as sample sizes of TCA relevance – even though the measurement is performed without any additional sample preparation nor under protective gas atmosphere. Additionally, the results from such a measurement have been shown to be comparable to established particle characterization

techniques regarding their analytical performance, while at the same time being superior regarding the measurement time and sample preparation effort. Especially for TCA, whose focus is rapid and easy analysis, LIBS and the developed methods open a whole new field of applications and analysis opportunities.

Based on this dissertation, further scientific work can take off. For one, the knowledge regarding multivariate calibration techniques and possible calibration techniques can be used for developing quantification models for various other materials and matrices. In the context of TCA, analyte quantification in metallic matrices, like copper, iron, or zinc matrices would be of interest – also considering the effect of mechanical pressure on the sample matrix composition and the effect the particle size on the quantitative result. With the proposed reference particle generation process, testing any developed calibration models on different TCA reference particles is easily and efficiently possible in any laboratory.

Especially in combination with the information on LIBS crater sizes and ablated volume, the quantification models of any matrix can be applied to generate maps regarding the element composition over a surface area. This could be applicable the analysis of solid-state electrolytes to map the lithium distribution in the sample, or silicon coatings on iron surfaces applied to increase the interaction with adhesives with the coated surface.

References

[1]: R. Noll, Laser-Induced Breakdown Spectroscopy: Fundamentals and Applications; Springer: Berlin, 2012.

[2]: D. Huber, M. Schuster. Development of a Composite Analysis Process with Laser-Induced Plasma Spectrometry and Multivariate Data Evaluation for Characterizing Particles in the Field of Technical Cleanliness Analysis. Dissertation, Technical University Munich, 2021.

[3]: M. Lanzinger, D. Huber, V. Merk, S. Kaufmann, M. Schuster, N. Ivleva. Development of Laser-Induced Breakdown Spectroscopy-Methods for Rapid Element Quantification in Alloy Particles in Technical Cleanliness Analysis. Spectrochimica Acta Part B: Atomic Spectroscopy 2023, 205, pp. 106691.

[4]: D. Bleiner, Z. Chen, D. Autrique, A. Bogaerts. Role of Laser-Induced Melting and Vaporization of Metals during ICP-MS and LIBS Analysis, Investigated with Computer Simulations and Experiments. Journal of Analytical Atomic Spectrometry, 2006, 21, pp. 910.

[5]: M. Lanzinger, S. Kaufmann, M. Schuster, N. P. Ivleva. LIBS as a Fast and Reliable Alternative to MXRF and SEM–EDX for Quantitative Analysis of Aluminium Alloy Particles in Technical Cleanliness Analysis. Microchemical Journal 2024, 207, pp. 111782.